VARIABLE SPEED CONSTANT FREQUENCY POWER CONVERSION WITH PERMANENT MAGNET SYNCHRONOUS AND SWITCHED RELUCTANCE GENERATORS

by

Geun-hie Rim

Dissertation submitted to the faculty of the
Virginia Polytechnic Institute and State University
in partial fulfillment of the requirements for the degree of

DOCTOR OF PHILOSOPHY

in

Electrical Engineering

APPROVED:

Krishnan Ramu

Krishnan Ramu, Chairman

Robert P. Broadwater

Robert P. Broadwater

Dan Y. Chen

Dan Y. Chen

Robert W. Hendricks

Robert W. Hendricks

Saifur Rahman

Saifur Rahman

February, 1992

Blacksburg, Virginia

VARIABLE SPEED CONSTANT FREQUENCY POWER CONVERSION WITH PERMANENT MAGNET SYNCHRONOUS AND SWITCHED RELUCTANCE GENERATORS

by

Geun-hie Rim

Committee Chairman: Krishnan Ramu
Electrical Engineering

(ABSTRACT)

Power electronics is inevitably concerned with the processing of variable speed power generations such as in wind turbines, aircraft systems and naval on-board ship systems. The nature of these types of energy is distinct in that their frequency and power vary depending on the speed of the prime-mover. To make use of the variable speed energy, a power processing scheme which transforms the variable speed energy into a constant frequency power is required. There are measures such as mechanical and electrical links for such purposes. Electrical link systems are chosen in this study due to their fast responses and high reliabilities. The power conversion stage may be a dc link with a line-commutated converter, a dc link with a self-commutated inverter, or a cycloconverter. The line-commutated converter and cycloconverter power stages require a fixed frequency supply for operation whereas the self-commutated inverter is capable of stand-alone operation, thus making it attractive.

Two cases of variable speed power generation using a permanent magnet synchronous machine (hereafter referred to as PMSM) and a switched reluctance machine (hereafter referred to as SRM) were studied in this dissertation. The possible use of PMSMs has been proved by the good correlation between the experimental results and the theoretically predicted results. Three different control strategies have been proposed, implemented in hardware, and experimentally verified. The efficiency of the VSCF power conversion with a self commutated converter were comparable to the one using a line-commutated converter.

A novel converter topology with no dc link capacitor has been proposed for the application of SRMs to the VSCF power conversion. The proposed topology directly links the constant frequency ac source to the SRM. This feature enhances the reliability of the power conversion scheme and reduces the weight and volume of the system. The correlation between the theoretical and experimental results of some key issues showed the feasibility of the proposed VSCF power conversion scheme.

In the course of the study, one stage ac to dc power conversion with a compact transformer was required for dc loads. However, phase-controlled ac to dc conversion has the disadvantages of low power factor and harmonic pollution on the utility side, particularly in the case where dc voltage regulation is required. Therefore, a novel single phase rectifier for dc load which provides ohmic isolation with a high frequency transformer is extensively investigated. The proposed scheme had a wide output variation on dc output while maintaining unity power factor and sinusoidal current in the ac input side. Three control strategies for the operation of the converter were proposed and verified experimentally. The harmonic spectra on ac and dc sides are analytically derived and experimentally proved under some load conditions.

Acknowledgements

In the name of my Lord, Jesus Christ, I would like to express my appreciation to Prof. K. Ramu for his encouragement and support during the course of this research work. His broad knowledge, creativity and patience have been truly helpful.

I also wish to thank Prof.s, R.P. Broadwater, D.Y. Chen, R.W. Hendricks and S. Rahman for their contributions as member of my doctoral committee, their teaching and suggestions regarding the documentation.

I also acknowledge the help and cooperations provided by my colleagues, A.S. Bharadwaj, Dr. P. Materu, X. Mang and all the students in the motion control system research group.

I am also indebted to Korea Electrotechnology Research Institute for their supports. Special thanks are due to the president, U.H. Ahn, the former president, C.S. Oh, managers S.B. Byun, D.S. Shin, Y. Kim, N. Kim, K. Kim, D. Na and other colleagues.

This work was made possible by the steadfast support and sacrifice of my family. In particular, I owe my gratitude to my parents, in-laws, and my uncle Mr. B.Y. Rim.

I thank my children Howon and Dawon for their successful adjustment to US life and being what they are.

I owe an enormous debt to my wife, Miae, for her care, support and understanding during my Ph.D study.

I dedicate this dissertation to the memory of my father in-law and grandmothers.

Table of Contents

List of Figures

List of Tables

Chapter 1
INTRODUCTION

1.1 Introduction

A number of prime movers for electric power generation shown in Figure 1.1 have variations in their speed. Some examples are wind turbines, aircraft, and naval on-board ship turbines. Power at constant frequency is desired for transmission, distribution, and utilization. That is made possible either by introducing a mechanical link to maintain a constant generator speed or by introducing an electric link to convert the variable speed power into the constant frequency power. The latter solution provides faster response, higher reliability, and greater feasibility in many systems compared to the mechanical link solution. The variable speed prime movers drive a synchronous or an induction generator. In the case of the synchronous generator, the output will be of varying voltage magnitude and frequency. The induction generator can be tied to the constant frequency supply directly, but the power flow is uncontrolled. In both cases, power converters are required to process power at constant frequency in the variable speed constant frequency (VSCF) case with the synchronous generator and to control the power flow in the induction generator case.

Two synchronous machines, a PM synchronous machine and a switched reluctance machine (PMSG and SRM), both considered in this study, are categorized as brushless machines. This advantageous characteristic simplifies the rotor construction by doing away with the rotor windings, slip rings, and brushes. In that process, the reliability of their operations has increased and is in their favor. They also have the advantages of high efficiency and power density, features very important for airborne applications.

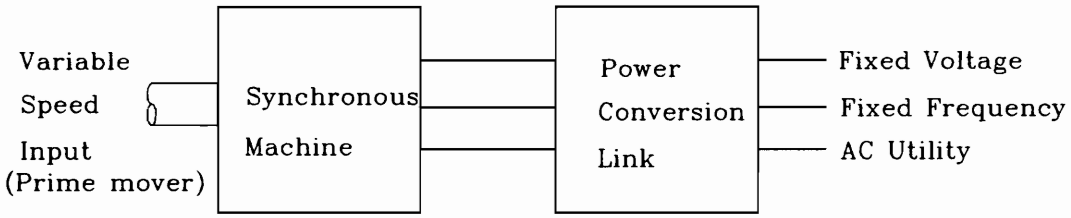

Figure 1.1: Power conversion link for variable speed mechanical input

1.2 Review of Previous Work

1.2.1 Static VSCF power conversion

Significant efforts have been made in static power converter designs to enhance the system efficiency or to process the renewable energies such as wind power [1]-[3], [13], and solar energy [7]. The recovery of energy from the machine is essential to increase the efficiency of the system [8], [9], and variable speed power can be interconnected to the power grid for power generation [1]-[6].

1.2.2 PWM converter

Power processing from dc to ac can be found throughout industry in applications such as the VAR-compensator [10], high voltage dc (hvdc) [11], ac motor drives [35]-[39], uninterruptible power supply (UPS) [46], [47], magnetic energy storage systems, etc. The major concerns in these power processings are:

(i) Minimization of harmonics [15]-[19].

(ii) Audible noise reduction [20].

(iii) Power factor correction [21]-[23].

To minimize the distortion of the waveforms two methods are most frequently adopted. They are:

(i) Pulse width modulation [24]-[26].

(ii) Pulse dropping [15], and [27].

However, the use of 3rd harmonic distortion to increase the output voltage is reported for balanced three phase inverter systems [17], [33]. Depending on the nature of the process, dc to ac power conversion is divided as follows:

(i) Current source inverter [40]-[42].

(ii) Voltage source inverter [43]-[44].

Due to their robustness and ease of control, phase-controlled converters using SCRs have been used for a long time. But they do not give a sinusoidal line current and the power factor is dependent on the control angle. These characteristics are undesirable in applications. The advent of self turn-off semiconductor devices gave control freedom in static power conversion, and made available the self-commutating high switching-frequency converter [45]-[47]. Due to these converters, good quality of waveforms with unity power factor can be produced and are considered for industrial applications [6], [22], and [23].

1.2.3 PM synchronous machine

PM synchronous machines are used for variable speed drive systems due to their compactness, high power density, ease of control and high efficiency. Generator applications of PMSM is attempted for the first time in [50], [51].

1.2.4 SRM

Switched reluctance machines have gained prominence due to the advent of inexpensive semiconductors for its control. The switched reluctance machines are inexpensive to build, maintain, and operate at a higher efficiency than conventional variable speed motor drives.

Since researchers started reinvestigating the SRM in the 60's, a considerable amount of research effort covers a wide range of topics which are described as follows:

(i) Design of SRMs [52]-[57]

(ii) Analysis SRM drives [58]-[62], [72], [73]

(iii) Device ratings of the SRM converters [63], [66]

(iv) Topology of the SRM converters [64]-[69]

(v) Controllers for the SRM converters [70]-[72]

(vi) Motor/Generator Operation of SRM [75]-[78]

Due to the nonlinearity and saturation of SRM, converter kVA requirements call for attention [63], [66]. The electromagnetic torque is proportional to the square of the applied

current in the machine which in turn requires only unidirectional current, making the converter topology simpler than other variable speed drives. Several converter topologies have been studied only for the motoring operation of the SRM [64]-[69].

The topology concerns the machine winding structure, the device ratings, and the minimization of the number of switches. Single switch per phase for bifilar-winding SRMs, and single switch per phase using the split dc source voltages or using dump resistor converters are proposed in [64], [66] and [69], respectively. Further research efforts, [65], [67], [68] and [74] describe the minimization in the number of switches by increasing the utilization of switches.

The possibility of using SRM for four quadrant operation is reported in [74]. Motoring/generation mode operations of SRM with battery sources are described in the literature, [75] and [77], with the two-switch per phase configuration being the most commonly used. The possible use of SRMs as generators is reported in [76] using two switch per phase and battery excitation.

1.2.5 Single phase ac/dc converter

Phase controlled ac to dc power conversion has the disadvantages of low power factor and harmonic pollution on the utility side, particularly in the case where dc voltage regulation is required. It is well known that a diode-bridge rectifier with an output capacitor-filter induces low power factor and pulse current problem on the ac side [83]. To minimize the lower frequency harmonics and enhance the power factor, the authors use a passive filter on the ac side in [84]. But these rectifiers give only fixed dc voltages. A high switching frequency PWM converter is reported for rectifier-inverter systems using IGBTs [85]. A study on programmed pulse-dropping ac chopper show that it is advantageous for low switching frequency [86]

1.3 Objectives and Contributions

1.3.1 VSCF scheme with a PMSM

The currently used systems and their typical problems are:

(i) Battery charging/discharging systems - low efficiency.

(ii) Cycloconverter systems - frequency limitations.

(iii) Line commutated converter systems - harmonics and low power factor.

To overcome these detrimental features of the VSCF scheme, the following objectives are formulated:

(i) Improvements in the overall system efficiency.

(ii) Removal of the frequency constraints.

(iii) Reduction of harmonics and minimization of filter sizes.

(iv) Improvements in power factor.

(v) Formulation of the scheme and its strategies.

(vi) Implementation and experimental verification of the scheme on a laboratory prototype.

1.3.2 VSCF scheme with an SRM

Various converter topologies have been reported for SRM drives [64]-[69]. But none of the presently known schemes are able to operate the SRMs as generators and motors directly from the ac supply. Realizing this deficiency, a new topology which is capable of performing motoring and generating operation is introduced in the present work. The objective of the study is to analyze the use of an SRM for VSCF power conversion and prove its feasibility with experimental verification.

1.3.3 Single phase ac/dc Converter

During the study of the scheme it became apparent that the system isolation between the dc load and the ac source needed to be achieved with a compact transformer. Volume-critical applications require compactness and light weight. Hence a study of single phase ac/dc conversion with the feature of light weight and good quality of power is investigated. Further high power and good quality waveforms are imperative in ac to dc power conversion.

1.4 Scope and Organization of the Dissertation

Two generation systems with PMSM and SRM in steady state are modeled, analyzed, and designed with a pulse width modulation (PWM) converter. Experimental verification with laboratory prototypes are presented along with the predicted result that confirm the validity of the modeling and the soundness of the feasibility of the schemes.

The line commutated converter cannot be used for dc to ac power conversion in the stand alone applications and the VSCF scheme needs a self-commutated converter in such cases. Introduction of such a converter facilitates the adjustment and control of power factor and shaping the waveform quality. One such power converter scheme for PMSM is described in Chapter 2. In this chapter each subsystem is modeled, analyzed, and integrated for steady state. The relationship between the generated voltage at the converter and the utility grid voltage is discussed with phase diagrams. This scheme removes the constraint of the other scheme in regard to harmonics and power factor. The feasibility of the scheme is proved by realizing a prototype and correlating the experimental results with the theoretically predicted results.

Chapter 3 describes the steady state characteristics of a topology with two quadrant operation (motoring/generating) of a four-phase SRM. Theoretical results in steady state for speed control applications are verified using a laboratory prototype. The study covers the topology configuration on the following issues:

(i) Formulation of the control strategies for speed control.

(ii) Impact of current advance and maximum PWM duty ratio with respect to speed and power.

(iii) Device ratings.

(iv) Power flow control in the scheme.

(v) Discussion of merits and demerits of the topology.

In Chapter 4, for the sake of completeness of VSCF power control, a single phase ac

to dc converter with unity power factor and sinusoidal ac input current are studied. This chapter addresses the following research objectives:

(i) Formulation of control strategies to reduce the total harmonic distortion of the ac input current.

(ii) Implementation of the various control strategies on a laboratory prototype.

(iii) Verification of correlation between the experimental and the theoretical results.

(iv) Isolation of ac source and load using a small high frequency transformer.

Chapter 2

VARIABLE SPEED POWER CONVERSION WITH A PMSM

Variable speed constant frequency power conversion schemes use wound rotor induction or synchronous machines for power generation. With the advent of high power density permanent magnets, the synchronous generators could be built compactly compared to the wound rotor type, resulting in the elimination of an external dc supply for rotor excitation, the slip rings, and brushes. Such machines are ideal for aircraft, naval on-board ship power systems and remote station applications such as on an island or a ranch. This chapter, realizing the need for such applications, contains the steady state modeling, performance evaluation and experimental verification of the key results of a VSCF power conversion scheme with a PMSM.

The line commutated converter cannot be used for dc to ac power conversion in the stand alone applications and therefore the VSCF scheme needs a self commutated converter. The introduction of such a converter facilitates the adjustment and control of power factor and shaping the waveform quality. One such power converter scheme is described in this chapter. The operation and design of the converter and its associated control circuitry are described in detail. An experimental verification of the VSCF scheme with a permanent magnet synchronous generator is included to validate the key assertions.

Nomenclature

I_g	Generator line current
I_s	Ac source line current
I_{dc}	Dc link current
V_{ai}	Ac input phase voltage of the inverter
V_{lai}	Ac input line to line voltage of the inverter
V_{as}	Phase voltage of the ac source
V_{ls}	Line to line voltage of the ac source
V_g	Generator phase voltage
V_{lg}	Generator line to line voltage
V_{dc}	Dc voltage of the rectifier
V_i	Inverted voltage of the controlled converter
R_s	Line reactor resistance
L_s	Line reactor inductance
R_g	Generator stator-winding resistance
L_d, L_q	Quadrature d,q axes inductance
α	Phase difference between V_{as} and V_{ai}
ω_s	Ac source frequency in rad/sec
ω_m	Generator frequency in rad/sec
ϕ_m	Phase difference between I_s and V_{as} for control strategy I
ϕ_c	Phase difference between I_s and V_{as} for control strategy II
ϕ_p	Phase difference between I_s and V_{as} for control strategy III
P_{in}	Input power
P_{oc}	Converter output power
P_o	Active power delivered into the utility
Q_o	Reactive power delivered into the utility
η	Efficiency
δ	Torque angle
E_f	Generator induced emf

2.1 Introduction

The possible use of permanent magnet synchronous machines has arisen with recent developments in permanent magnet technology and its application to large machines approaching MVA ratings. The permanent magnet machines have the advantages of high efficiency and power density, features very important for airborne applications with their requirement of no external dc supply for rotor excitation. The latter advantage simplifies the rotor construction by doing away with the rotor windings, slip rings and brushes. This increases the reliability of its operation. The permanent magnet synchronous machine has, in addition, a very low synchronous reactance, thus making it a stiff source of power with a higher steady state and transient capability than its counterpart, the wound rotor type. It is to be noted that a study with permanent magnet synchronous machines lends itself to a study of the superconducting generator with very few modifications. Such a study is necessary and almost imminent in light of present higher temperature superconductor research and the possibility of their realization in the future.

There are two kinds of permanent magnet synchronous machines. The classification is based on the nature of the induced emf waveform. The one with the trapezoidal induced emf waveform is known as a permanent magnet dc brushless machine and the other, with a sinusoidal induced emf waveform goes by the name of a permanent magnet synchronous machine (PMSM). The PMDC brushless generator has approximately 15 % more power density than the PMSM but has yet to be produced in larger ratings than the PMSM. Their use in wind energy schemes and their applications is of recent origin [4]-[6], and [51] .

The power conversion stage may be a dc link with line-commutated converters or a dc link with a self-commutated inverter or a cycloconverter. The line-commutated converters and cycloconverter power stages require a fixed frequency supply for operation whereas the self-commutated inverter is capable of stand-alone operation. This makes the self-commutated inverter attractive for remote applications where the wound rotor synchronous and induction machines are used for power generation with variable speed prime movers.

A constant frequency supply is required for both the line-commutated converter and the

cycloconverter power stage in the power conversion scheme. However, a self-commutated inverter is different in that it can be operated without any external fixed frequency supply. Hence, the self-commutated converter is attractive for remote applications such as on a ranch, an island, or in an aircraft system where the wound rotor synchronous and induction machines are used for power generation with the variable speed prime movers. The primary issues addressed in this chapter are:

(i) Introduction of a self commutated converter structure for the VSCF power conversion scheme.

(ii) The study of the operation and design of the power converter in the VSCF scheme to enhance waveform quality and to control the power factor.

(iii) Determination of the modulation strategy and its impact on the switching frequency, selection of the switches, filter size, and upper power limits for VSCF generation with the permanent magnet synchronous machines.

(iv) Transient response characteristics for step changes in the speed of the prime mover and the required margin in the power rating of the converter.

Experimental verification is made with a laboratory prototype to validate the modeling procedure. The advantages and disadvantages of this scheme are described with the help of the performance characteristics of the system. A systematic design of the scheme is presented with the ratings of the power switching devices and PMSM.

2.2 VSCF Generation with PMSM

The VSCF generation scheme with PMSM is shown in the Figure 2.1. The PMSM is driven by a prime mover whose speed is varying as in the case of a wind turbine. The output voltages of the PMSM are rectified through a diode bridge rectifier and smoothed through a capacitor filter. The smoothed dc power is inverted through a PWM converter to get a fixed frequency sinusoidal power. The switching converter proposed here is as shown in Figure 2.2. The three phase source may be connected to the utility grid or may be a stand alone system.

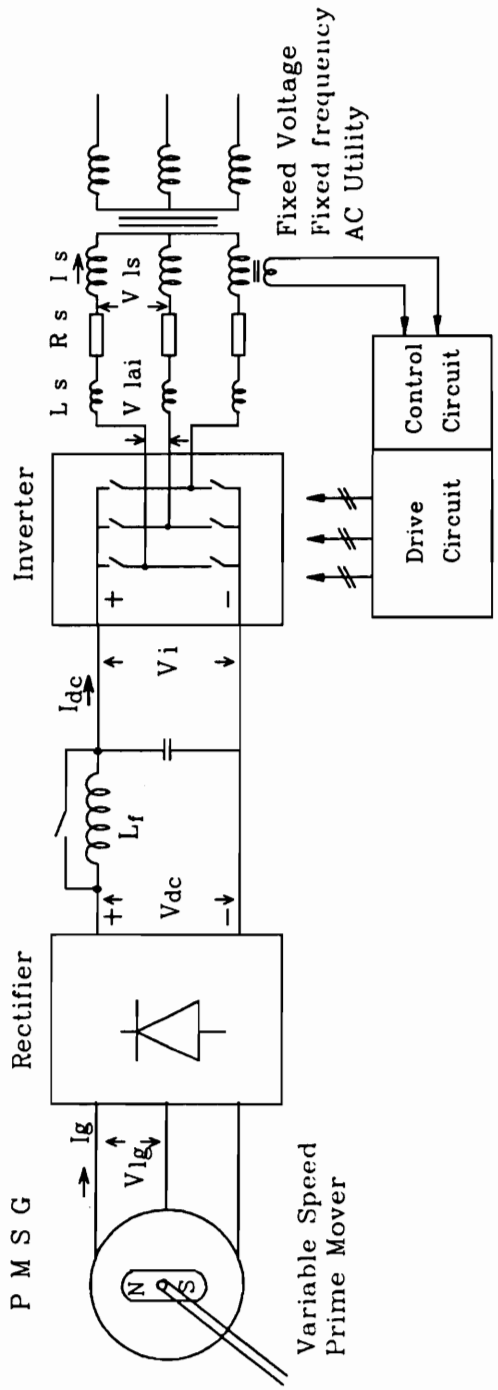

Figure 2.1: VSCF power conversion scheme using a PWM converter

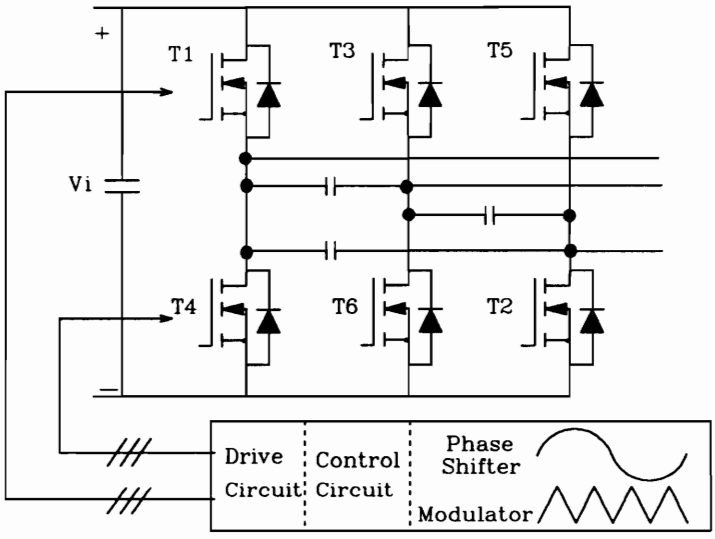

Figure 2.2: The PWM converter construction

The VSCF generation scheme with PMSM [5], and PM dc brushless [4] machines have been studied with line commutated converters. The line commutated converter requires an ac source for its operation and introduces considerable harmonics and low power factor. Due to these drawbacks, it is proposed here to consider a self commutated converter structure for the power conversion link [6]. Such power conversion schemes are reported for use in ac and dc drives. The major limitation in most of these structures has been the necessity for large filters both on the dc and ac sides. But the investigation of these converter configurations has not been applied to many applications such as VSCF generation including that of UPS systems. Their potential for use in a large number of applications requires an understanding of the following aspects:

(i) Normalized relationship between the converted power and the rating of the switches.

(ii) The filter size, the impact of the switching frequency on the selection of switches, and upper power limits of power conversion with each of the schemes.

(iii) The design and operation of the power conversion scheme.

(iv) The design and implementation of the control circuitry for the power conversion scheme.

(v) An experimental verification of the key theoretical results and the design procedure for the power converter.

These issues are addressed in the following sections.

2.3 Input Power and Terminal Voltage of the Machine

2.3.1 Input power

In VSCF with PMSM, power factor equals 1 in the generator. The phasor diagram of the PMSM is shown in Figure 2.3, where δ is the power angle. The input power is,

$$P_i = 3E_f I_g \cos\delta. \tag{2.1}$$

where E_f is induced emf, I_g is line current of the generator.

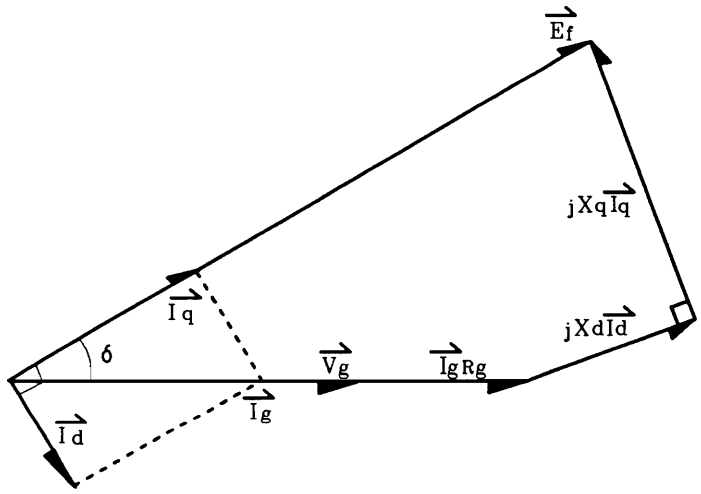

Figure 2.3: Phase diagram of the PMSM

Writing the dc link current, I_{dc}, in terms of generator line current, I_g, and induced emf, E_f, as a function of speed, ω_m, as

$$I_{dc} = K_1 I_g \tag{2.2}$$

where K is a proportionality constant.

$$E_f = K_b\, \omega_m. \tag{2.3}$$

Hence the input power from (2.1), (2.2), and (2.3) is

$$P_i = 3E_f I_g \cos\delta \tag{2.4a}$$

$$= 3\left(\frac{K_b}{K_1}\right)\omega_m I_{dc}\cos\delta. \tag{2.4b}$$

The base quantities used for normalizing the equations are,

$$P_b = \text{Base power} \tag{2.5a}$$

$$= 3V_b I_b \tag{2.5b}$$

$$V_b = \text{Base voltage} \tag{2.6a}$$

$$= \text{RMS phase voltage} \tag{2.6b}$$

$$I_b = \text{Base current.} \tag{2.7}$$

Hence the normalized input power is,

$$P_{in} = \frac{P_i}{P_b} \tag{2.8a}$$

$$= \frac{3\left(\frac{K_b}{K_1}\right)\omega_m I_{dc}\cos\delta}{3V_b I_b}. \tag{2.8b}$$

The base voltage is,

$$V_b = K_b \omega_b \tag{2.9}$$

where ω_b is the base speed in rad/sec. Substituting (2.9) in (2.8b), the input power is

$$P_{in} = \left(\frac{1}{K_1}\right)\omega_{mn} I_{dcn}\cos\delta \tag{2.10}$$

where the normalized variables are,

$$\omega_{mn} = \frac{\omega_m}{\omega_b} \tag{2.11}$$

$$I_{dcn} = \frac{I_{dc}}{I_b} \tag{2.12}$$

$$P_{in} = \frac{P_i}{P_b} \tag{2.13}$$

and

$$K_1 = \frac{\pi}{\sqrt{6}}. \tag{2.14}$$

Usually ω_{mn}, I_{dcn}, and P_{in} are known variables. From equation (2.10), the torque angle is written as

$$\delta = \cos^{-1}\left\{\frac{P_{in}}{\left(\frac{1}{K_1}\right)\omega_{mn} I_{dcn}}\right\}. \tag{2.15}$$

2.3.2 Terminal voltage of the machine

The quadrature and direct axis currents are

$$\vec{I}_q = \vec{I}_g \cos\delta \tag{2.16}$$

$$\vec{I}_d = \vec{I}_g \sin\delta. \tag{2.17}$$

Therefore the machine terminal voltage is

$$\vec{V}_g = \vec{E}_f - j\vec{I}_q X_q - j\vec{I}_d X_d - \vec{I}_g R_g. \tag{2.18}$$

2.4 Control Strategies and Operation of the Self Commutated Power Converter

Power conversion employing SCR power devices has a fundamental disadvantage in terms of switching frequency and hence in the magnitude and order of harmonics. To overcome or to mitigate this demerit, a three phase sinusoidal PWM inverter version of the VSCF scheme using power MOSFET transistors is proposed for this study. Unlike in the case of a current source inverter, the phase voltages of a voltage source inverter should be kept at finite voltage levels, which enforces a complementary switching of the upper leg with respect to the lower leg or vice versa. The terminals a, b, and c shown in Figure 2.4 are connected either to the positive or negative rail of the dc link depending on the required switching levels.

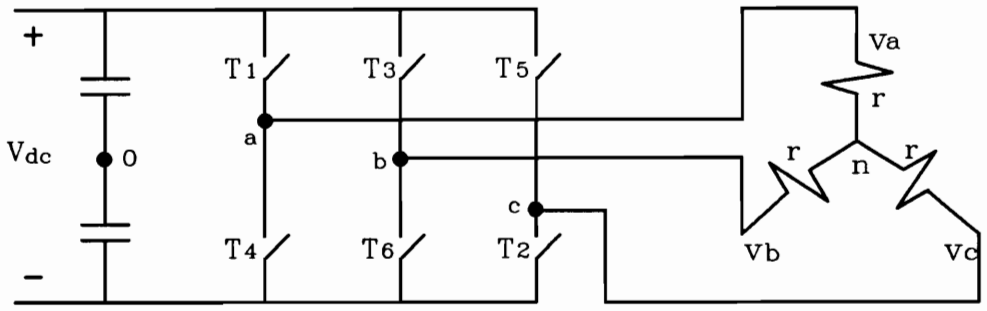

Figure 2.4: Inverter and load connections

For resistive loads, the phase voltages are determined by voltage division using the eight possible switching configurations as shown in Figure 2.5. The phase voltages and line to line voltages are easily found from the switching configurations without using any equations. The three-phase system is also verified by the balanced three-phase voltage equations;

$$V_{ab} + V_{bc} + V_{ca} = 0 \tag{2.19}$$

and

$$V_{an} + V_{bn} + V_{cn} = 0. \tag{2.20}$$

The basic six-step inverter is a particular case of the PWM inverter and is shown in Figure 2.6 with the corresponding switch configurations. Only six cases occur out of the eight configurations. The phase voltages can be obtained by the three-phase balanced system equations,

$$V_{an} = \frac{2}{3}V_{ao} - \frac{1}{3}(V_{bo} + V_{co}) \tag{2.21}$$

$$V_{bn} = \frac{2}{3}V_{bo} - \frac{1}{3}(V_{co} + V_{ao}) \tag{2.22}$$

$$V_{cn} = \frac{2}{3}V_{co} - \frac{1}{3}(V_{ao} + V_{bo}). \tag{2.23}$$

But the phase and line voltage waveforms are found using the table of the switch configurations. This waveform generation method becomes more useful as the carrier frequency increases.

The normalized frequency ratio, $R = \frac{f_c}{f_s}$ takes an important role in the output voltage harmonic spectrum, where f_c is the carrier frequency and f_s is the reference sinusoidal frequency. A single phase inverter needs an odd number of R to avoid even harmonics. However, for the three phase inverter, one more constraint is added due to the phase displacement of $\frac{2\pi}{3}$ from phase to phase. It needs the normalized frequency, R, to be in multiples of three. Therefore the required normalized frequency of the three phase inverter is,

$$R = 6m + 3 \text{ where m=1, 2, 3,} \cdots \tag{2.24}$$

Figure 2.7 shows PWM waveforms for $f_c/f_o = 9$. Quarter waveform symmetry in phase voltage ensures the requirement of the frequency ratio of the carrier and reference voltage.

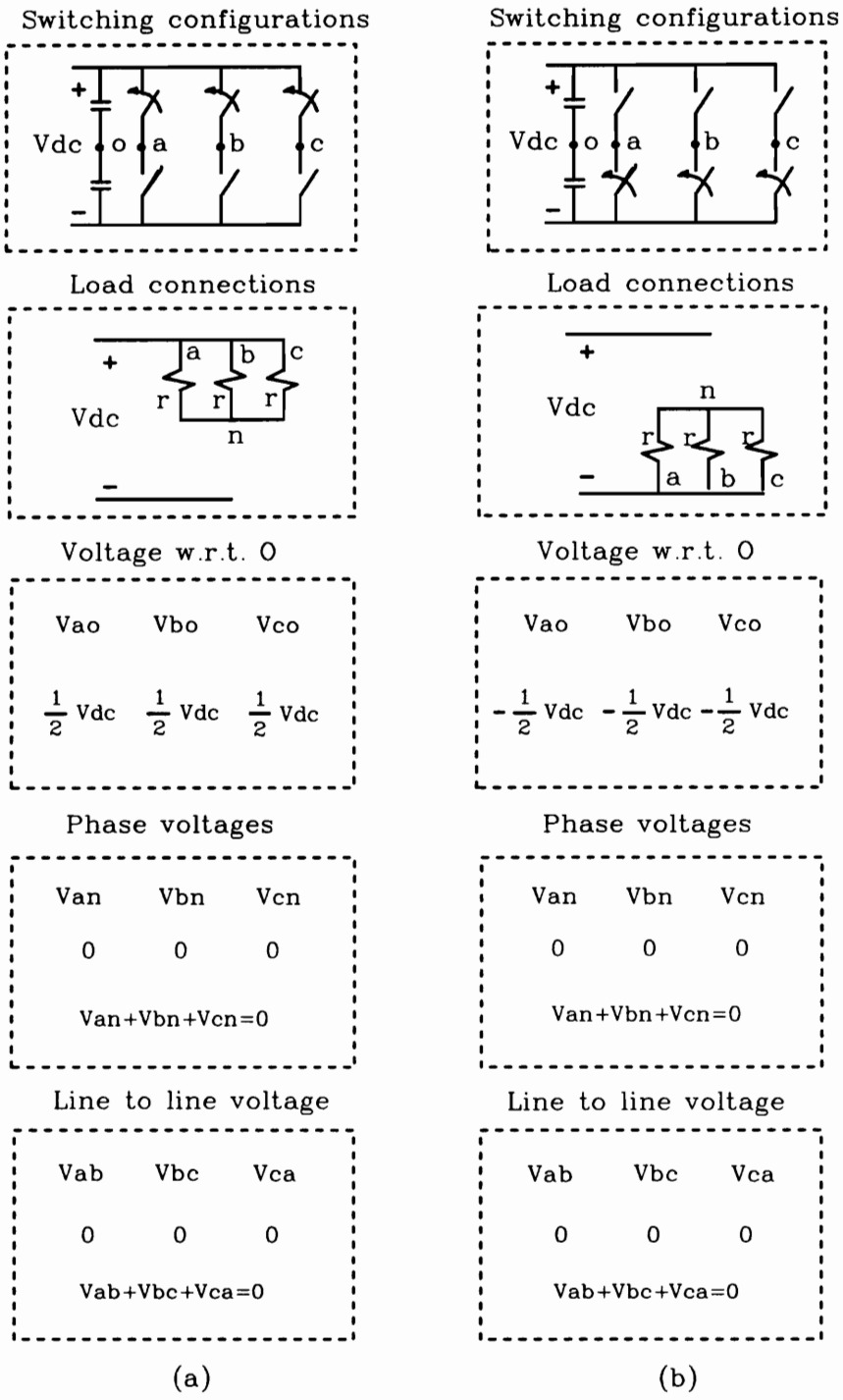

Figure 2.5: Switching configurations

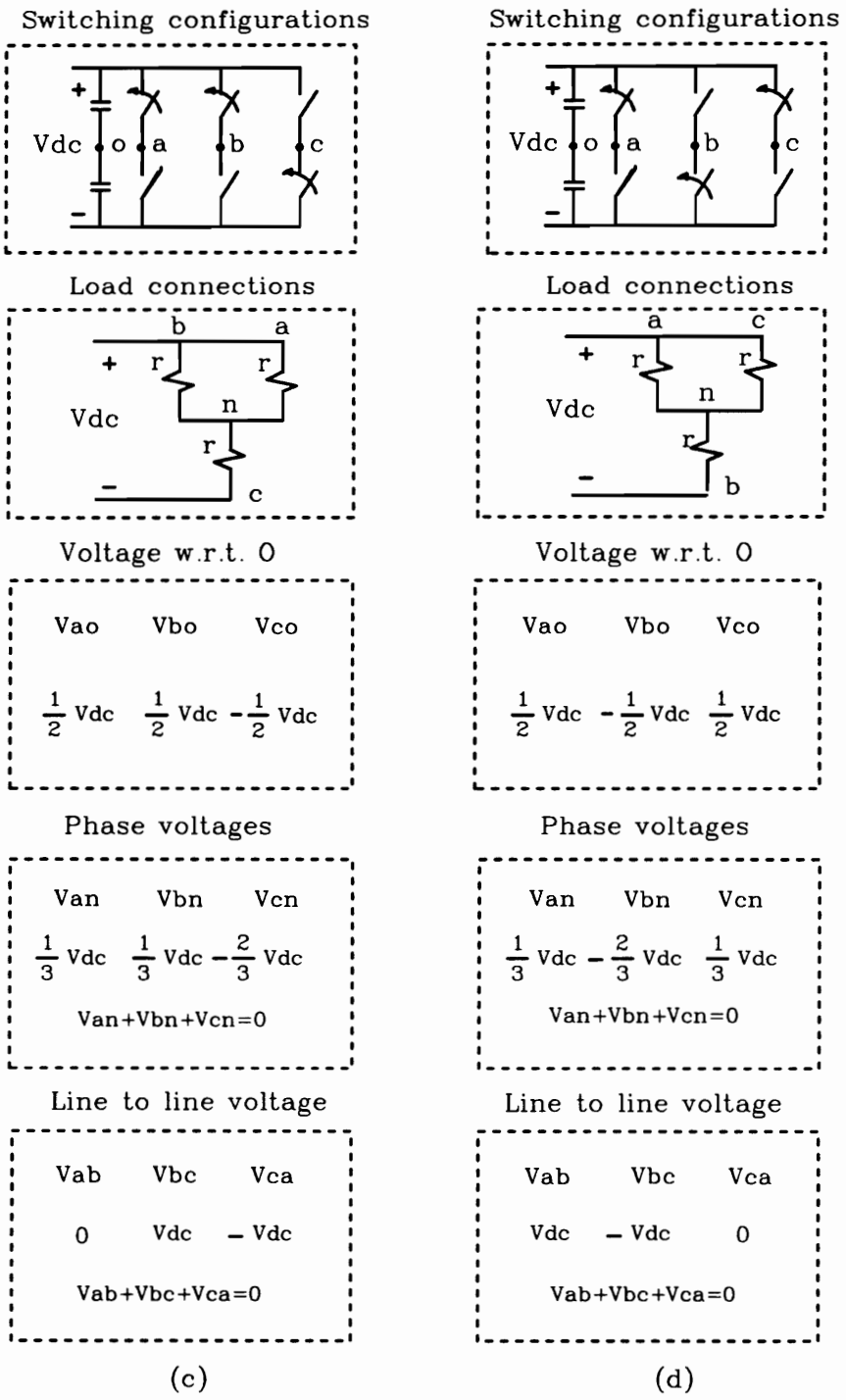

Figure 2.5: Continued

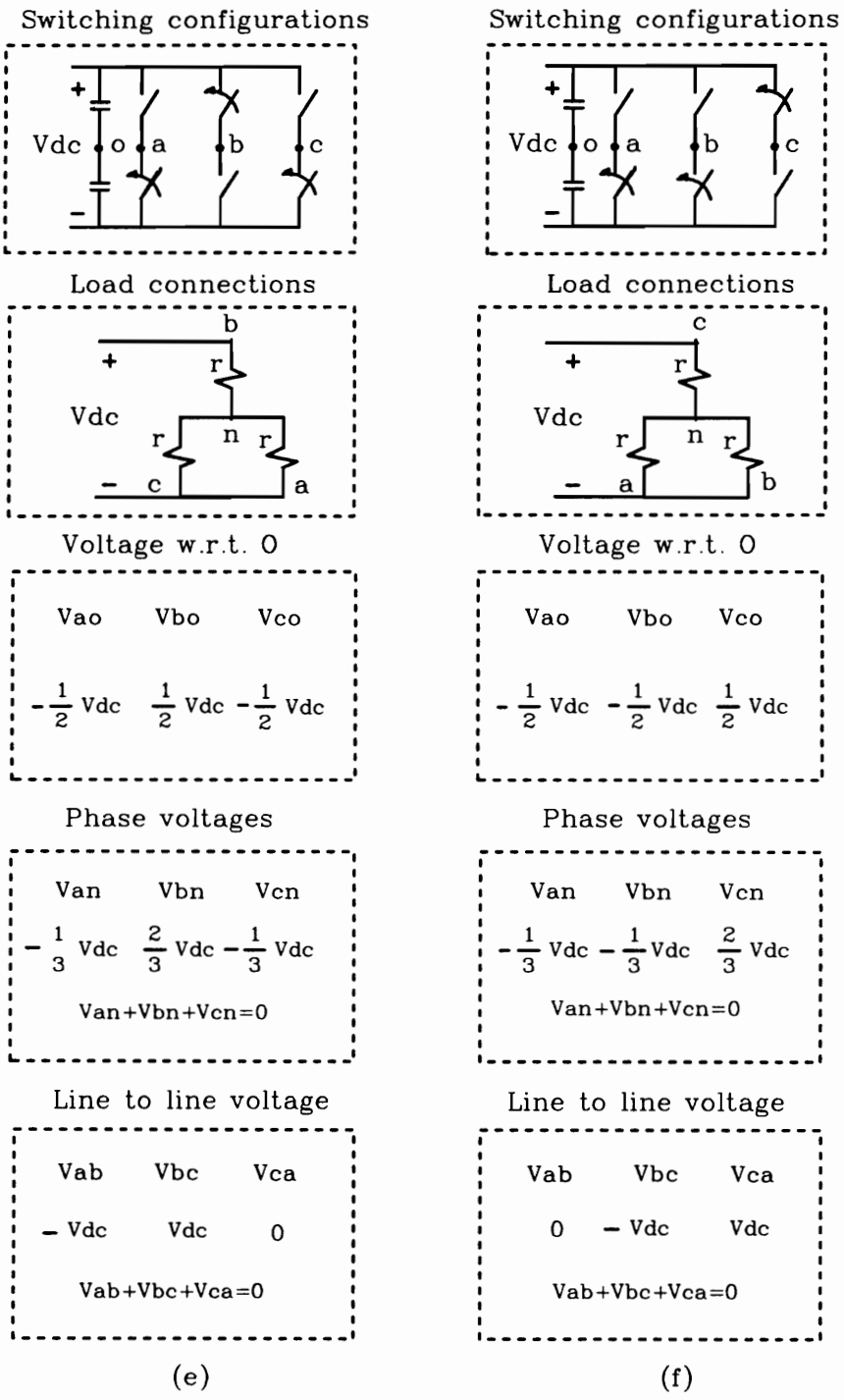

Figure 2.5: Continued

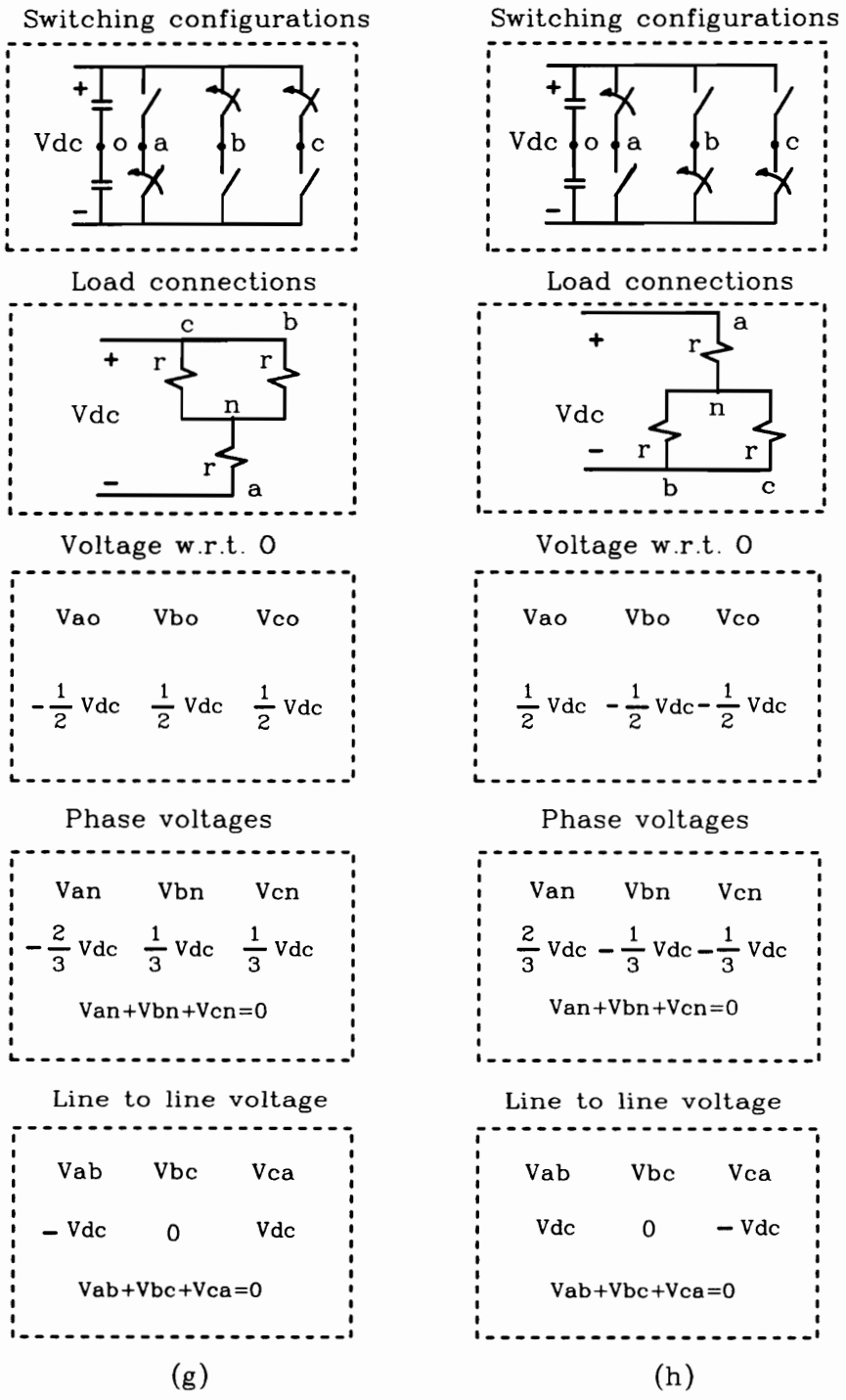

Figure 2.5: Continued

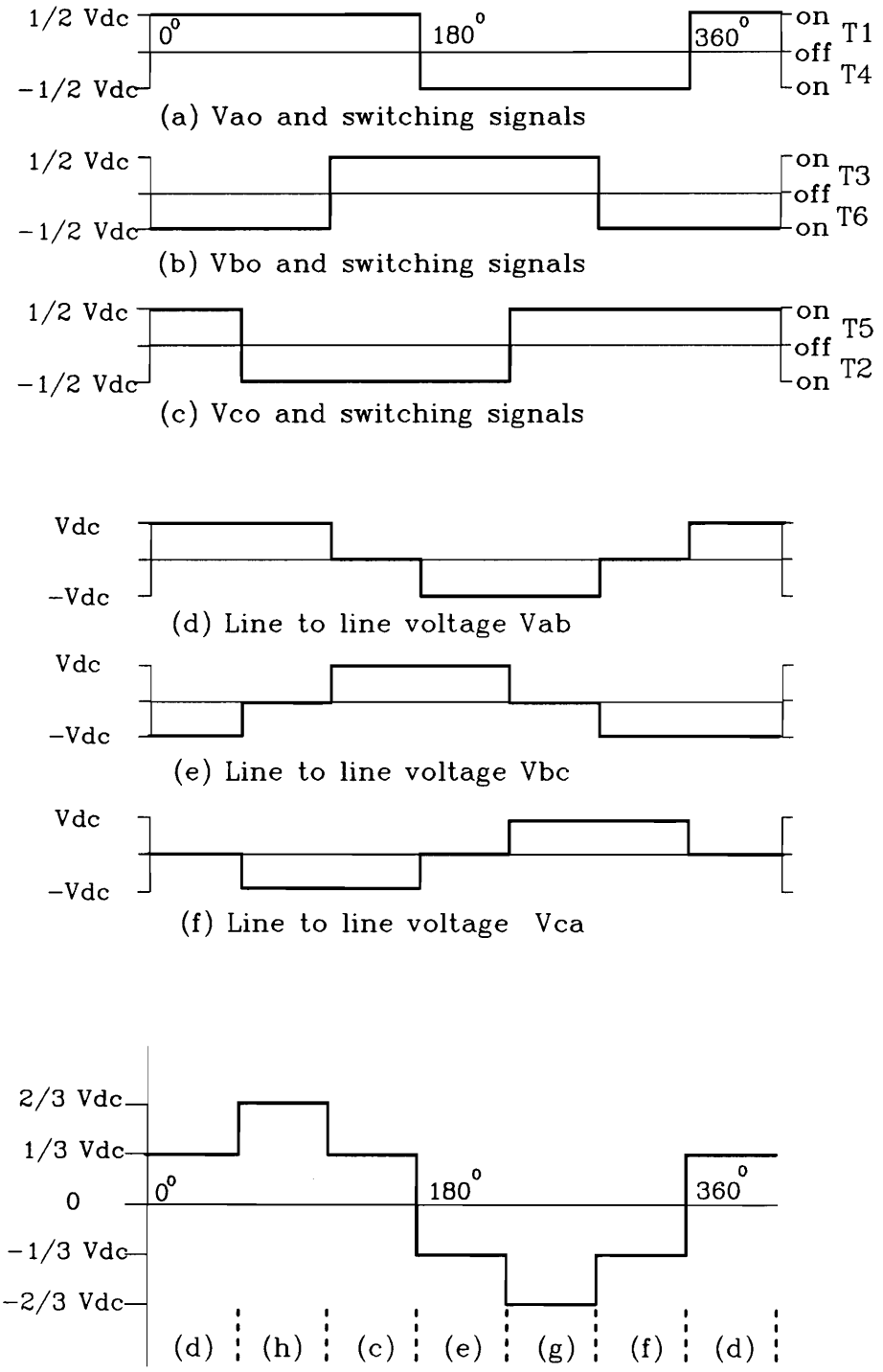

Figure 2.6: Six pulse inverter

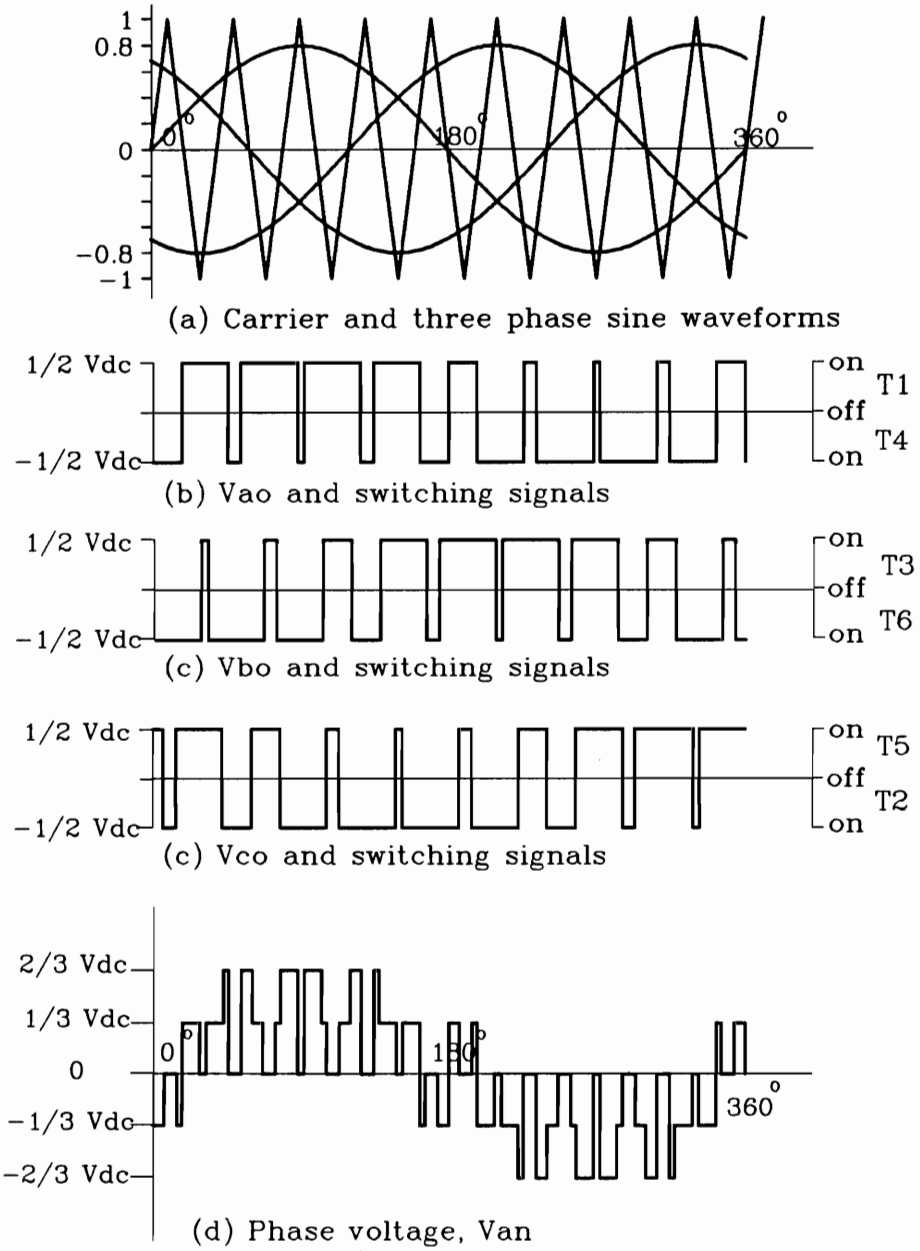

Figure 2.7: PWM waveforms for fc/fs=9

The experimental signals of the PWM inverter are shown in Figure 2.8. The frequency of the triangular carrier is 999 Hz for this study. The switching of the upper switches (T1, T3, T5) and lower switches (T4,T6,T2) is complementary. Due to prime-mover speed variations, the rectified generator voltages vary. As the ac utility grid voltage is of constant frequency and fixed voltage, control strategies are required to tie a varying dc bus with a fixed ac bus. Three control strategies are proposed and investigated in this section.

2.4.1 Control strategy I (Modulation control)

The purpose of this control strategy is to transfer constant energy at constant frequency from a variable speed energy source, regardless of the prime mover speed. As the utility voltage is a constant, the line current determines the constant power to be converted at a certain lead or lag phase difference, ϕ_m, between the line current and the utility phase voltage. Once the line current is predetermined, the voltage drop across the line reactor follows. Hence the constant phase voltage of the inverter is obtained by modulating the PWM signal for a varying dc bus voltage. Figure 2.9 shows the phasor diagram for this control strategy for a fixed power factor, $\cos\phi_m$. The relationship between the variables is described by,

$$\vec{V}_{ai} = -\vec{V}_{as} + \vec{I}_s(R_s + j\omega_s L_s) \tag{2.25}$$

where ω_s is the utility frequency, $\vec{V}_{ai}$ is the phase voltage of the converter, $\vec{V}_{as}$ is the phase voltage of the utility, $\vec{I}_s$ is line current, and R_s and X_s are the resistance and reactance of the line reactor, respectively.

Normalizing the inverter phase voltage

$$\vec{V}_{ain} = \frac{\vec{V}_{ai}}{V_b} \tag{2.26a}$$

$$= \frac{\vec{V}_{as}}{V_b} + \frac{\vec{I}_s R_s}{I_b R_b} + j\frac{\vec{I}_s X_s}{I_b Z_b} \tag{2.26b}$$

$$= \vec{V}_{asn} + \vec{I}_{sn} R_{sn} + j\vec{I}_{sn} X_{sn} \tag{2.26c}$$

where I_b, V_b, and Z_b are the base current, base voltage, and base impedance, respectively. The normalized variables are defined as

$$V_{asn} = \frac{V_{as}}{V_b} \quad \text{p.u.} \tag{2.27}$$

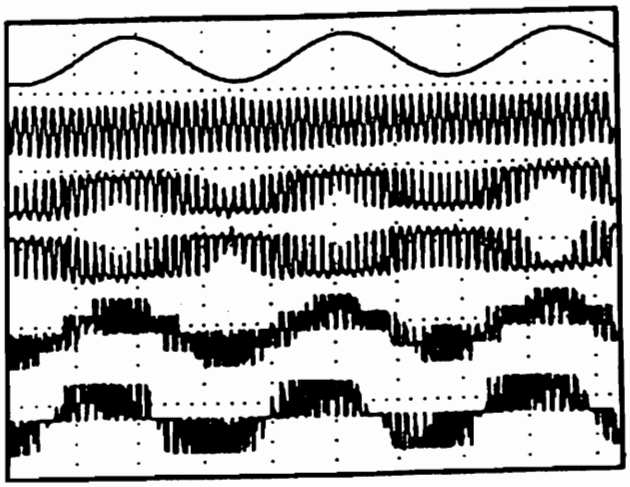

Figure 2.8: Experimental switching operation of the PWM inverter for resistance load (Sinusoidal reference, Triangular carrier, Switching signals for T_1, T_4. Phase voltage and line voltage of the converter with 999 Hz, $m = 0.78, V_{dc} = 38$V and 5 ms/div)

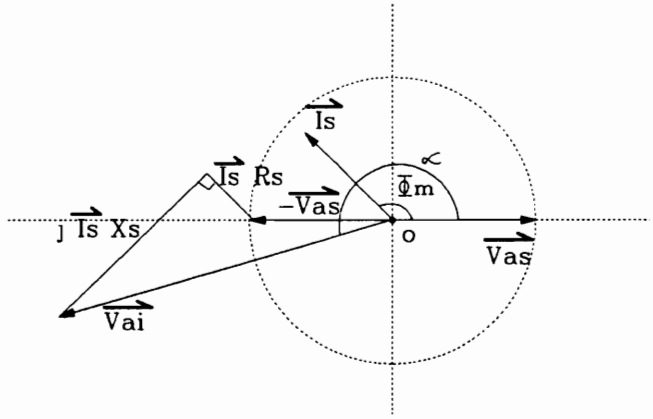

Figure 2.9: Phasor diagram for control strategy I

$$I_{sn} = \frac{I_s}{I_b} \quad \text{p.u.} \tag{2.28}$$

$$R_{sn} = \frac{R_s}{Z_b} \quad \text{p.u.} \tag{2.29}$$

$$X_{sn} = \frac{X_s}{Z_b} \quad \text{p.u.} \tag{2.30}$$

The output power of the converter is,

$$P_{oc} = 3V_{as}I_s \cos\phi_m + 3I_s^2 R_s. \tag{2.31}$$

And power fed to the constant frequency source is given by

$$P_o = 3V_{as}I_s \cos\phi_m. \tag{2.32}$$

Normalizing the output power,

$$P_{on} = V_{asn}I_{sn} \cos\phi_m. \tag{2.33}$$

This strategy transfers constant power to the utility. The losses increase as the prime mover speed increases, resulting in lower efficiency at higher operating speed. That is a disadvantage of this control strategy.

2.4.2 Control strategy II (Maximum current clamping control)

This control scheme transfers power to the utility proportional to the prime mover speed. No voltage modulation is required, but current clamping is needed for the converter to be protected against over-current and transients. The phase relation between the utility and the inverter phase voltage is as shown in Figure 2.10. For a constant power factor, $\cos\phi_c$, the higher inverter phase voltage resulting from the higher speed of the prime mover has the loci oa. This results in a current increase. Hence, the output power of the inverter is,

$$P_{oc} = 3I_sV_s \cos\phi_c + 3I_s^2 R_s. \tag{2.34}$$

For negligible resistance of the line reactor, the normalized output power of the inverter feeding into the utility is

$$P_{on} = V_{asn}I_{sn} \cos\phi_c. \tag{2.35}$$

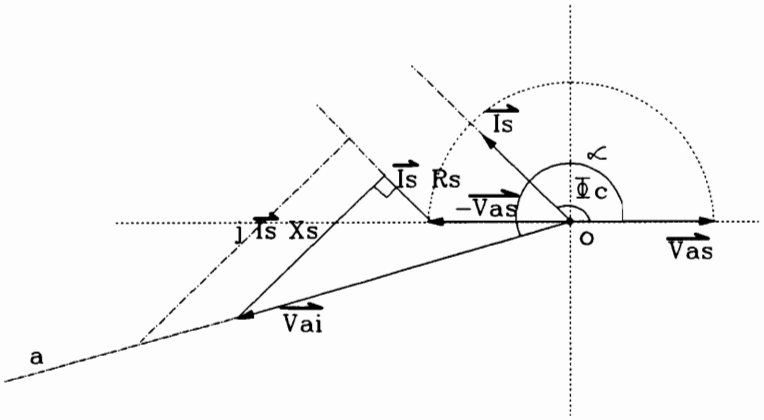

Figure 2.10: Phasor diagram for control strategy II

If the phase voltage of the utility is set as the base voltage, then

$$\frac{P_{on}}{I_{sn}} = \cos\phi_c. \tag{2.36}$$

Since the ratio of normalized power to normalized current is constant for a fixed ϕ_c, the normalized power is directly proportional to the normalized line current. This strategy lets the VSCF scheme produce varying power proportional to the speed of the prime mover, which makes the scheme very efficient. In the experimental study, due to the large resistance of the line reactance, the efficiency is lower at the higher operating speed.

2.4.3 Control strategy III (Phase angle control)

This control strategy is designed to change the phase of the line current with respect to the phase voltage of the utility. As shown in Figure 2.11, the loci of the inverter phase voltage moves on the circle $o'abc$ which is determined by a constant line current and utility phase voltage. If the minimum operating speed point is c, then the operating speed range of the prime mover is from point c to a. The maximum output power $P_{on} = V_{asn}I_{sn}$ is at the point b where the power factor is unity. Between points a and c the scheme draws reactive power from the utility, but between the maximum power point b and d, the scheme supplies reactive power to the utility. To enlarge the operating speed range, it is noted from Figure 2.11 that a large line current is needed. The normalized active power, P_{on}, and reactive power, Q_{on}, are given as follows,

$$P_{on} = I_{sn}V_{asn}\cos\phi_p \tag{2.37}$$

$$Q_{on} = I_{sn}V_{asn}\sin\phi_p \tag{2.38}$$

The phase angle can be varied by adjusting the phase shifter.

2.5 The Analysis of the VSCF Characteristics

The performance equations for the VSCF scheme are given here. The PMSM phase voltage is given in the equation 2.12 as the following:

$$\vec{V}_g = \vec{E}_f - j\vec{I}_q X_q - j\vec{I}_d X_d - \vec{I}_g R_g \tag{2.39a}$$

$$= K_b\omega_m \angle\delta - j\vec{I}_q\omega_m L_q - j\vec{I}_d\omega_m L_d - \vec{I}_g R_g \tag{2.39b}$$

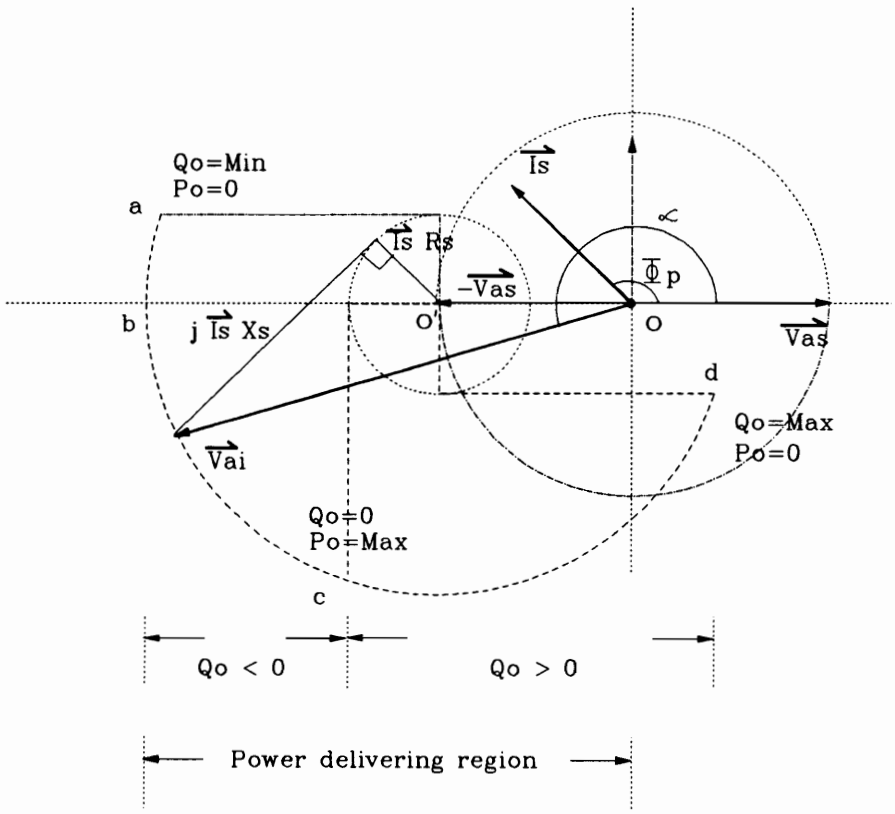

Figure 2.11: Phasor diagram for control strategy III

which in normalized variables is

$$\vec{V}_{gn} = \frac{\vec{V}_t}{V_b} \tag{2.40a}$$

$$= \frac{K_b\omega_m \angle\delta}{V_b} - j\frac{\vec{I}_q\omega_m L_q}{V_b} - j\frac{\vec{I}_d\omega_m L_d}{V_b} - \frac{\vec{I}_g R_g}{V_b} \tag{2.40b}$$

$$= \omega_{mn}\angle\delta - j\vec{I}_{qn}X_{qn} - \vec{I}_{dn}X_{dn} - \vec{I}_{gn}R_{gn}. \tag{2.40c}$$

The voltage across the capacitor in normalized form is

$$V_{dcn} = 1.35\sqrt{3}V_{gn}. \tag{2.41}$$

Introducing the PWM modulation ratio [33], the fundamental line to line input voltage of the inverter is defined to be

$$V_{lai} = \frac{\sqrt{3}}{2}mV_{dc}\sin\left(\omega_s t + \frac{\pi}{6} + \alpha\right) \tag{2.42}$$

where α is the phase difference between the fundamental component of the inverted voltage and the ac source voltage, ω_s is the utility frequency or the sinusoidal reference voltage frequency and m is the modulation ratio, which is defined as the following:

$$m = \frac{A_s}{A_t} \tag{2.43}$$

where A_s, and A_t are the peak amplitudes of the sinusoidal reference and triangular carrier, respectively. Using equation (2.42) and voltage drop across the line reactor, the normalized phase voltage(V_{ain}) of the converter can be written in terms of the normalized source voltage(V_{asn}), the normalized source current(I_{sn}), and the normalized impedance of the line reactor(R_{sn} and X_{sn}). Hence,

$$\sqrt{2}V_{ain}\sin(\omega_s t + \alpha) = \frac{1}{2}mV_{dcn}\sin(\omega_s t + \alpha) \tag{2.44a}$$

$$= \sqrt{2}V_{asn}\sin(\omega_s t) + \sqrt{2}\vec{I}_{sn}\sin(\omega_s t + \phi)(R_{sn} + jX_{sn}) \tag{2.44b}$$

from which

$$V_{asn}\sin(\omega_s t) = \frac{mV_{dcn}\sin(\omega_s t + \alpha)}{2\sqrt{2}} - \vec{I}_{sn}\sin(\omega_s t + \phi)(R_{sn} + jX_{sn}) \tag{2.45a}$$

$$= 0.827mV_{gn}\sin(\omega_s t + \alpha) - \vec{I}_{sn}Z_{sn}\sin(\omega_s t + \phi + \psi) \tag{2.45b}$$

where

$$Z_{sn} = \sqrt{R_{sn}^2 + X_{sn}^2} \tag{2.46}$$

$$\tan\psi = \frac{X_{sn}}{R_{sn}}. \tag{2.47}$$

2.5.1 Analysis for control strategy I

The idea of this strategy is to obtain constant power from variable speed power by modulating the PWM signal. From the phasor diagram, shown in Figure 2.9,

$$V_{ain}\cos\alpha = 0.827mV_{gn}\cos\alpha \tag{2.48a}$$

$$= -V_{asn} + I_{sn}R_{sn}\cos\phi_m - I_{sn}X_{sn}\sin\phi_m \tag{2.48b}$$

$$V_{ain}\sin\alpha = 0.827mV_{gn}\sin\alpha \tag{2.49a}$$

$$= I_{sn}R_{sn}\sin\phi_m + I_{sn}X_{sn}\cos\phi_m \tag{2.49b}$$

where V_{asn}, R_{sn}, X_{sn}, and V_{gn} are known variables for a certain speed of the prime mover. Once the output power is fixed, I_{sn} and ϕ_m are also known variables. Therefore the phase angle between V_{asn} and V_{ain} is

$$\alpha = tan^{-1}\left\{\frac{I_{sn}R_{sn}\sin\phi_m + I_{sn}X_{sn}\cos\phi_m}{-V_{asn} + I_{sn}R_{sn}\cos\phi_m - I_{sn}X_{sn}\sin\phi_m}\right\}. \tag{2.50}$$

Hence,

$$mV_{gn} = \frac{I_{sn}R_{sn}\sin\phi_m + I_{sn}X_{sn}\cos\phi_m}{0.827\sin\alpha} \tag{2.51a}$$

$$= \text{constant.} \tag{2.51b}$$

Hence, the PMSM voltage variation, which depends on the prime mover speed, is matched at the converter end by changing the modulation ratio. The constant power is determined when the modulation ratio is fixed, which gives the power balance across the inverter:

$$I_{dcn}V_{dcn} = 3I_{sn}V_{asn}\cos\phi_m + 3I_{sn}^2R_{sn}. \tag{2.52}$$

Hence, the normalized dc link current is

$$I_{dcn} = \frac{3I_{sn}V_{asn}\cos\phi_m + 3I_{sn}^2R_{sn}}{V_{dcn}} \tag{2.53a}$$

$$= \frac{3I_{sn}V_{asn}\cos\phi_m + 3I_{sn}^2R_{sn}}{1.35\sqrt{3}V_{gn}}. \tag{2.53b}$$

The output power and the overall efficiency are,

$$P_{on} = I_{asn}V_{asn}\cos\phi_m \tag{2.54a}$$

$$= \text{constant} \tag{2.54b}$$

$$\eta = \frac{\text{output power}}{\text{PMSM air gap power}} \tag{2.54c}$$

$$= \frac{I_{sn} V_{asn} \cos \phi_m}{V_{gn} (0.779 I_{dcn}) + (0.779 I_{dcn})^2 R_{gn}}. \tag{2.54d}$$

2.5.2 Analysis for control strategy II

This control strategy lets the VSCF scheme transform the variable speed energy in the most efficient way. The power across the inverter is balanced over the entire operating speed range. Therefore the output power is

$$P_{on} = V_{dcn} I_{dcn} - 3 I_{sn}^2 R_{sn} \tag{2.55a}$$

$$= 3 V_{asn} I_{sn} \cos \phi_c \tag{2.55b}$$

and the efficiency is given by

$$\eta = \frac{V_{asn} I_{sn} \cos \phi_c}{V_{gn} (0.779 I_{dcn}) + (0.779 I_{dcn}) R_{gn}} \tag{2.56}$$

where I_{sn}, V_{gn}, and I_{dcn} vary depending on the speed of the prime mover. The maximum power limit of the VSCF scheme using this control strategy is determined by the ratings of the converter and PMSM.

2.5.3 Analysis for control strategy III

For control strategy III, the operating speed range of the prime mover is mainly dependent on the phase difference between the line current and the utility phase voltage. The scheme produces the inverter phase voltage proportional to the prime mover speed by which the phase difference, ϕ_p, is determined. The VSCF scheme generates lagging or leading reactive power depending on the phase shift. From the power balance equation (2.52) and phasor relationship

$$I_{dcn} = \frac{3 V_{asn} I_{sn} \cos \phi_p + 3 I_{sn} R_{sn}}{V_{dcn}} \tag{2.57}$$

$$0.827 m V_{gn} \cos \alpha = V_{asn} + I_{sn} R_{sn} \cos \phi_p - I_{sn} X_{sn} \sin \phi_p \tag{2.58}$$

$$0.827 m V_{gn} \sin \alpha = I_{sn} R_{sn} \sin \phi_p + I_{sn} X \cos \phi_p. \tag{2.59}$$

From the above three nonlinear equations, I_{dcn}, ϕ_p, and α can be solved for given I_{sn}, V_{asn}, V_{dcn}, and m. Then the output power and the overall efficiency are,

$$P_{on} = 3V_{asn}I_{sn}\cos\phi_p \tag{2.60a}$$

$$\eta = \frac{V_{asn}I_{sn}\cos\phi_p}{V_{gn}(0.779I_{dcn}) + (0.779I_{dcn})^2 R_{an}} \tag{2.60b}$$

where ϕ_p, V_{gn}, and I_{dcn} are varying depending on the speed of the prime mover, and α is the phase angle between phase voltages of the utility and the inverter.

The operating speed range is determined by the phase voltage levels of the utility and the lower operating speed. But increasing the range of speed of the prime mover causes problems due to an increase in phase current and hence increased line losses and that resulting high rating of the converter at high speed. Therefore the operating speed range and the phase voltage of the utility are chosen based on a compromise. Note that this feature also affects the transformer ratings.

2.6 Impact of Switches and Switching Frequency on Filter Size

2.6.1 Switches

The impact of switches and switching frequency on the ac side filter are examined in this section. The switching frequency of the inverter is a function of the available power switches and their ratings. For 1/4 MW and above, GTOs are ideal switches with a switching frequency up to 500 Hz. The Darlington transistors with a switching frequency of 2 kHz can handle up to the 250 kW power levels. For lower power levels, IGBT and MOSFET switches are considered with switching frequencies above 2 kHz.

2.6.2 Filter size

The relationship between the inductive filter, the maximum ripple current, and the switching frequency is derived based on the following assumptions:

(i) The current has a linear rise and decay during a switching cycle.

(ii) The dc link voltage is constant during switching.

(iii) The current is maintained within $\pm\Delta i$ band.

The switching cycle time is

$$T = \frac{1}{f_c} \tag{2.61}$$

where f_c is the switching frequency in Hz. The rate of change of current is

$$\frac{2\Delta i}{\frac{T_c}{2}} = 4 f_c \Delta i \tag{2.62}$$

where Δi is the variation of current from its mean value and it may be either positive or negative.

This is also equal to the available voltage to inductance ratio given as

$$4 f_c \Delta i = \frac{(0.5 V_{dc} - V_{as})}{L_f} \tag{2.63}$$

where L_f is the filter inductance per phase with a maximum occurring at $V_{as} = 0$. Hence the minimum filter inductance is given by

$$L_f = \frac{V_{dc}}{8 f_c \Delta i} \tag{2.64}$$

As for the size of the capacitive filter in the dc link, it is designed based on the minimum operating speed of the synchronous generator, the number of poles, and the ripple voltage permitted in the dc link.

2.7 Experimental Results

2.7.1 Experimental results

A laboratory prototype VSCF power conversion scheme with the PMSM has been designed and realized to verify the key theoretical predictions. The PMSM details are given in section A.1.1 of Appendix-A. The inverter was made with MOSFET switches and had a peak power capability of 3kW. The nominal switching frequency is 1 kHz but can be varied up to 20 kHz. Apart from the power isolation transformer, filters on the ac side have been introduced for this study. The leakage inductance of the isolation transformer may be used as a filter since the external filters may not be desirable for large applications.

(i) **Control strategy I (Modulation control):** Figure 2.12 shows the experimental results of the system performance using control strategy I. The line current on the utility side is maintained constant even though the prime mover speed is changed from 743 rpm to 960 rpm. The transients are not shown in this figure. To maintain the line current constant at 1.5 A, the modulation ratio has been changed from unity to 0.778. Note that the dc link voltage has changed from 55.4 V to 74.4 V. The power factor is leading.

(ii) **Control strategy II (Maximum current clamping control):** In this control strategy, the modulation ratio is maintained constant. Hence an increase in prime mover speed results in a proportional change in the dc link voltage. This results in an increase in the utility side current resulting in a larger power output. Experimental results reinforcing this reasoning are shown in Figure 2.13. The left half of the figure corresponds to a prime mover speed of 657 rpm and the right half to 875 rpm. The dc link voltage increases from 50 V to 64.1 V resulting in a line current on the utility side from 1.05 A to 2.01 A.

(iii) **Control strategy III (Phase angle control):** The phase angle between the line current and utility voltage is changed in this control strategy. This results in the utility line current being maintained constant but output power is correspondingly varied. Figure 2.14 shows the experimental results for the prime mover speeds of 1090 and 817 rpm to the left and right, respectively. The line current is maintained at 3A whereas the phase angle changes from 25° to 68.8°, leading in both cases. This control strategy facilitates the use of the inverter for generation of reactive power and hence the scheme as a source of static VAR compensation.

(iv) **Effects of the dc link filter on the system performance:** Figure 2.15 shows the effects of dc link filter on the system performance. The wave shape of the line to line voltage of the PMSM drastically changes from trapezoidal to sinusoidal when an inductor is introduced in the dc link. The line current of the PMSM has changed to 120°s of rectangular shape. As for the line current on the utility side, there is no change either in magnitude or in phase. The introduction of the dc link inductor will

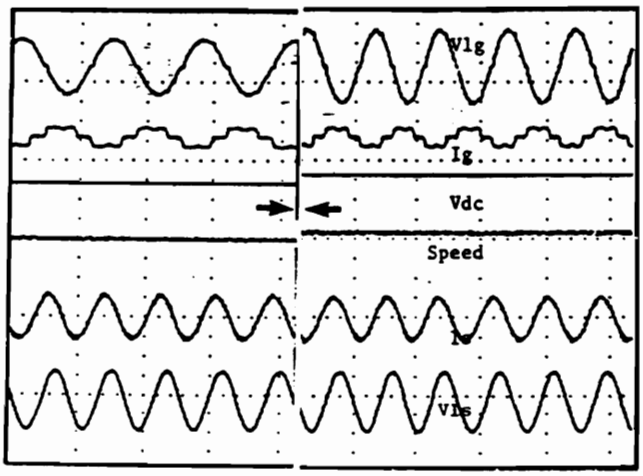

Figure 2.12: Experimental results with control strategy I at two different speeds of the prime mover. (Left half for 743 rpm and right half for 960 rpm with modulation of 1.0 and 0.776, respectively)

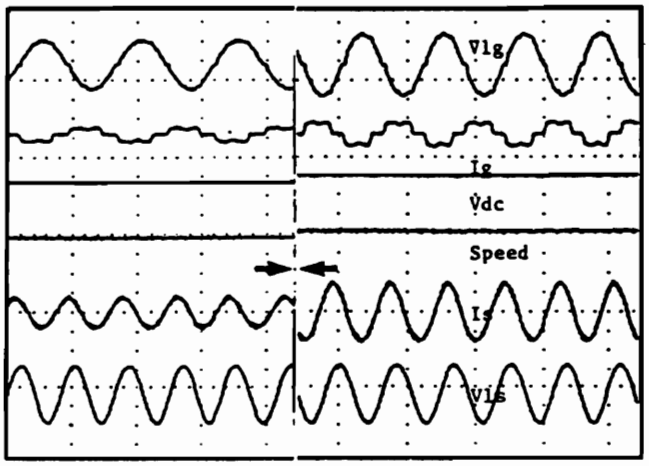

Figure 2.13: Experimental results with control strategy II at two different prime mover speeds of 657 and 875 rpm. (The lower speed characteristics are shown to the left and the higher speed characteristics to the right.)

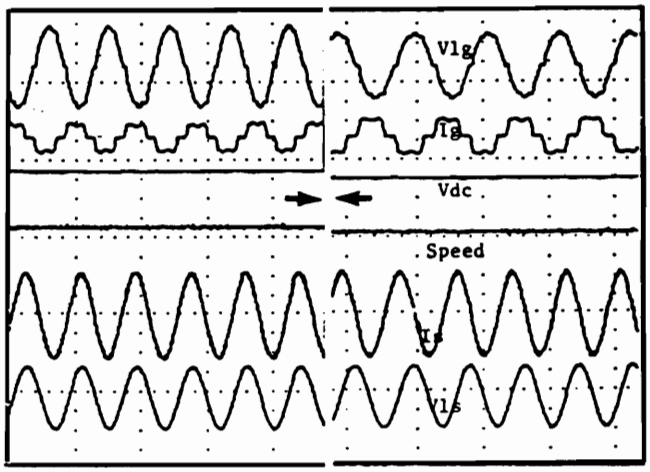

Figure 2.14: Experimental results with control strategy III at the prime mover speeds of 1090 and 917 rpm, shown from left to right.

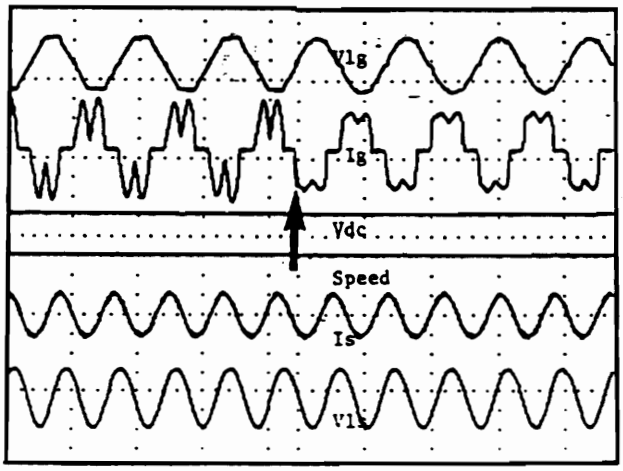

Figure 2.15: Experimental performance due to the impact of dc link filter on system characteristics. (Left half for no inductive filter and right half with inductive filter, both performances at the prime mover speed of 750 rpm.)

decrease the harmonic losses in the PMSM but will have no impact on the utility side variables.

(v) **Dynamics of the VSCF scheme with the PMSM:** The dynamic performance of the proposed VSCF power converter scheme when the PMSM is started from standstill is shown in Figure 2.16. It is run up to 956 rpm which corresponds to a dc link voltage of 74.5 V. The line current is maintained at a maximum of 2.4A by modulation ratio control. Note the change in the phase angle in the utility as it goes from a lagging angle to zero degrees. The delay in the rise of the dc link voltage is due to the dc link filter and PMSM electrical time constants. The proposed system handles the transients very well as seen from this test result.

2.7.2 Experimental steady state performance characteristics

The experimental steady state performance characteristics for the three control strategies as a function of speed are shown in Figures 2.17 - 2.19. The impact of control strategies on the net output and efficiency is considered in this section. Control strategy-I, while maintaining constant output power, is unable to utilize the increasing input power as the prime mover speed increases. This results in low efficiency and never exceeds 54% for the prototype. With increasing speed, the efficiency drops as much as 12.5%. This can be explained as follows. The modulation ratio is decreased with increasing dc link voltage due to the higher speeds. This increases more turn-off times for the inverter switches and more conduction times for the integral body diodes which are freewheeling the energy. The diodes have larger losses for the chosen MOSFETs, and are approximately two to three times the device losses. Added to that factor is the high frequency core losses of the PMSM itself. These enhanced losses decrease the overall efficiency as speed increases. In control strategy-II, the modulation ratio is maintained constant and hence most of the dc link power is transferred to the ac side. This results in higher output with increasing speed and hence higher efficiency. From Figure 2.18, it is seen that the efficiency goes up from 66.4% to 71.7%.

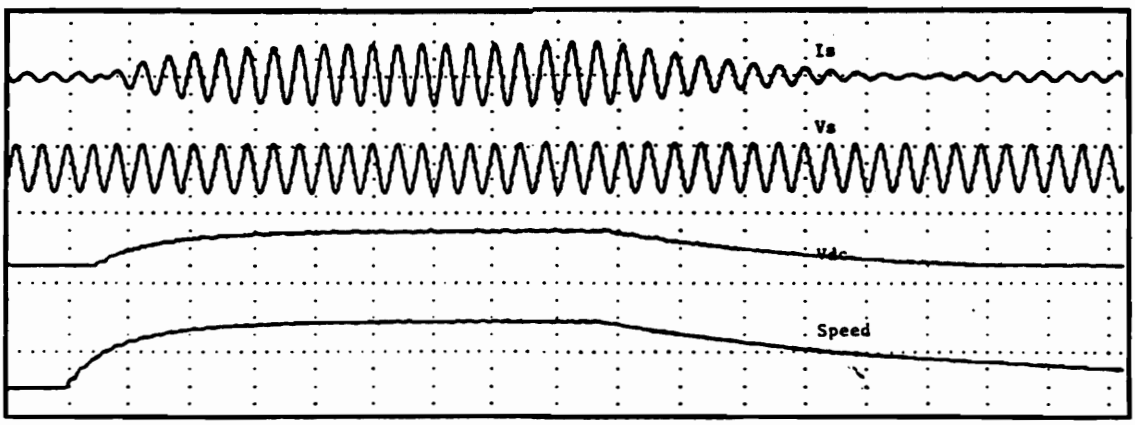

Figure 2.16: The starting and stop performances of the VSCF with the PMSM from stand-still to running speed of 956 rpm and then stop operation.

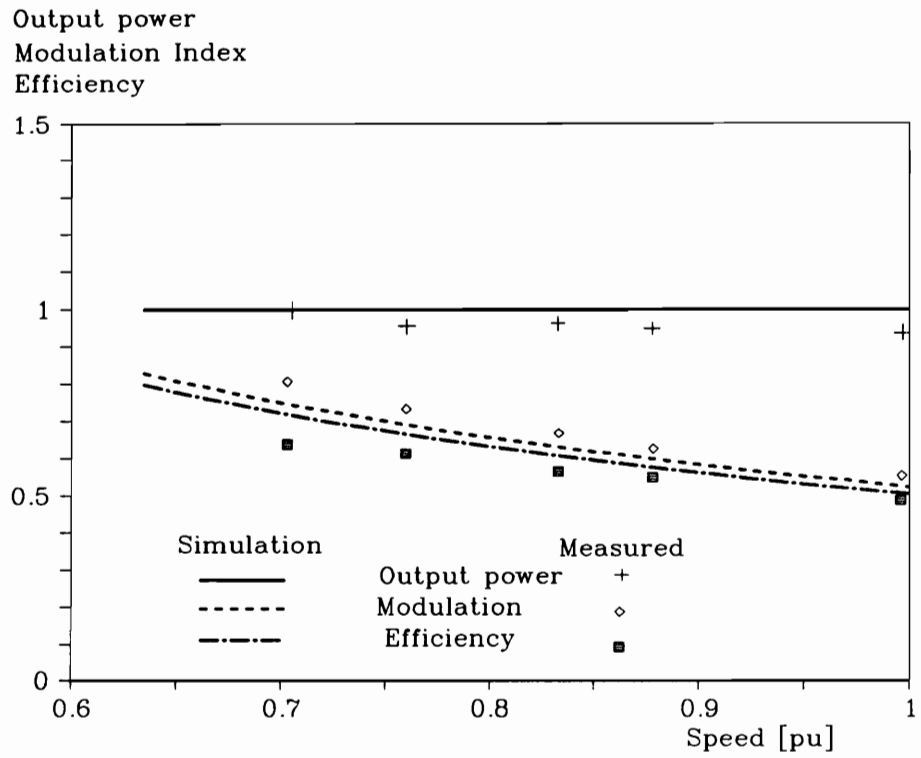

Figure 2.17: Experimental and predicted results for control strategy I

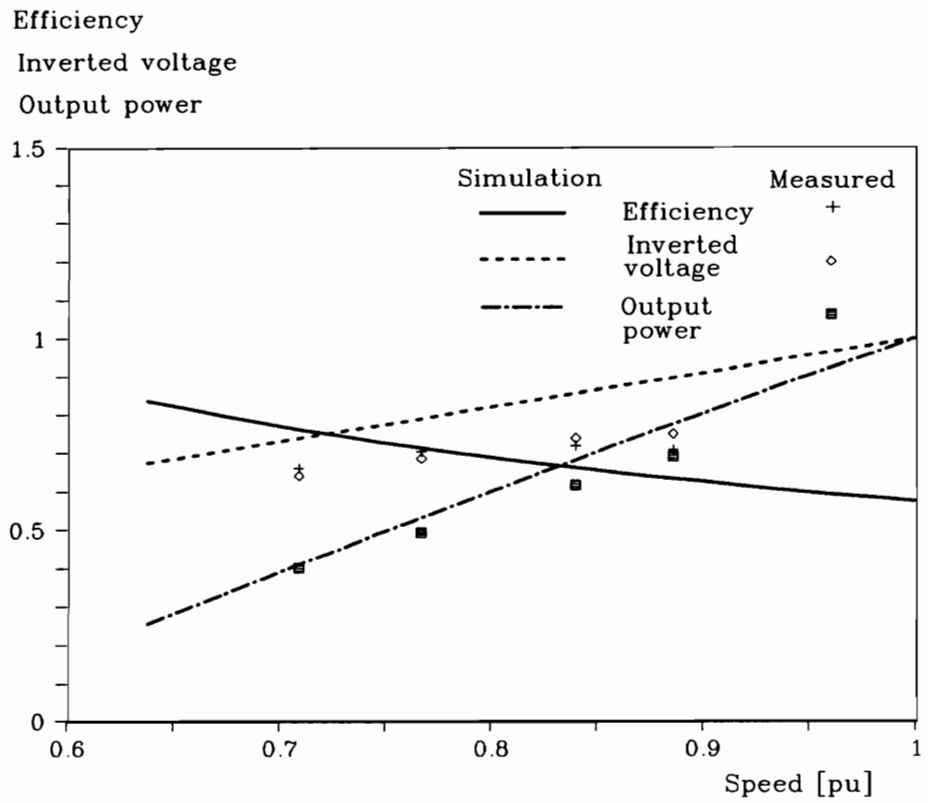

Figure 2.18: Experimental and predicted results for control strategy II

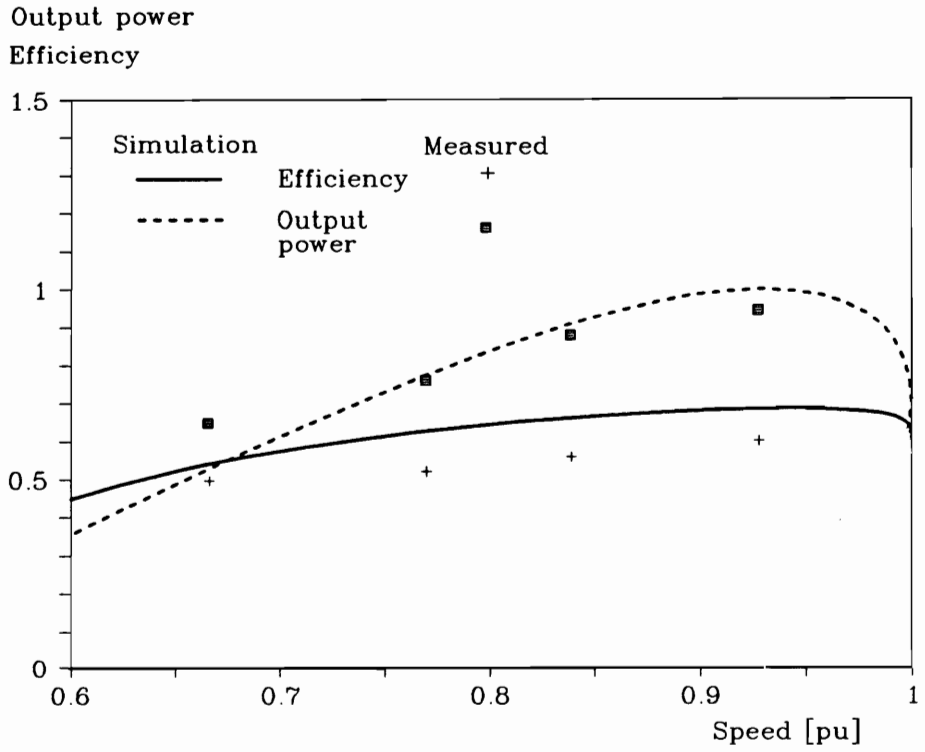

Figure 2.19: Experimental and predicted results for control strategy III

Figure 2.19 shows the performance characteristics using control strategy III. As the speed of the prime mover increases, the power factor goes from lagging to leading which helps to increase the efficiency to 60%. Even though the output power increases, it is not in proportion to the input power. The enhanced losses due to the power factor being other than unity reduces the efficiency of the VSCF power conversion scheme with this control strategy. It is noted that this control strategy gives better performance than control strategy I but is definitely inferior to control strategy II.

2.8 Conclusion

The following conclusions may be drawn from this study of a VSCF power conversion scheme with the PMSM:

(i) A novel scheme for VSCF with PMSM has been proposed which can be operated with a self commutating inverter.

(ii) The output current on the ac side is sinusoidal and power factor is adjustable, thus eliminating two of the major disadvantages with existing schemes.

(iii) Three different control strategies have been proposed: Control of the magnitude of the ac line current, control of the output power, and control of the power factor angle. All these control strategies have been realized in hardware, implemented in the VSCF scheme, and experimentally verified.

(iv) Control strategy II (Modulation control) gives the highest efficiency whereas control strategy III (Phase angle control) gives a variable power factor angle.

(v) A variable power factor angle makes this VSCF scheme useful as a VAR generator.

(vi) For high efficiency, the modulation ratio has to be fixed at unity. This is verified with control strategy II (Maximum current clamping control).

(vii) The switching frequency of the inverter does not exceed 1 kHz in most cases in order to obtain a good sinusoidal waveform in the line current. This is a very attractive

feature of this scheme and may find applications in high power schemes using GTOs, Darlington transistors, and IGBTs.

(viii) The impact on system performance of using an inductor in the dc link is found to be negligible.

(ix) The efficiency of the VSCF power conversion scheme with the PMSM is comparable to the one using a line-commutated converter.

(x) The transient performance of the VSCF power conversion scheme is smooth and has no detectable oscillations.

Chapter 3

VARIABLE SPEED POWER CONVERSION WITH AN SRM

The origin of SRM can be traced back to 1838. The advent of inexpensive high power switching devices revived the interest in the machine. In the late 60's, the potential of SRM for traction application attracted researchers. Since then the progress in research of the SRM drive has been phenomenal.

In this chapter, a review of the basic principle of operation of the SRM, currently available converter topologies, the controller requirements and some design considerations are included. A novel converter topology for the VSCF application is proposed and analyzed.

Nomenclature

$\delta\omega_m$	Incremental mechanical energy
$\delta\theta$	Angle increment
L_{max}	Maximum phase inductance of SRM
L_{Min}	Minimum phase inductance of SRM
N_s	Number of stator poles of SRM
N_r	Number of rotor poles of SRM
p	Number of ac supply phases, usually $p = 3$
q	Number of machine phases
T	Elecromagnetic torque

θ_i	Rotor position at i^{th} inductance break point
θ_a	Conduction starting angle or current advancing angle
θ_c	Dwell angle
$\theta_f = \theta_a + \theta c$	Falling angle
T_a	Shaft average torque
P_o	Average output power
W_m	Mechanical speed in [rad/sec]
W	Work per stroke
v_{dc}	Front-end converter output voltage
η_s	System efficiency
D	Duty ratio
I_{FCrms}	Front-end converter rms current rating
I_{MCrms}	Machine-side converter rms current rating
L	Self inductance of SRM phase
M	Mutual inductance due to phase coupling
R_w	Stator winding resistance
P_W	Instantaneous power of a phase winding
J	Moment of inertia of machine
B	Coefficient of viscous friction
β_s	Stator pole arc
β_r	Rotor pole arc
v_a, v_b, v_c	Instantaneous ac phase voltages
i_a, i_b, i_c	Instantaneous ac line currents
P_i	Instantaneous shaft power
$P_{Wmagnetic}$	Variation of the magnetic field energy in a phase winding
$P_{Wmechanic}$	Mechanical power of a phase winding
η	Efficiency across the machine and its converter

3.1 Introduction

It is known that in comparing with the present variable speed induction drive, the SRM drive has simpler construction and better than or at least equal performance in terms of torque per unit volume, efficiency, and volt-ampere requirements. One of the distinct features of SRM is the absence of windings or permanent magnets in the rotor, which results in a mechanically and thermally robust and maintenance-free machine.

The SRMs are doubly salient machines with an unequal number of poles in the stator and rotor, for instance, 8/6 or 6/4 poles in the stators and rotors, respectively, for four or three phase machines. Such typical machines are illustrated in Figure 3.1.

3.2 Basic Principles of SRMs

The section includes the discussion on the salient features [63], [94] of SRMs. The schematic diagram of an SRM with eight stator poles and six rotor poles are shown in Figure 3.1 (a) and its idealized inductance profiles is shown in Figure 3.2.

3.2.1 Torque production

The operation of the machine is as follows. When a pair of the stator windings which are diagonally opposite in the stator across the rotor are excited, the rotor moves until it reaches aligned position with the axis of the excited phase. This position is referred to as aligned position and it corresponds to the maximum inductance. The unaligned position is reached when two diagonally-located rotor poles are half a rotor pole-pitch away from the excited phase. If the next phase is excited before the rotor is fully aligned with the currently excited phase then the rotor moves towards and produces one more work stroke. Similarly, by switching the phase current sequentially the rotor continues to move. Hence the movement of the rotor produces torque and hence mechanical power. The direction of rotation of the machine can be reversed by changing the switching sequence of the phase currents. Therefore this drive is capable of four quadrant operation.

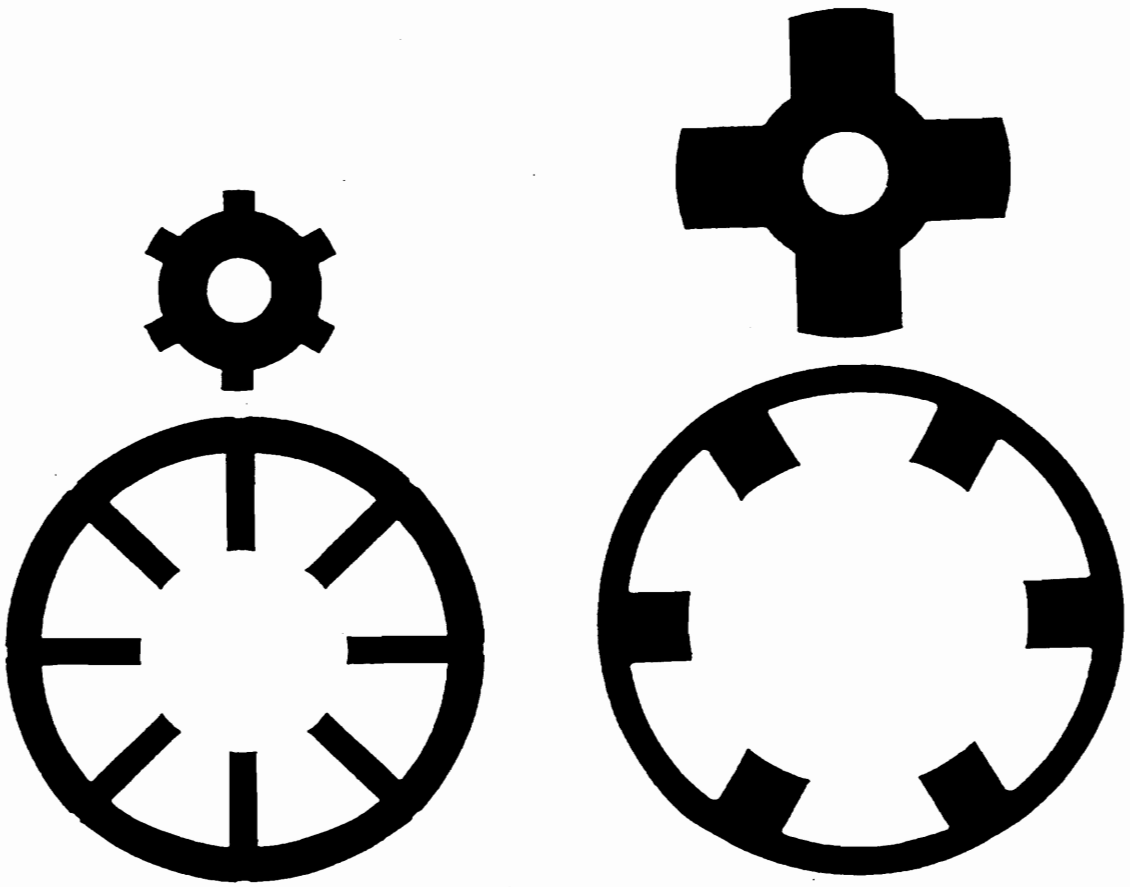

(a) 8/6 pole SRM structure (b) 6/4 pole SRM structure

Figure 3.1: SRM structures

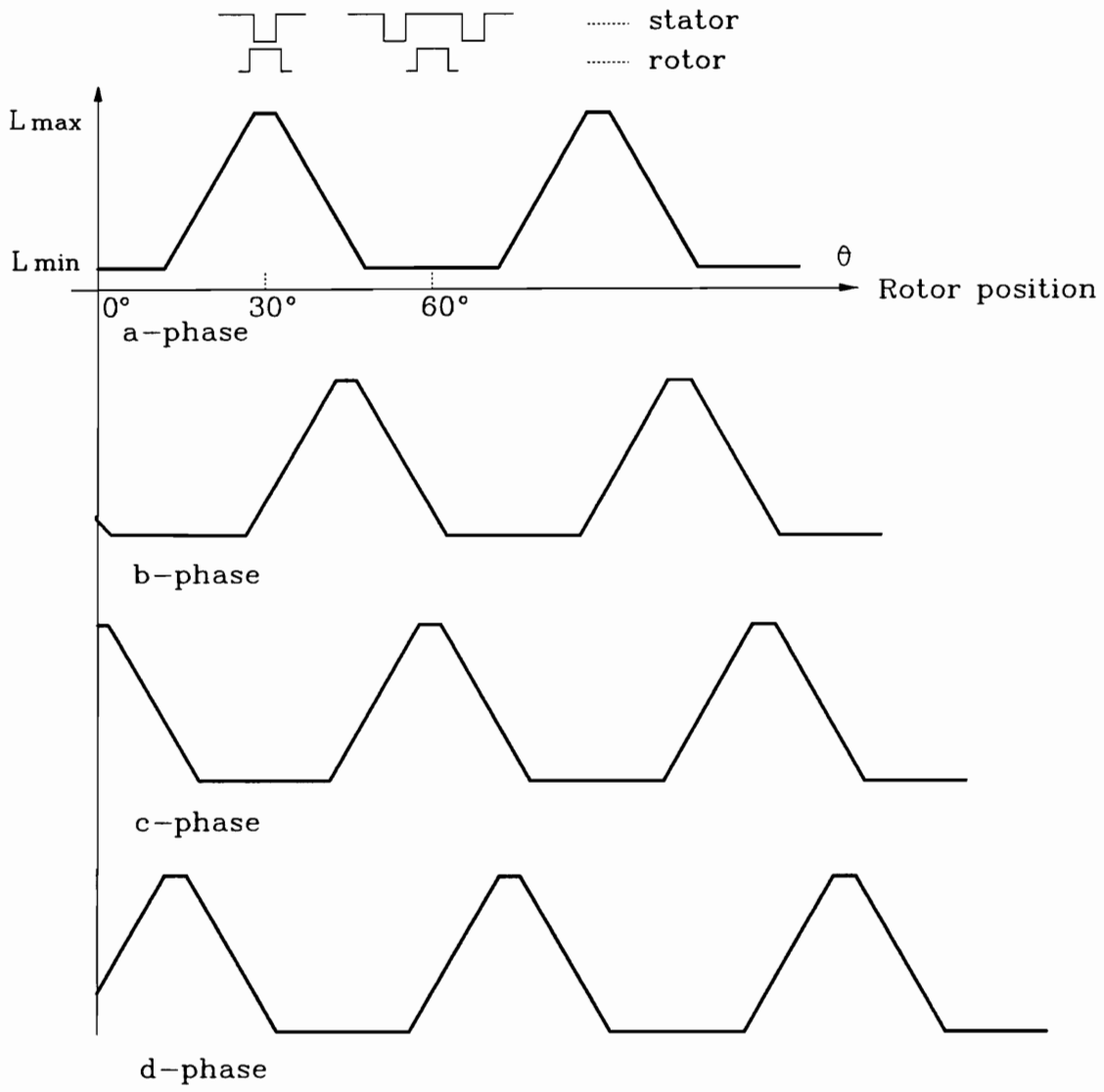

Figure 3.2: Inductance variation of a four phase machine

In the case of a rotating machine, the relationship between the mechanical energy and torque is,

$$\delta W_m = T\delta\theta \tag{3.1}$$

where $\delta W_m, T, \delta\theta$ are the incremental mechanical energy, electromagnetic torque, and the incremental mechanical angle, respectively. Hence

$$T = \frac{\delta W_m}{\delta\theta} \tag{3.2}$$

Assuming constant excitation and linear inductance, the incremental torque due to the rotor movement from θ_1 to θ_2 is,

$$\begin{aligned}
\delta T &= \frac{\delta W_m}{\theta_2 - \theta_1} && \text{(3.3a)} \\
&= \frac{L(\theta_2, i) - L(\theta_1, i)}{\theta_2 - \theta_1} \cdot \delta i && \text{(3.3b)} \\
&= i \cdot \delta i \cdot \frac{\delta L(\theta, i)}{\delta\theta} && \text{(3.3c)} \\
&= \frac{1}{2} i^2 \cdot \frac{\delta L(\theta, i)}{\delta\theta} && \text{(3.3d)}
\end{aligned}$$

where L is the self inductance of the circuit at the rotor position of θ. The torque equation (3.3d) implies,

(i) The electromagnetic torque is proportional to the square of the winding current, which results in

- The independence of torque with respect to the direction of current flow and hence one switch per phase winding requirement.
- A good starting torque production.

(ii) The torque is also directly proportional to the slope of the inductance and rotor position. Hence, a negative torque (generating mode) is made possible with unipolar current by operating the machine on the negative slope of the inductance and position.

3.2.2 Inductance variation and torque

Neglecting the fringe effect and magnetic saturation, Figure 3.3 (b) shows the inductance variation of one-phase with respect to rotor position. Each rotor position at which the slope

of inductance profile changes significantly is determined in terms of the stator and rotor pole-arcs and number of rotor poles. From Figures 3.3 (a) and (b), the various angles are derived as:

$$\theta_1 = \frac{1}{2}\frac{2\pi}{N_r} - \frac{1}{2}(\beta_s + \beta_r) \tag{3.4a}$$

$$\theta_2 = \theta_1 + \beta_s \tag{3.4b}$$

$$\theta_3 = \theta_2 + (\beta_r - \beta_s) \tag{3.4c}$$

$$\theta_4 = \theta_3 + \beta_s \tag{3.4d}$$

$$\theta_5 = \theta_4 + \theta_1 \tag{3.4e}$$

where β_s and β_r are pole arcs of the stator and rotor, respectively, as shown in Figure 3.3 (a).

The number of cycles of inductance variation per revolution is proportional to the number of rotor poles, and its period is equal to the rotor pole pitch, θ_5 and is given by,

$$\theta_5 = \frac{2\pi}{\text{No. of rotor poles}} \tag{3.5a}$$

$$= \frac{2\pi}{N_r} \text{ rad} \tag{3.5b}$$

The physical interpretation of inductance at each stator-rotor position is,

$\underline{0 - \theta_1:}$ The stator and rotor poles are not overlapping and the inductance stays at L_{min}.

$\underline{\theta_1 - \theta_2:}$ The rotor pole starts to overlap with the stator pole at θ_1 and the inductance increases until the poles are fully overlapped at θ_2 where the inductance has its maximum value L_{max}.

$\underline{\theta_2 - \theta_3:}$ The inductance remains constant at L_{max} until complete rotor-stator overlap is over. During this period no torque is produced. However, it is desired to have this flat inductance region to prevent significant negative-torque generation. The unequal rotor and stator pole arcs allow the flat-top inductance profile. Usually the stator pole arc is smaller than the rotor pole arc to get more winding space.

$\underline{\theta_3 - \theta_4:}$ The inductance decreases linearly until it reaches L_{min} and the poles are not overlapping anymore.

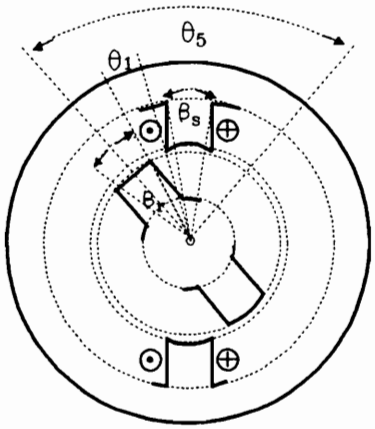

(a) Rotor and stator position

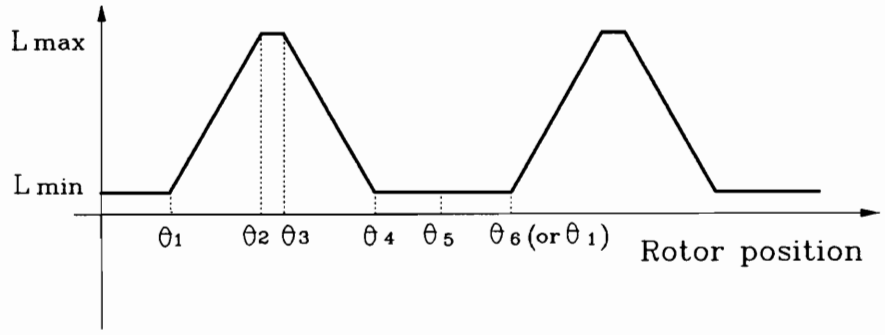

(b) Inductance profile

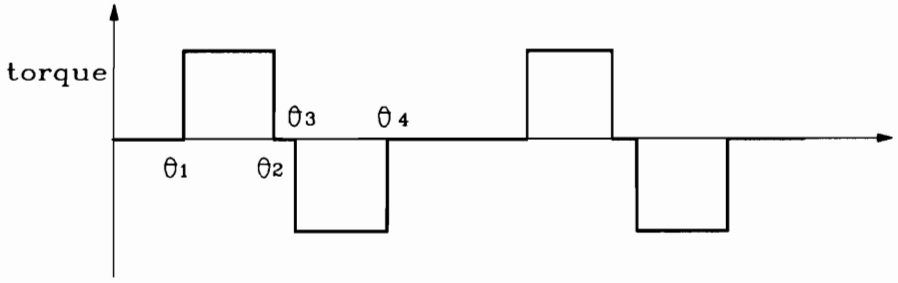

(c) Torque production

Figure 3.3: Rotor position and torque

$\underline{\theta_4 - \theta_5:}$ The inductance remains at L_{min}. Applying a constant current on the stator winding, the resultant torque is shown in Figure 3.3(c). Depending on the slope of the inductance and position, the machine produces either a positive (motoring mode), or a negative torque (generation mode) as seen from the torque equation (3.3d). Note that due to the machine back emf and inductive circuit characteristics, the current is usually advanced.

3.2.3 Steady state performance of the SRM

Energy conversion

In one revolution, for a q-phase machine, there are qN_r work strokes per revolution. The idealized relationship between the inductance profile and flux linkage-current characteristic for a flat-topped current waveform is shown in Figure 3.4. The points in both Figures 3.4 (a) and (b) are similarly labeled on both the figures. In Figure 3.4(b) the area OAEFO is possible energy conversion area, but due to the inductive circuit characteristics the early current commutation is required to avoid a significant negative torque. This causes the reduction of the available energy loop from the area OAEFO to OABC. In order to optimize the energy conversion, it is essential to convert the whole field energy into mechanical energy. In practice part of the field energy returns to the electric source. To maximize the energy conversion efficiency the following is to be achieved:

(i) Keep the current flat during the positive slope of the phase inductance. To do that advance energization of the winding may be essential.

(ii) Commutate the current as fast as possible so that the residual current does not produce the negative torque.

Current waveforms

As shown in Figure 3.3 the polarity and magnitude of the torque of the SRM rely on the variation of inductance and position, when the pulse current is applied. Since the inductance is also a function of current, the current shapes are to be considered in the energy conversion.

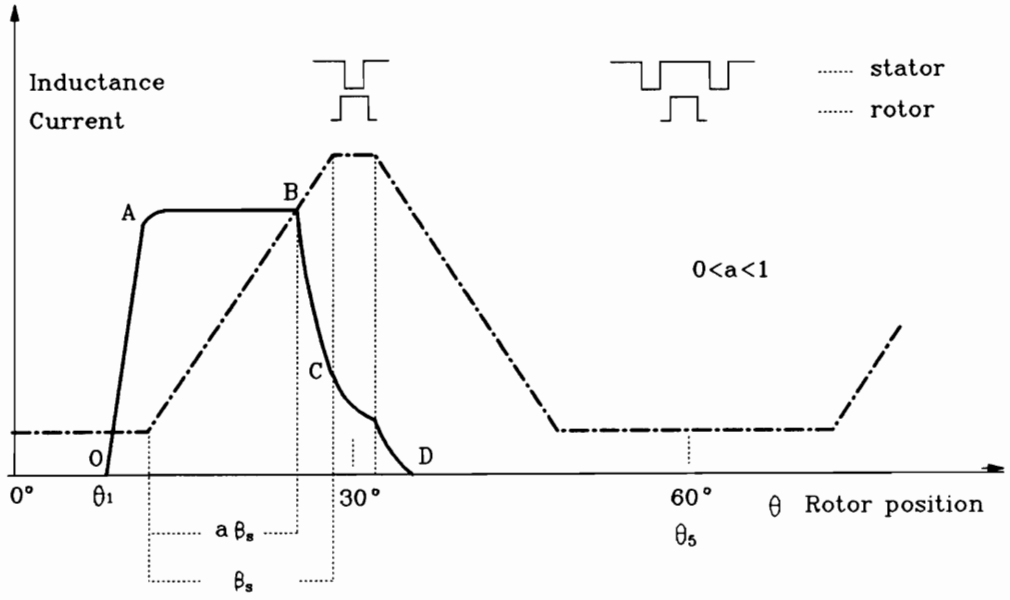

(a) Flat–topped current waveform and phase inductance

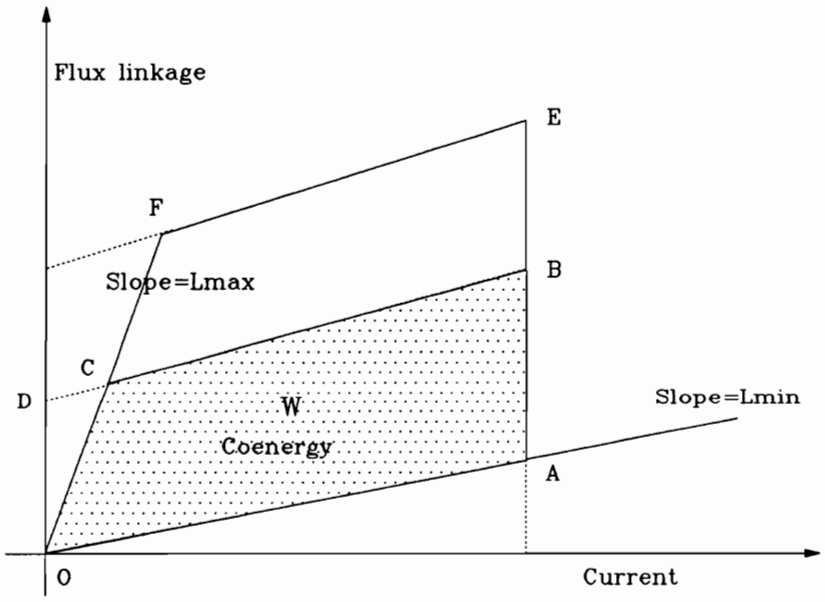

(b) Flux linkage vs current for energy conversion

Figure 3.4: Flat-topped current and energy conversion

In practice, the source voltage obtained from batteries or rectified dc sources is fixed, the source voltage is assumed remain constant at 1 pu in the discussion of current waveforms. The current shape varies with speed, load torque and the time of energization of the windings. The flat-topped pulse currents are expected around the base speed. At low speed, the rate of current rise is high because of the large voltage difference between the source voltage and the back emf. The slow inductance variation is in favor of the current increase, too. Therefore current chopping is required at low speed to limit the current magnitude. On the contrary, at the high speed, the increased back emf and short time for the rise of the current do not allow the current to build up fast. As a result more advanced turn-on of the phase windings are required for higher speed operation.

Typical current and their experimental waveforms using a four phase machine are shown in Figure 3.5. Figure 3.5(a) shows the effects of late commutation. The high rate of current rise and longer current rise-time explicable by the chopped current waveforms in Figure 3.5 (b) after advancing the turn-on timing 7° from θ_1 shown in Figure 3.3. At the base speed which is defined as the speed at which back emf is equal to the source voltage, a nearly flat-topped pulse current flows as shown in Figure 3.5(c) But at higher speed, enough advance in turn-on timing is required for the current to be built up. Compared to that of the base speed, more than two times of advanced angle is provided for the speed of 4200 rpms shown in Figure 3.5(d). Note that these two different advanced angle are almost of the same time duration, i.e. 7° = 0.65 ms (@ 1800 rpm) and 15.4° = 0.61 ms (@ 4200 rpm). An asymmetrical bridge converter shown in Figure 3.6 (a) is used in the current waveform measurements.

Average torque and power output

The coenergy in Figure 3.4 is used to calculate the average torque calculation. The average torque, T_a is given by

$$T_a = \frac{\text{Work}}{\text{Stroke}} \cdot \frac{\text{No. of stroke}}{\text{Revolution}} \cdot \frac{1}{2\pi} \tag{3.6a}$$

$$= W \cdot N_r \left(\frac{N_s}{2}\right) \cdot \frac{1}{2\pi} \tag{3.6b}$$

$$= \frac{W N_r N_s}{4\pi}, \text{ Nm} \tag{3.6c}$$

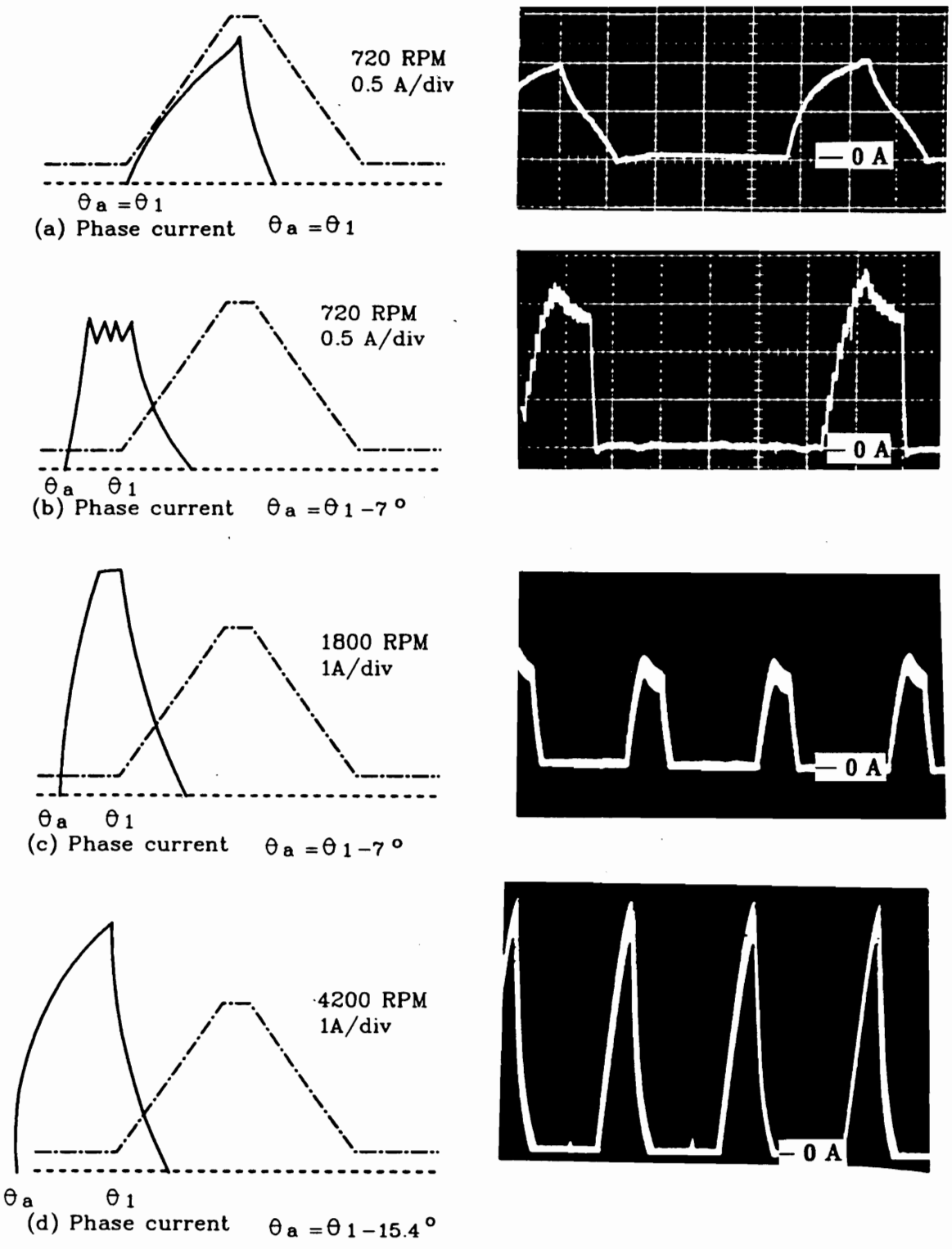

Figure 3.5: Typical current waveforms at different speed

where W is the work per stroke, N_s is the number of stator poles, N_r is the number of rotor poles. The average power output is,

$$P_o = T_a \cdot W_m \tag{3.7a}$$

$$= \frac{W N_r N_s W_m}{4\pi}, \text{ Watts} \tag{3.7b}$$

where W_m is the mechanical speed in rad/sec.

3.3 Review of the Topologies

Many SRM-converter topologies have been proposed to control the unidirectional phase currents. The cost minimization and performance maximization are the two important but sometimes conflicting requirements in selecting the converter topologies for SRM drives. That is, single switch per phase configurations are appropriate for low performance applications because of their use of minimum number of power devices and components, and resulting simplicity of the drive circuitry, whereas two switch per phase converters are needed for high performance drive system for them to have more freedom in controlling the phase currents in spite of the cost differential compared to the single switch per phase configuration.

It is well known that the SRM drives require only one switch per phase winding since the torque is independent of the direction of the winding current. However, in practice, some difficulties lie in the realization of single switch per phase configuration because of SRM's highly inductive circuitry. Hence, provisions for diversion of current path are to be given before switching off the current. Otherwise, the converters experience high voltage-spikes, resulting in the failure of the switching devices. This factor is one of the major issues to be considered in the discussion of the SRM converter. The control complexities are the result of the SRM-converter topologies and hence the need for a clearer understanding of the converter topologies. But the inductance of the winding contributes to the device protection in case of a shoot through fault. Since each phase winding is connected in series with a switch or switches, it limits fast current rise. In this section, the presently available major topologies are reviewed in regard to the number of switches, operations, control flexibility, and device ratings, etc.

3.3.1 Converter configurations and operations

Many converter topologies have been used in various applications. The configurations are classified as in the following:

(i) Asymmetric bridge converter.

(ii) Bifilar-winding configuration.

(iii) Split dc supply converter.

(iv) C-dump configuration.

(v) R-dump configuration.

(vi) Switch-shared configuration.

In spite of the different configurations, they have the following common features:

(i) Series connection of the switches and the phase winding, resulting in the immunity to shoot through faults.

(ii) Independent operation of each phase, resulting in the operation of healthy phase even in the presence of some phase failures.

(iii) Energy return paths when the switches are turned off to prevent the high voltage spikes.

Asymmetric bridge converter

The converter, as shown in Figure 3.6(a), requires two switches and two freewheeling diodes per phase. There are three stages of operation for this configuration. The first stage occurs when both switches are turned on. The source voltage, V_{dc} is applied across the phase winding to build up the current. In the second stage, one or two switches are turned off while current is flowing in the winding, the current free wheels through one diode and one switch or it flows back to the source through the two freewheeling diodes to reduce the current magnitude, depending on the control strategy. The last stage is performed when both switches, T_1 and T_2 are turned off to commutate, forcing the current to flow against

the source voltage through diodes, D_1 and D_2. The energy stored in the winding is depleted at this stage and recovered. Among the currently known SRM drive topologies, this has the maximum freedom in the control capability and has no constraints on the number of phase windings.

Bifilar-winding configuration

Figure 3.6(b) shows a simple converter for an SRM with bifilar stator windings. Current increases in the main winding when the switch, T_1, is turned on and the stored energy in the winding is transferred to the source through the auxiliary winding and diode when the switch is turned off. The simplicity of the converter is achieved with the bifilar wound machine which has a poor winding space factor, additional copper, more terminals in the machine. The high voltage spikes resulted from the imperfect coupling and winding turns ratio may be more than twice the source voltage when the switch is turned off. Therefore the voltage rating of the switching devices is more than twice that of the SRM winding.

Split source converter

This also meets the minimum switching device requirement and is shown in Figure 3.6(c). Phase A is energized by turning on T_1. The current circulates through T_1, C_1 and phase-winding A. If T_1 is off, the current continues to flow through phase winding A, D_1 and C_2. Note that C_2 is at $\frac{1}{2}V_{dc}$. Hence the stored energy in the winding is depleted fast.

C-dump configuration

C-dump configuration shown in Figure 3.6(d) requires one more switch and diode than the number of machine phases and additionally a capacitor and an inductor. When T_1 is switched off while A-phase winding current flows, the current commutates to D_1 and begins to charge the dump capacitor C_d. The rising voltage across the capacitor reduces the decaying time of the phase current. The trapped energy is recovered with the step-down chopper made up of T4, D4 and the inductor L_d. The configuration has the disadvantages of relatively high voltage rating of the power devices and energy recovery losses and increased capacitor use.

R-dump configuration

Figure 3.6(e) shows a converter configuration with one switch and one diode per phase. When T_1 is switched off, the winding current freewheels through D_1 and an external resistor R_d. Compared to the other source-recharging type converters, this configuration is disadvantageous in that it takes longer time to extinguish the winding current at commutation possibly causing negative torque and further it dissipates a part of the winding energy in the resistor, reducing the overall efficiency.

Switch-shared configuration

This configuration is categorized into the following two types.

q+1 switch topology: q is the number of phases. Figure 3.6 (f) shows a converter circuit in which one end of all phase winding is connected to one common midpoint between a switch and a diode. Other ends of the windings are connected separately at the similar points. To excite phase-A winding T_c and T_1 are turned on. When the phase A is enabled the common switch, T_c remains turned on and the phase switch T_1 is switched on and off for current control, or keep the phase switch, T_1 on , and switch on and off the common switch, T_c for freewheeling control. Only after completing the depletion of the energy stored in the phase winding, the next phase can be energized. The converter is fit for SRMs which do not have inductance overlap because it can control only one phase current at a time. Therefore it is suitable for SRMs with low number of phases and not for high performance applications where multiple phase energizations may be required.

1.5q switch topology: A power converter circuit for an even number of phase machine is shown in Figure 3.6(g). Top switch, T_{12} is shared by two phases. Note that it is shared by phase A and phase C, and T_{34} is shared by phase B and phase D so that each phase has enough time to deplete the winding energy. The top switch controls one phase current at a time since there are no overlap current in phases A and C (or phases B and D). The peak current through the switches are equal but the rms currents are different. Hence the switching and conduction losses are not evenly distributed, but the converter has almost the same flexibility in control as an asymmetric bridge converter.

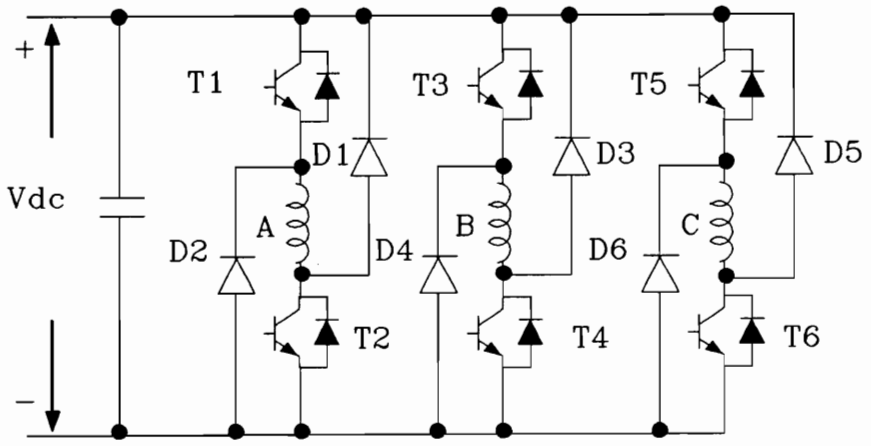

(a) Asymmetric bridge converter

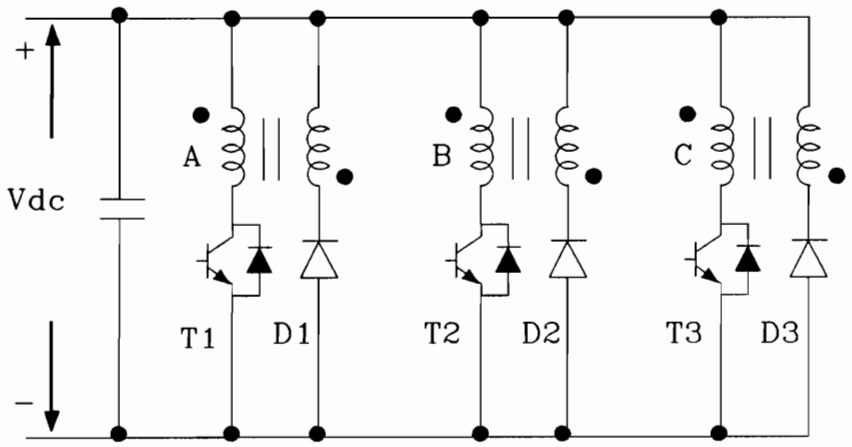

(b) Bifilar–winding machine configuration

Figure 3.6: SRM converter topologies

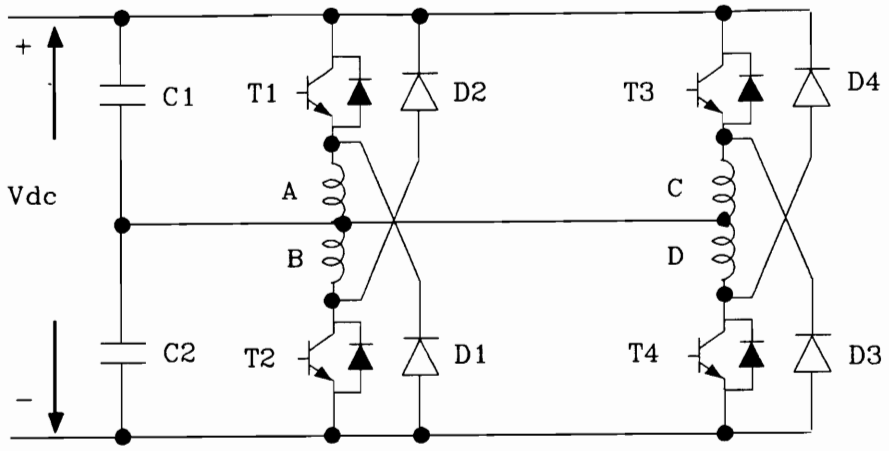

(c) Split source converter

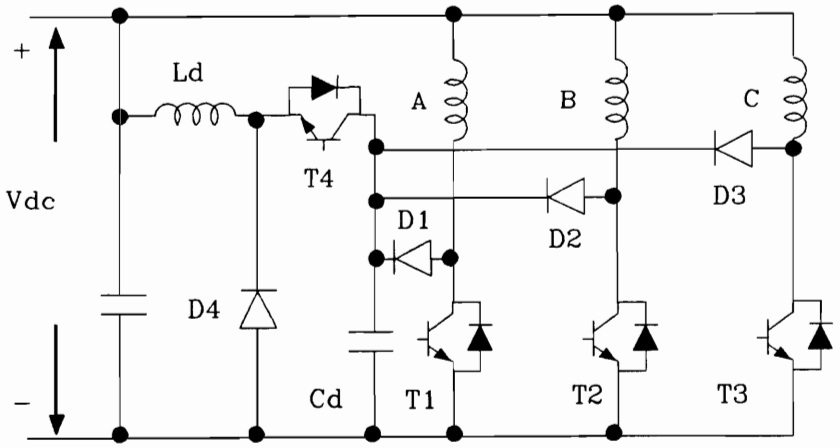

(d) C–dump configuration

Figure 3.6: Continued

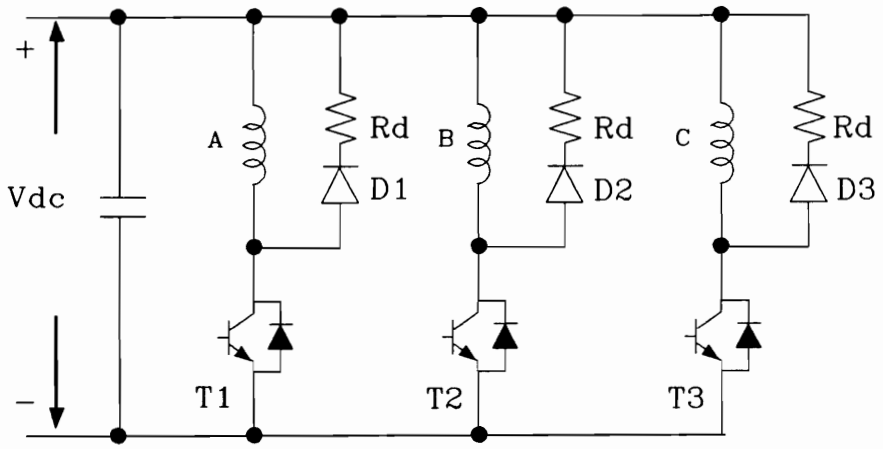

(e) R–dump configuration

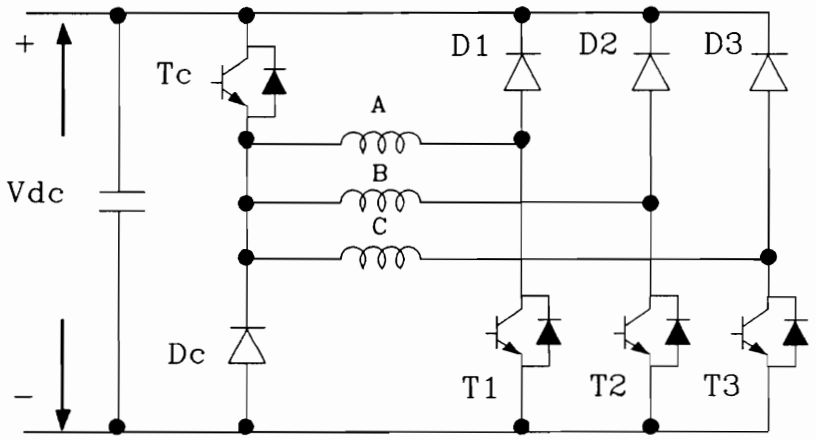

(f) q+1 switch topology

Figure 3.6: Continued

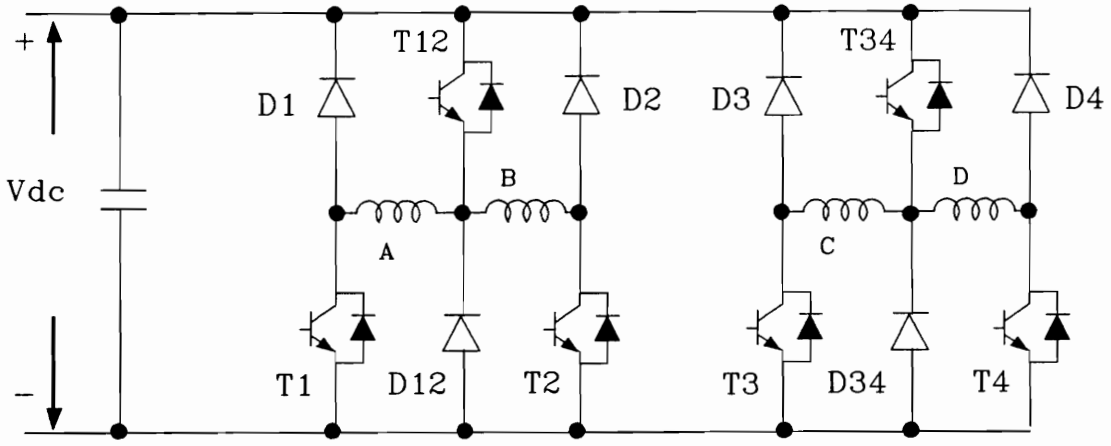

(g) 1.5q switch topology

Figure 3.6: Continued

3.3.2 Control strategy

The control flexibilities are mainly dependent on the converter topology and to an extent on the machine characteristics. Depending on the topology, some of the control strategies may not applicable as summarized in Table 3.1.

Angle control

In SRM drives, two angles are controllable; one is current advance-angle and the other is conduction-angle. High speed, or heavy load torque requires more current, resulting in large advance-angle. But the conduction angle remains constant, otherwise, longer current decaying time may cause a significant negative torque. At low speed or light load, the machine can be controlled by reducing the conduction angle or by chopping current. The former gives large torque ripples (accompanied by acoustic noise), whereas the latter produces less torque ripple but causes more switching losses. In high performance applications, the specifications allow a small torque ripple. In those cases, overlap current may be desirable to meet the requirements. It is achieved by increasing the conduction angle.

Current control (chopping)

At low speeds the back-emf is low, and as the inductance increases slowly, the current rises fast. Consequently the phase current rises to a higher level than it is required. It is controlled simply by turning on and off the switching devices. Current control is achieved either by chopping or by conduction angle control. Two strategies are involved in current chopping; one is freewheeling control and the other is regeneration control. When a phase switch is turned off while the current flows, the freewheeling control lets the current circulate through the winding and a freewheeling diode (and a phase switch). Hence it reduces the system efficiency in the case of a R-dump configuration, on the contrary, it enhances the system efficiency for an asymmetric bridge converter. Regeneration control is acceptable only in the limited topologies as shown in table 3.1. It gives a higher system efficiency than the energy-dump type configurations, but it also has demerits such as high switching losses, large current through dc link capacitor and high voltage fluctuations in the dc link.

Table 3.1: Comparisons of the converter topologies

Configuration	Device				Motor winding rating	Control capability
	No. of		Ratings			
	SW.	Diode	Voltage	Current		
Asymmetric bridge converter	2 q	2 q	> Vdc	$\frac{Ip}{\sqrt{q}}$	Vdc	Very flexible
Bifilar winding converter	q	q	> 2Vdc	$\frac{Ip}{\sqrt{q}}$	Vdc	No freewheeling control
Split source converter	q	q	> Vdc	$\frac{Ip}{\sqrt{q}}$	$\frac{1}{2}$ Vdc	No freewheeling control
C–dump configuration	q+1	q+1	>2Vdc	$\frac{Ip}{\sqrt{q}}$	Vdc	No freewheeling control
R–dump configuration	q	q	>2Vdc	$\frac{Ip}{\sqrt{q}}$	Vdc	No regeneration No overlap current
q+1 switch Topology	q+1	q+1	> Vdc	$\frac{Ip}{\sqrt{q}}$ Ip	Vdc	No overlap current control Tc
1.5q switch Topology	$\frac{3}{2}$ q	$\frac{3}{2}$ q	> Vdc	$\frac{Ip}{\sqrt{q}}$ $2\frac{Ip}{\sqrt{q}}$	Vdc	Very flexible T12, T34

Table 3.1: Continued

Configuration	Merits	Demerits	Misc.
Asymmetric bridge converter	- High efficiency - Fast regeneration - High control capability	- High count of devices - High voltage drop (across the devices)	- Good for lower No. of phases
Bifilar winding converter	- Fast regeneration - Low count of devices	- Poor thermal management - Low power density - High voltage ratings of devices - Extra copper & connections	- Good for low voltage low power level
Split source converter	- Low count of devices - Fast regeneration - Relatively high efficiency	- Phase dependence - Extra capacitor - Even No. of phases - Low reliability	
C-dump configuration	- Low count of devices - Relatively high efficiency	- One Extra switch - Extra inductor - High count of components	
R-dump configuration	- Simplicity - Low count of devices	- Low efficiency - Slow current decay - Limited conduction angle - High voltage rating of machine	- Low performance applications - Low power level
q+1 switch Topology	- High efficiency - Fast regeneration - Low count of devices - Simplicity	- Limited conduction angle - Extra switch - Not even power dissipation of devices - Limited conduction angle - High voltage rating of switch	- Low performance applications
1.5q switch Topology	- Fast regeneration - Relatively low count of devices	- Even No. of phases - Uneven power dissipation of devices	

Current control (commutation)

Fast current decay, recovery of the stored energy, and small torque ripples are the key features in phase commutation. The first two can be carried out by regeneration through the freewheeling diodes in most of the available topologies and the torque ripple can be reduced by overlapping phase currents. However, the R-dump configuration is not acceptable for this requirement and it gives a large torque ripple because of the limited conduction angle. q+1 switch converter topology has a large torque ripple for the same reason.

3.3.3 Device ratings

Selection of switching devices

The selection of switching devices takes an important place in designing a converter. The following factors are the key issues to be considered:

(i) Power level.

(ii) Source and transient voltage.

(iii) Peak and continuous current.

(iv) Switching frequency or switching speed.

(v) Cost.

(vi) Simplicity of driving circuit.

In the SRM drives, forced commutated converters are required. Therefore the converters consist of the switching devices such as GTOs, BJTs, IGBTs, and MOSFETs. For low power range converters, the MOSFETs and IGBTs are the attractive candidates. Judging from the peak and continuous current ratings, MOSFETs are the most suitable devices for the SRM converters.

Current rating of the switching devices

Depending on the control strategies and converter topologies, the current rating is varying. The peak current rating and the continuous current ratings should be defined first in

any case. From the given specifications, the peak current, I_{peak} is defined as the following.

$$I_{peak} = \frac{P_o}{\eta_s D V_{dc}} \tag{3.8}$$

where P_o is the peak output, D is the duty ratio, V_{dc} is the dc source voltage, and η_s is the efficiency of the system. The continuous current rating is equal to or less than the peak current of the winding. Assuming the continuous current equal to the rms current per phase, the rms current is determined from a flat-topped current. Allowing no overlap current and no phase-shared switch, from Figure 3.7 (a) the rms current is given as,

$$I_{rms} = \sqrt{\frac{1}{2\pi}\int_0^{\theta_c} {I_p}^2 d\theta} \tag{3.9a}$$

$$= \sqrt{\frac{\theta_c}{2\pi}} I_p \tag{3.9b}$$

if $\theta_c = \frac{2\pi}{q}$ then $I_{rms} = \frac{I_p}{\sqrt{q}}$ where q is the number of phases, θ_c is the conduction angle for each phase, and I_p is the peak current value.

The top switches in the q+1 and 1.5q switch converter topologies have the rms current as in the following:

$$I_{rms} = \sqrt{\frac{1}{2\pi}\left[\int_0^{\theta_c} {I_P}^2 d\theta + \int_{\frac{2\pi}{q}}^{\frac{2\pi}{q}+\theta_c} {I_p}^2 d\theta\right]} \tag{3.10a}$$

$$= \sqrt{\frac{\theta_c}{\pi}} I_p \tag{3.10b}$$

If $\theta_c = \frac{2\pi}{q}$, then

$$I_{rms} = \frac{\sqrt{2}}{\sqrt{q}} I_p \tag{3.11}$$

When there are overlap currents through the switches of the asymmetric bridge converter or through the switches in the similar conditions, the rms current is given,

$$I_{rms} = \sqrt{\frac{1}{2\pi}\int_0^{\frac{2\pi+\theta_o}{q}} {I_p}^2 d\theta} \tag{3.12a}$$

$$= \sqrt{\frac{1}{q} + \frac{\theta_o}{2\pi}}\, I_p \tag{3.12b}$$

where θ_o is the overlap angle. The switch T_c in Figure 3.6(f) is a particular case and its rms current is given from Figure 3.7(b) as,

$$I_{rms} = q\sqrt{\frac{1}{2\pi}\int_0^{\theta_c} {I_p}^2 d\theta} \tag{3.13a}$$

$$= q\sqrt{\frac{\theta_c}{2\pi}}I_p \tag{3.13b}$$

In practice the rms current is less than the calculated value, since the current is usually chopped to control the magnitude and the duty ratio is less than unity. When the switches are turned off while the current is flowing, the freewheeling diodes take over the current, resulting in the reduction of the switch rms currents.

Voltage rating of the switches

The voltage rating of the switching devices is dependent on the source voltage and the converter topologies involved. As discussed earlier, the voltage rating of devices in a bifilar winding machine is the worst case, where the minimum voltage rating is at least twice of the winding voltage for the turns-ratio of 1:1. Other topologies, even the split source configuration, need the device voltage rating of $V_{dc} + \Delta V$, where V_{dc} is the dc link voltage and ΔV is a voltage margin to allow the increased voltage dc link voltage at commutation and the voltage spikes at turn off due to the circuit stray-inductance.

Freewheeling diodes

If the phase switches are turned on, the freewheeling diodes are reverse-biased by the source voltage. Hence, the minimum reverse voltage blocking capability is equal to the switch forward-blocking voltage. In the SRM drives, fast-recovering diodes must be used in conjunction with the switches because fast forward and reverse recovery are required to ensure fast current transfer at turn-off and fast blocking of diodes at turn-on of the switches. When phase switches are off, the freewheeling diodes conduct. The peak current rating of the diodes is the same as the peak on time current of the drive. But the rms current rating is not obvious because it is a function of the duty ratio and the machine inductance. Table 3.1 summarizes the key features of the SRM converter topologies. The merits and demerits are also included.

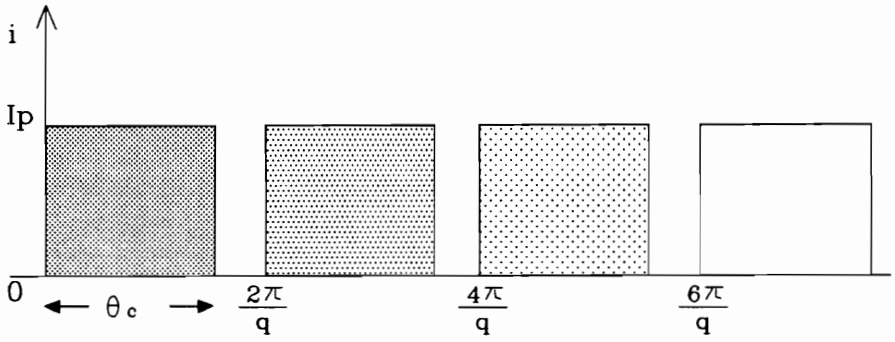

(a) Flat–topped current without overlap current

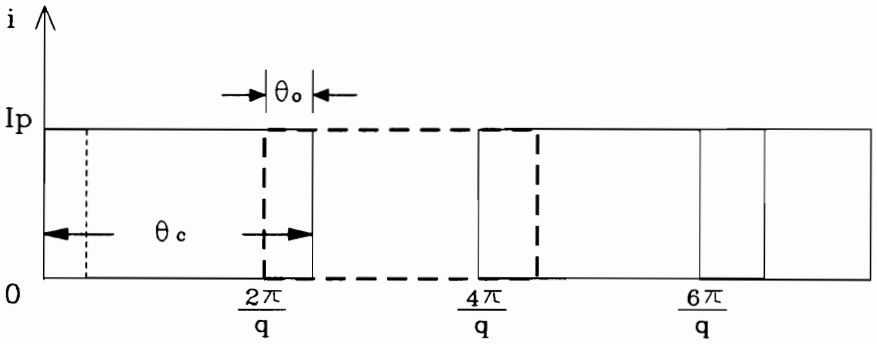

(b) Flat–topped current with overlap

Figure 3.7: Rms current calculations using a flat-topped current

3.4 VSCF Power Conversion with an SRM

The overall power conversion scheme is shown in Figure 3.8. The scheme works for both generating and motoring operations. In the generator mode, the shaft is driven by a prime mover. The electro-magnetic torque developed in the generator (when it delivers power) opposes the torque of the prime mover. The losses due to the copper and iron core, friction and converter causes the difference between these two torques. In a motor the electromagnetic torque developed in the machine except the losses is delivered to the shaft which drives the mechanical load. In this scheme, the SRM is directly connected to the shaft of a prime mover which has a variable-speed power such as an aircraft starter-generator. In the experimental set-up, a dc machine is mechanically coupled to the SRM. For generation the dc machine provides the variable-speed power to the system as a prime mover, and for motoring it takes power from the system as a load. The SRM rotor position is obtained from an optical encoder which is installed on the rotor shaft. The machine interfaces to the three phase mains through the proposed converter. During motoring, the converter acts as an inverter and drives the SRM as a motor. For generating operation, the power converter provides excitation to the SRM and extracts the resulting generated power directly to the ac mains.

3.4.1 Topology

A converter topology which is capable of four-quadrant (motoring and generation) operation is proposed for the VSCF power conversion scheme. The new converter topology for the VSCF power conversion scheme is made of two functional stages. One is converting stage which consists of six switches and six diodes and it interfaces a three-phase 60 Hz ac supply and a single-phase variable-frequency ac source. The other is the commutating stage through which each phase-winding is energized. The former is referred to as a front-end converter, the latter is referred to as a machine-side converter hereafter.

The functions of these converters for SRM drives may be briefly described as follows. When the rotor is appropriately positioned with respect to the stator, unidirectional current pulses are applied across the phase windings to energize.

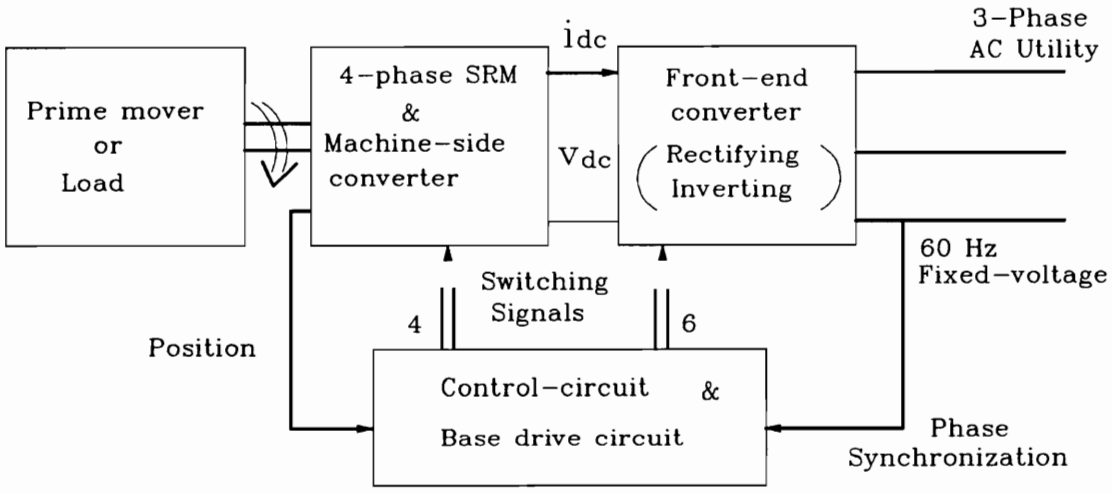

Figure 3.8: Overall conversion scheme using an SRM

If a desired current is commanded, a rapid response is needed for the demanded phase current level, which requires a two quadrant power converter, which is capable of applying equal positive and negative phase voltage when necessary. This is done usually by reversing the current direction of the phase winding through feedback diodes, on the contrary, the proposed converter keeps the source current direction, and changes the voltage polarity instead. Most of the SRM drives(the rectifier-capacitor source) except battery-source cases can not directly feed the energy to the source due to the diode bridge and the current limitation of the electrolytic power-capacitor, thus only limited amount of returned energy is stored in the capacitors and reused. As a result, an extra circuit such as dump resistor across the capacitor may be required to limit the voltage rise in the dc link, this resulting in a low efficiency. In such cases the reversed current affects the life-time of the capacitor due to the frequent charging and discharging actions. However the new converter can return the power from the machine to the source directly without any limitations and eliminates the dc link capacitor. The elimination of dc link capacitor resulting in cost savings and enhancement of the reliability of the scheme and increasing the power density of the scheme due to lower weight.

Front-end converter

The proposed converter configuration is shown in Figure 3.9. It is realized by cascading one switch with a diode for a switching block. It comprises six MOSFET switches(T1 to T6) and six diodes(D1 to D6). The three phase ac is connected to the mid point of each leg and the output is applied across the phase winding. The MOSFETs withstand the positive off-voltage and the diodes block the negative voltage excursion. Each MOSFET is provided with a turn-off snubber circuitry(not shown in the figure) to reduce the turn-off switching stress. The capacitors on the ac side provide current path when both top and bottom switches are off. It is a two quadrant converter. Note that the switching block eliminates shoot-through faults, namely, any number of switches can be activated simultaneously without detrimental outcome. This feature is greatly advantageous in controlling the converter, and will be discussed in detail in the section on converter control. To verify the feasibility, the front-end converter is tested for a resistive load.

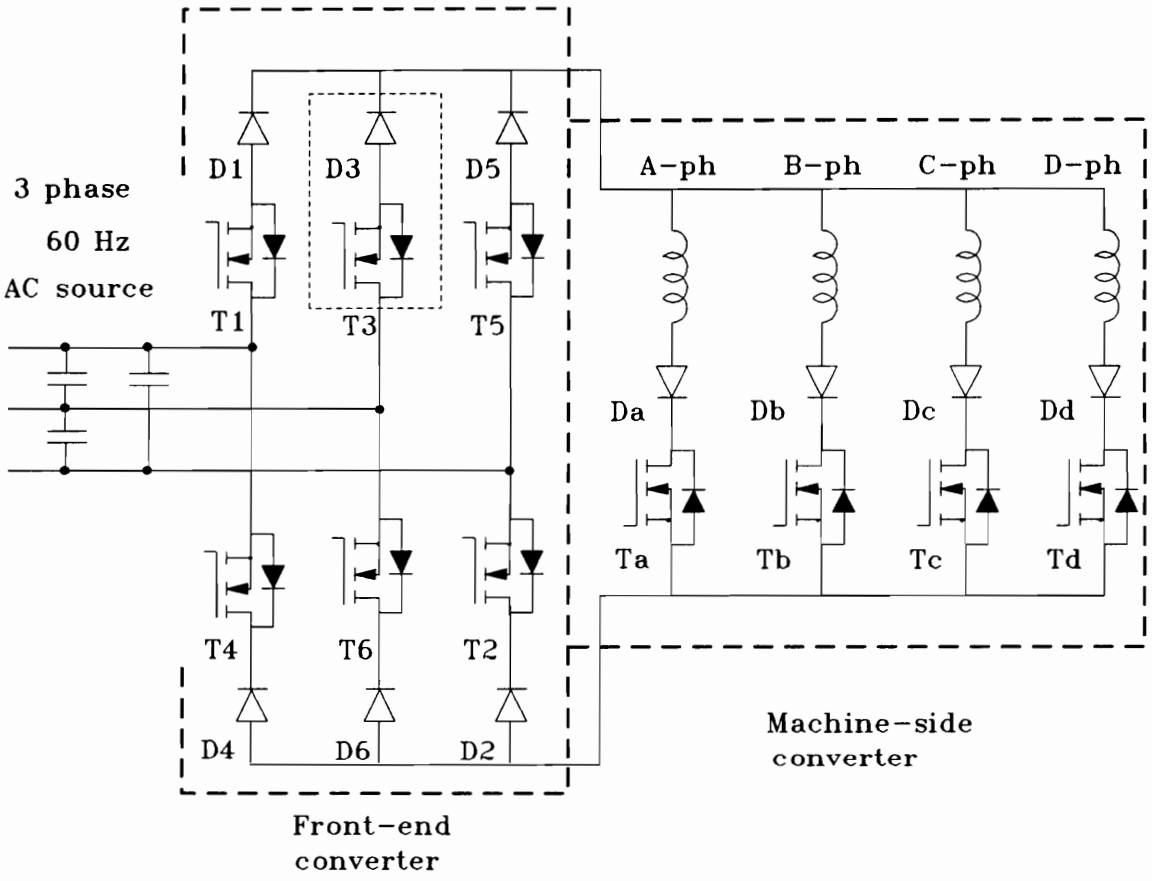

Figure 3.9: The proposed converter configuration for the VSCF scheme

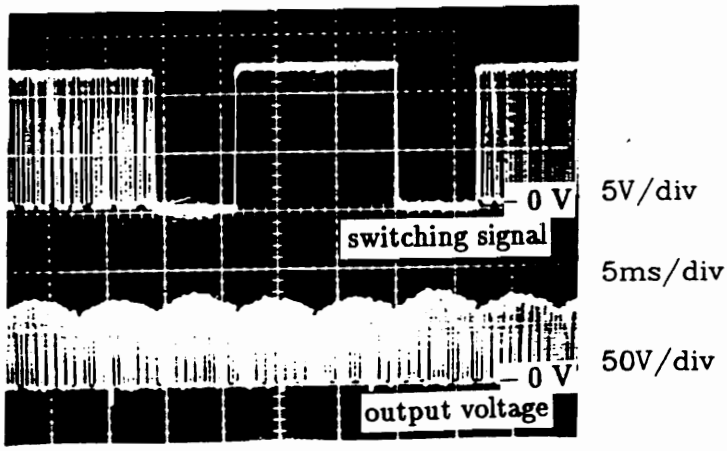

(b) Switching signal and output voltage for resistive load

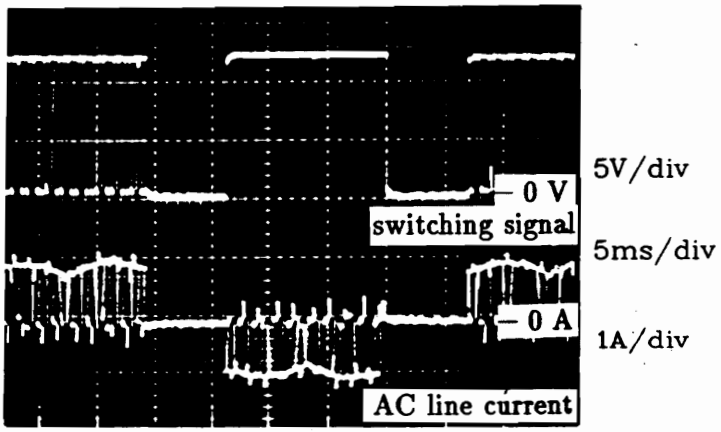

(c) Switching signal for T1 and ac line current

Figure 3.9: Continued

The output voltage and a switching signal in the PWM mode is shown in Figure 3.9 (b), where the output voltage waveform shows clearly six order harmonics riding over a dc voltage. The waveform is very similar to a conventional three-phase diode bridge output with chopping. Note that despite the solid turn-on signal during some period the output voltage is not affected at all due to the reverse-biased diodes. An ac line current is also shown with a switching signal in Figure 3.9 (c).

Peak currents through devices are determined primarily by the machine phase current. The voltage ratings are dependent on the peak voltage of the three phase ac source.

Machine-side converter

Each phase winding of the SRM is connected in series with a MOSFET and a diode. Therefore a four-phase machine needs four MOSFETs and four diodes for a machine-side converter. The diodes prevent the phase current reversal which may happen through the anti-parallel diodes of the MOSFETs when the polarity of the applied voltage is changed by the front-end converter for generation. Compared to the front-end converter the switching frequency of this converter is very low, because it is used only for phase commutation purposes. At the point of commutating there is no current flowing in the phase winding, which reduces turn-off stresses of the MOSFET switches greatly.

Peak currents through devices are determined primarily by the machine. The peak current and voltage ratings of the devices are the same as the front-end converter.

3.4.2 Control of the converter

The objective of controlling the SRMs is to obtain smooth torque at a desired speed. This can be accomplished by controlling the phase current as a function of rotor position. The essential feature of the control logic for the front-end converter is to synchronize the switching signals with the mains. Figure 3.10(a) depicts the block diagram of the control circuit for the front-end converter. Three phase sinusoidal signals are compared with each other by three comparators, which sets phase relationships of each phase at logic signal level.

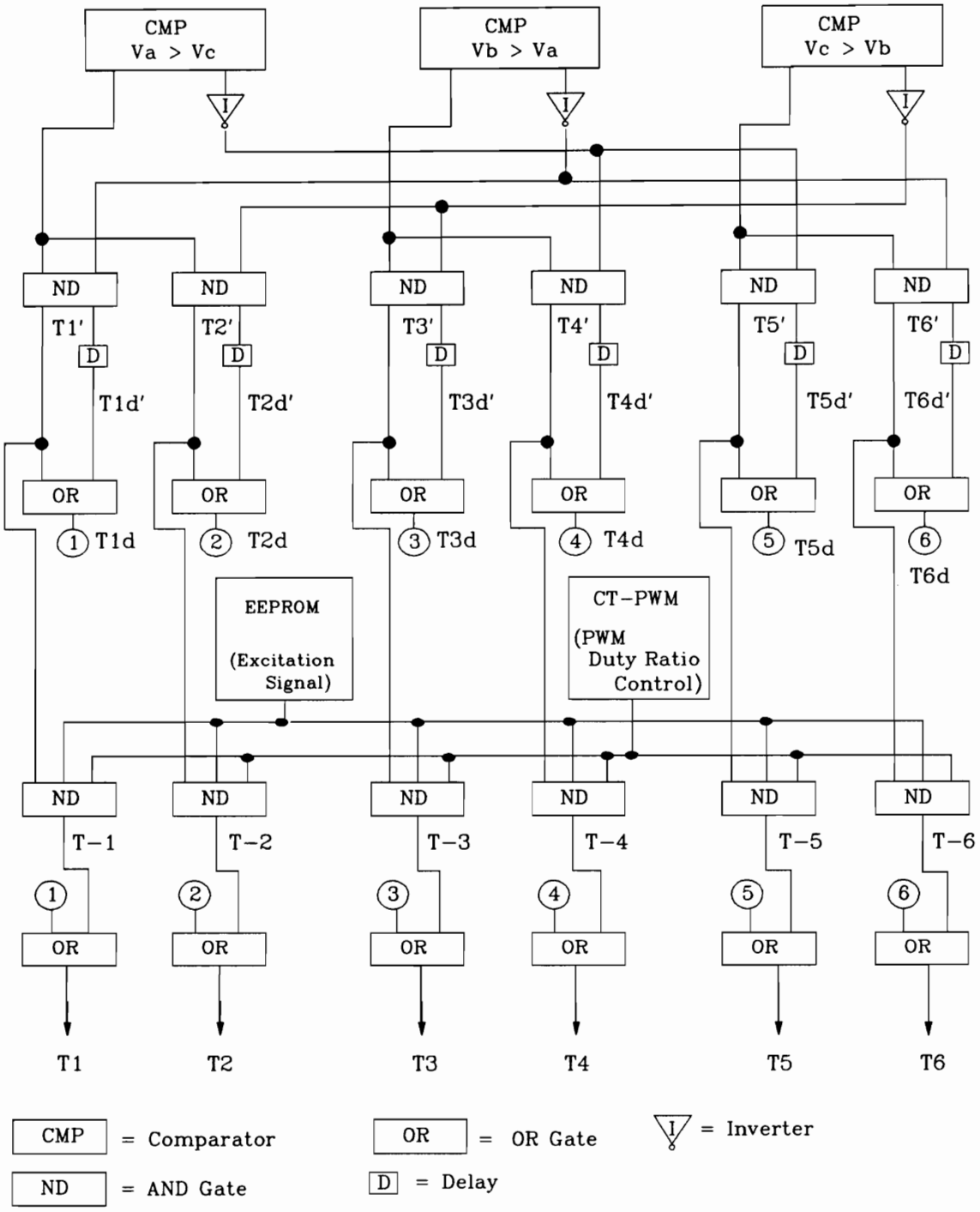

(a) Block diagram of the control circuit for the front-end converter

Figure 3.10: Control circuit & signals for the front-end converter

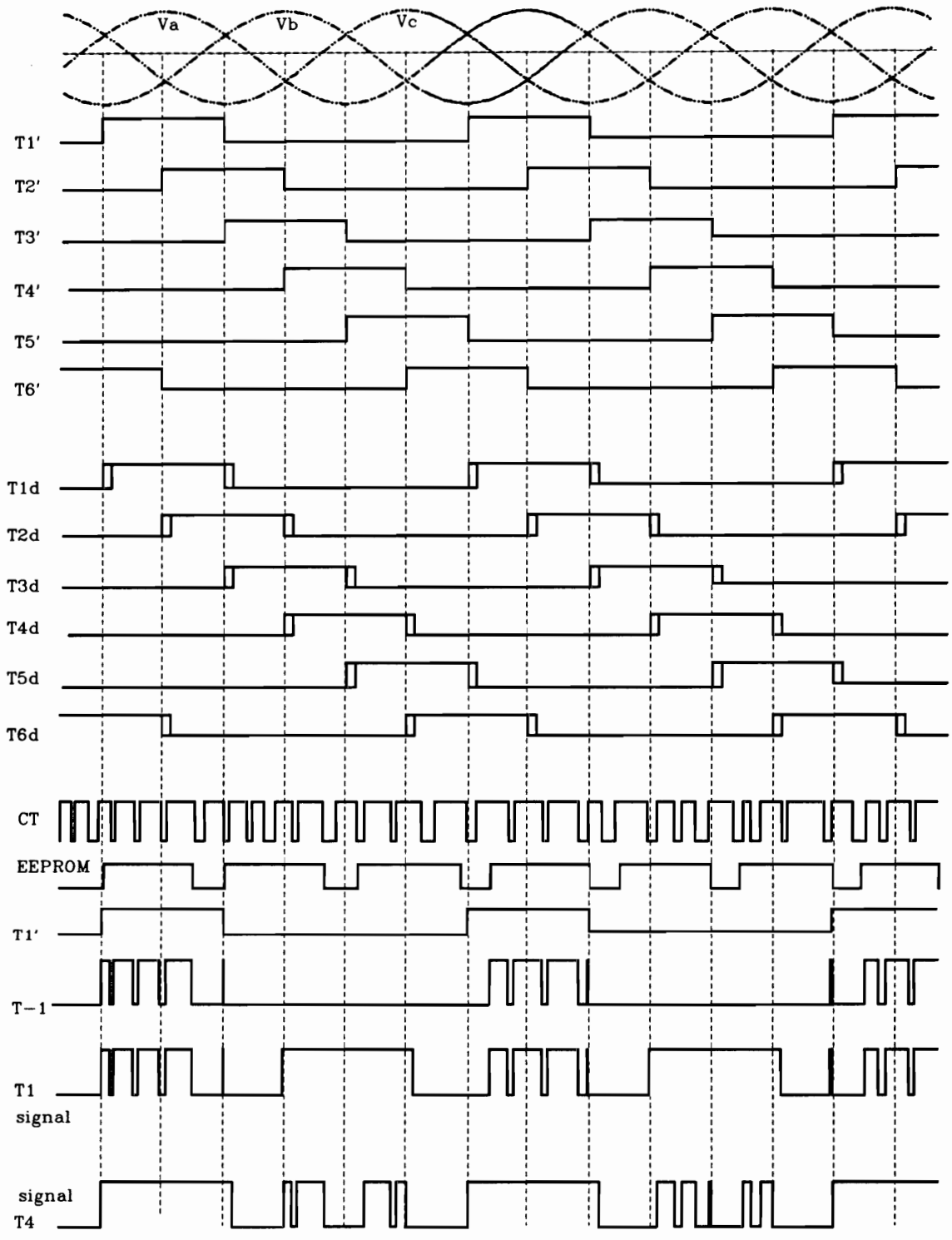

(b) Control signals at each block diagram points

Figure 3.10: Continued

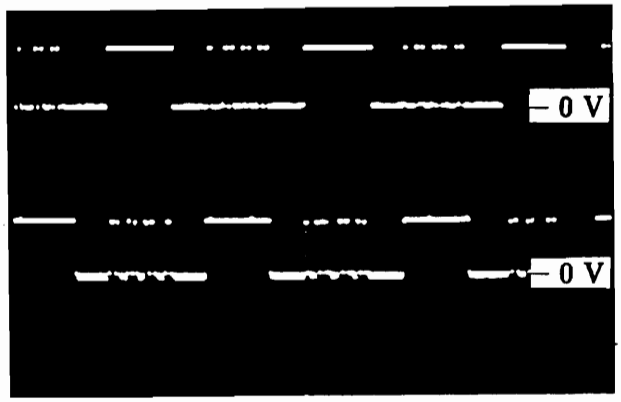

(c) Switching signals for T1 & T4 (5V/div, 1ms/div)

Figure 3.10: Continued

Appropriate combinations of the comparator outputs through six AND-gates give 120° high signals per cycle. Each signal has 60° of phase shift with regard to each other. These signals ensure the turn-on time of the six switches(T1 - T6). During the on-time current limiting signal from CT-PWM circuit and excitation signal from EEPROM governs the switching signal through a three input AND-gate. The resultant signal(T-1) is shown in Figure 3.10(b). To avoid destructive high voltage stresses in the converter, a continuous current-path should be arranged for inductive current of the circuit. Using a simple RC delay circuit the switching signals(T1' - T6') for each switch are extended(T1d - T6d), which lets the converter provide a path for the ac line current.

In the SRM drive, as discussed earlier, current is controlled using regenerative schemes for fast response, and is done by reversing the polarity of the voltage in this scheme. In Figure 3.10(b), if one of the top switches(T1, T3, or T5) and one bottom switch(T2, T4, or T6) of a different leg are turned on with forward-biased diodes, then a phase-current begins to flow. After the period, if turn-off signals are commanded, the other two switches of the same legs (which are already turned on) take over the current. When the current path is shifted from top to bottom, or vice versa, the voltage-reversal across the machine-winding occurs.

Note that even though the two switches of the same rail are turned on, only one switch on whose diode is forward biased conducts. This eliminates the shoot through faults of the converter. The experimental switching signals in Figure 3.10(c) confirms the last two signals shown in Figure 3.10(b).

Key features of two control circuits, phase shifting and position sensing circuits follow the functional diagram of the CT-PWM controller in Figure 3.11.

Phase shifting circuit

Since the front-end converter deals with a three phase ac source, the phase information of each phase of the ac source is required to activate the converter. In the discussion, a balanced 60 Hz three-phase ac source is assumed. A simple phase-shifting circuit(PSC) design[82] and its performance are discussed in this section.

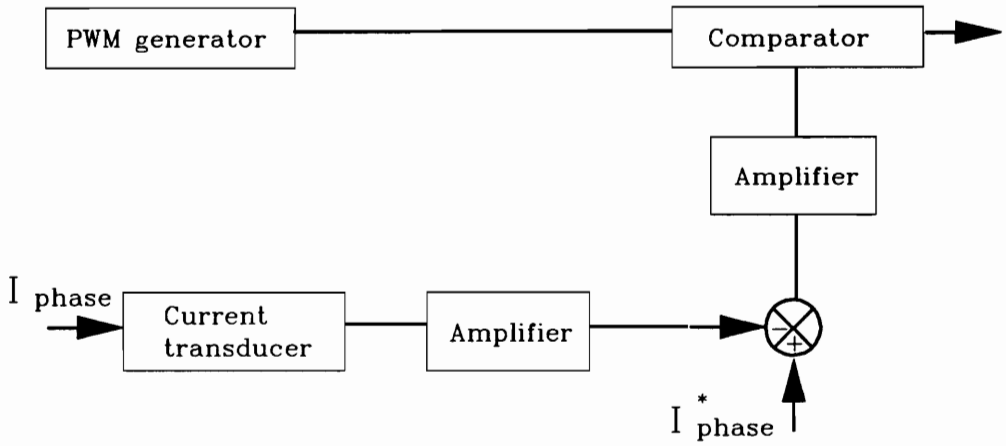

Figure 3.11: Functional diagram of CT and PWM circuits

The use of the PSC eliminates the necessity of all the three-phase references directly from the main source. Only one line to line voltage, or a phase voltage is required as a reference signal. Figure 3.12(a) shows the schematic diagram of the PSC. As can be seen from the schematic, a sinusoidal voltage is fed to the PSC as an input signal. The output is a sinusoidal voltage of which phase can be varied by trimming the resistance, Rp. The last operational amplifier, OP-4, is a gain changer. Note that the polarity of the output-signal is not changed, and the gain is greater than unity. The peak of the input signal should be less than the amplifier source voltage (usually, Vcc = 12 V), otherwise, the signal-waveform is distorted severely.

The transfer function of the given circuit is,

$$F(s) = \frac{V_{out}}{V_{in}} \tag{3.14a}$$

$$= \frac{1 - sCR}{1 + sCR} \tag{3.14b}$$

Since s can be replaced by $j\omega$ in the steady state, the gain $|F(s)|$ and the phase $\angle F(s)$ are given as the following.

$$|F(s)| = \frac{|1 - sCR|}{|1 + sCR|} \tag{3.15a}$$

$$= \frac{\sqrt{1 + (\omega CR)^2}}{\sqrt{1 + (\omega CR)^2}} \tag{3.15b}$$

$$= \text{unity} \tag{3.15c}$$

$$\angle F(s) = -2\arctan(\omega CR) \tag{3.16}$$

It is found from the above equations that the resistance, R_p affects the phase $\angle F(s)$. However it does not have any effects on the gain. But in practice, due to the parasitic components of the circuits, the gain amplification (OP-4) is required to control the signal gain.

As shown in Figure 3.12(b), the PSC permits continuous phase control about 0° to 180° with a unity gain of the output signal. The maximum phase-shift range is dependent on the Rp, and Cp values. For example the PSC has the maximum phase-shifts of 148.5° for Cp=0.47 μF and Rp=20 KΩ, and 173.5° for Cp=0.94 μF and Rp=50 KΩ.

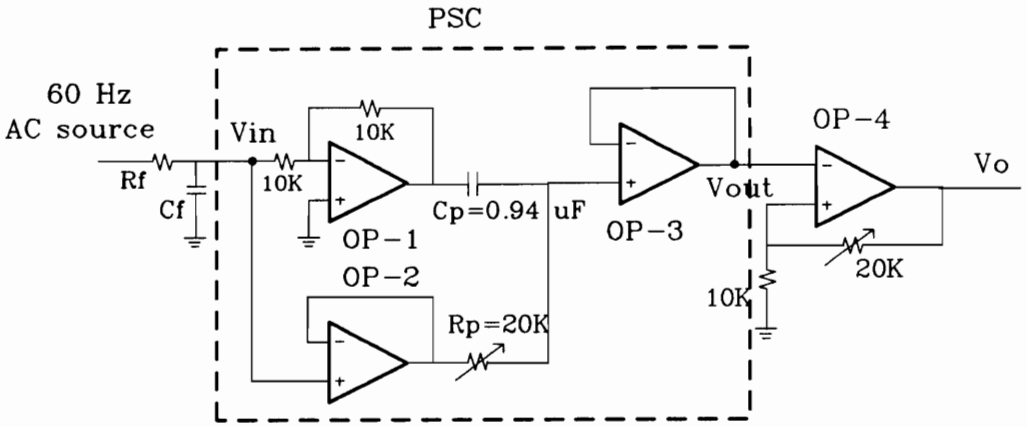

(a) Phase shifting circuit

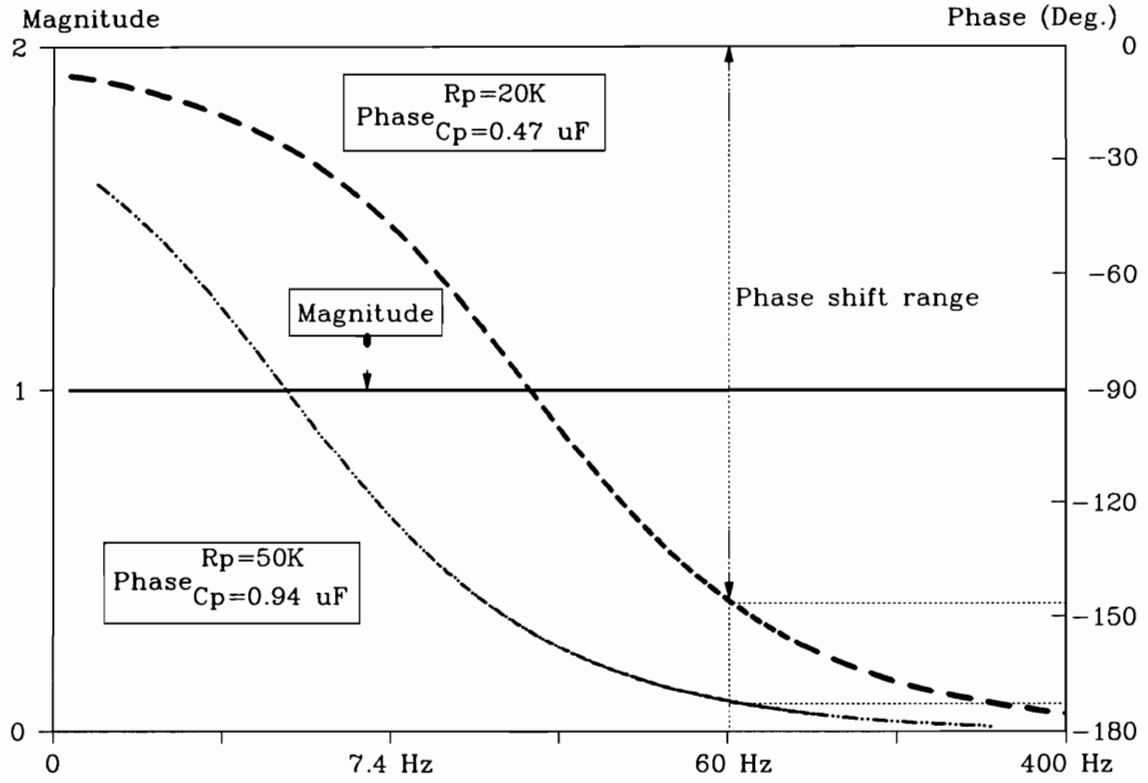

(b) Magnitude & phase of the transfer function

Figure 3.12: Phase shifting and three-phase signal generation

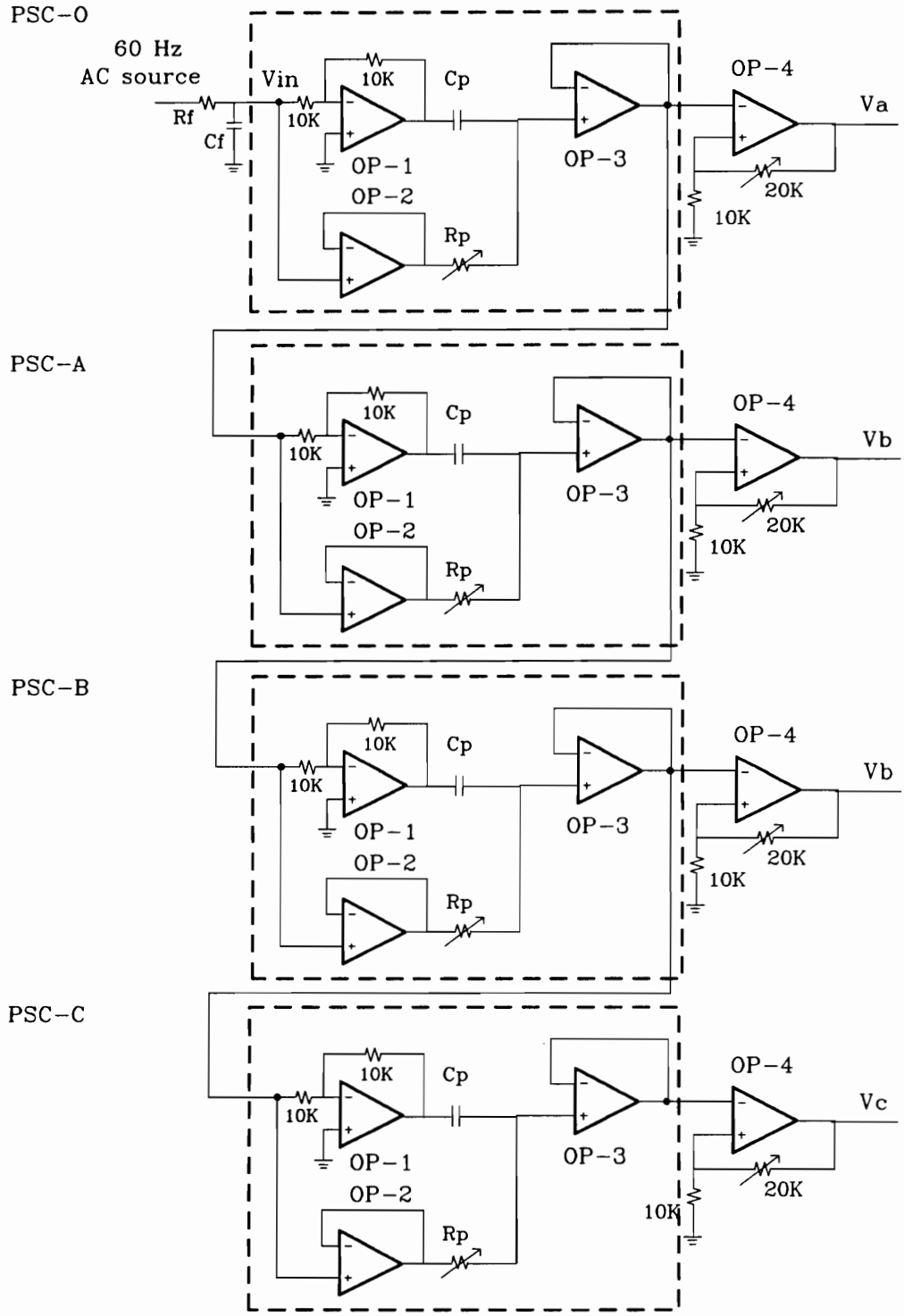

(c) Three phase sinusoidal generator

Figure 3.12: Continued

Three-phase sinusoidal generating-circuit using the PSC is shown in Figure 3.12(c). Four PSCs are cascaded in series to control the phase of the input signal as required at each stage. The reference sinusoidal input to the PSC-O is fed through a low-pass filter. The PSC-O ensures synchronization or phase shifting(α) of the generated three-phase signals with respect to the three-phase main source. The trimming resistances of the next three-PSCs are fixed (Rp=4.887 KΩ, Cp=0.94 μF) so that the PSCs have 120° of phase shift and unity gain.

Position sensing and commutation

SRM drives require the information of the rotor position as in a brushless PMSM drive. In some cases the pulse train from the shaft position sensor can be used, however, at low speeds a large number of pulses per revolution is needed. This can be obtained by using an encoder or resolver or by phase-locking a high frequency oscillator to the commutation sensor such as LED sensors. In this study, an 8 bit (in binary code) encoder is used for position sensing. An EEPROM 2864 is used as an external memory chip. It is programmed to give 5 output signals; one is for excitation signal of the front-end converter output voltage, the rest are for commutations. The clock for the chip is the LSB of the rotor position signal from the encoder. Since the LSB of the encoder generates 256 pulses per revolution the commutation timings are not even for an 8/6 pole machine which has 24 strokes per revolution. That is, each machine stroke has a different pulse-width and is calculated as,

$$\text{No. of pulses for each stroke} = \frac{\frac{256 \text{ pulses}}{\text{rev.}}}{\frac{24 \text{ strokes}}{\text{rev.}}} \tag{3.17a}$$

$$= 10.67 \frac{\text{pulses}}{\text{stroke}} \tag{3.17b}$$

This results in the uneven widths of the strokes. They are to be 11 pulses or 10 pulses. Due to the uneven machine-stroke widths, the phase currents may not be same even in the steady state. To avoid the undesirable results, high resolution encoders, or position sensors are required for high performance drives. The inter-connections of the EEPROM and the encoder including the output signals are shown in Figure 3.13. The commutation signals(Ta - Td) for the machine-side converter are directly obtained from the predetermined tables for different advance and conduction angles stored in the EEPROM.

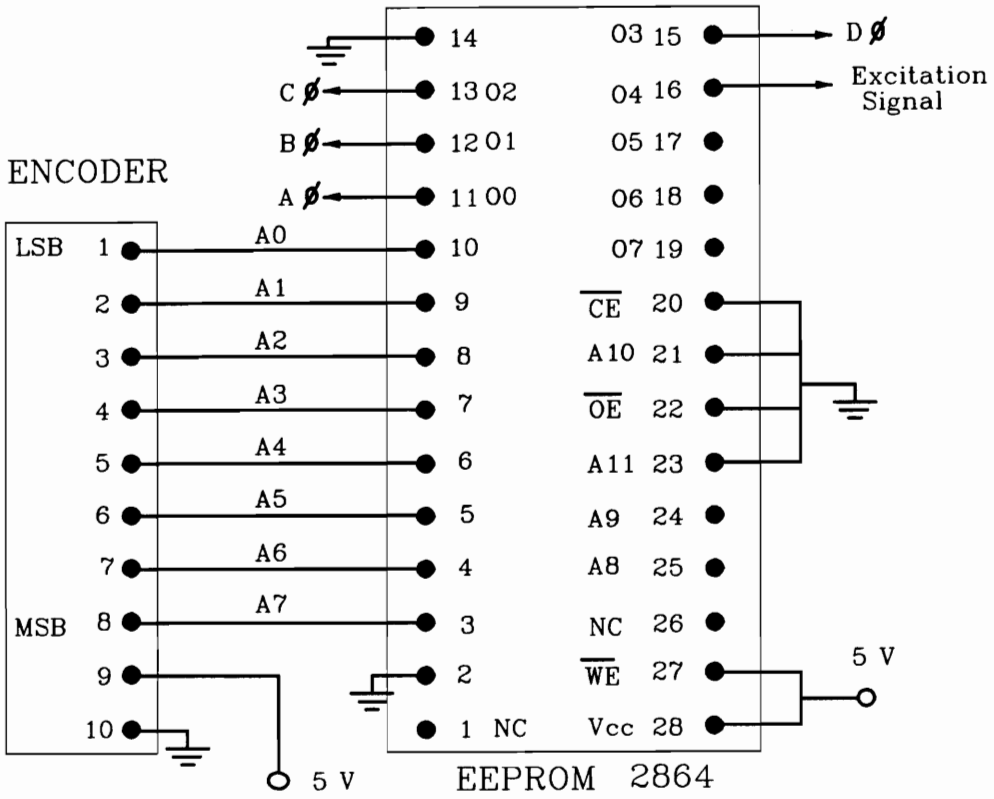

(a) Encoder and EEPROM connection

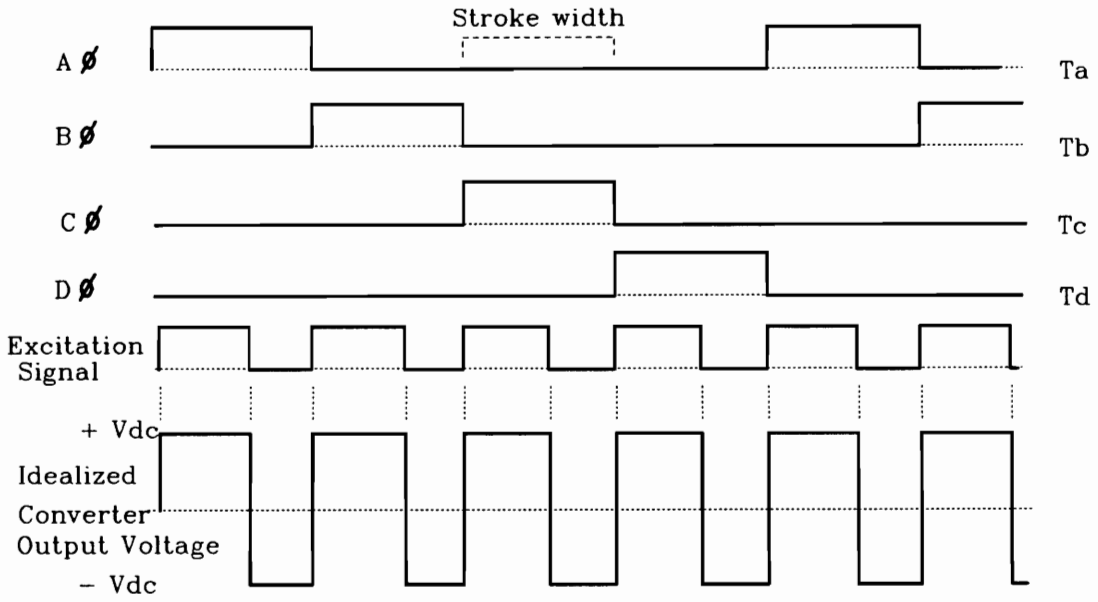

(b) Output signals and converter output voltage

Figure 3.13: Inter-connections of the EEPROM and the encoder

With the input of the rotor position, the corresponding switching signals are commanded. For a two quadrant operation of SRM controller, at least two tables are necessary. For the 8 bit encoder used in the experimental prototype, each table occupies 256 bytes. Since the current in the winding should be depleted before phase commutation occurs, the energization time is limited both in motoring and generating operations. It is commanded by the fifth signal(excitation signal) of the EEPROM(O_4) in Figure 3.13.

The direction of torque is determined by the time relationship between the instantaneous rotor position and the stator current for a particular stator pole. Thus, motoring and generating operations are easily achieved by the control signals of the machine-side converter. The control variables are the advance angle at which the phase switches(Ta - Td) are turned on, and the timing of excitation when the polarity of the voltage is reversed by the front-end converter.

3.4.3 Operation of the scheme

The most commonly used four-phase machine with 8 stator poles and six rotor poles are used in the study. Motoring and regenerative operations are explained in this subsection with the proposed scheme.

Motoring operation

In Figure 3.9, the phase current is controlled by one pair of switching devices in the front-end converter with one of the phase switches closed. If a pair of the front-end switches (one from top and the other from bottom in the different leg) with the diodes next to them forward-biased are turned on, the phase current builds up through one of the phase switch(chosen by the position sensor) in the machine-side converter. During the period, the other two switches of the same legs in the front-end converter are also turned-on with no current conduction due to the reverse-biased diodes. Two switching-signals (T1 and T4) of the same leg are depicted in Figure 3.10(b). If the two current-carrying switches are turned off to reduce the phase current, the voltage across the winding is reversed since the other two switches are already turned on and take over the current. During this time the

inductive energy is returned to the source and the current decays. In motoring operation the regenerated power is much less than the power supplied by the source. The difference of the two powers is transformed into mechanical power and consumed by the load and parts of the power is dissipated in the form of losses such as the iron, copper, windage, friction and converter losses. A high-speed motoring operation needs turn-on time to be advanced before the rising inductance point(θ_2 in Figure 3.3), when the circuit inductance is small, allowing the current to establish to the desired level before the rotor reaches the torque-producing region. High back-emf of the machine opposes the fast current build up during high speed. The speed change of the machine also demands the conduction angle variation responding to the changed inductance of the circuit and the phase current. Establishing current in the phase winding before θ_1 increases copper loss but does not generate more torque as much as the current does after θ_1. In high speed operation, the phase current never reaches the current set-point, and hence current chopping is not enforced any more, which is called single-pulse mode. Typical profiles of inductance, voltage, current and power of a phase winding are shown in Figure 3.14 for single-pulse mode operation.

Generating operation

When operating in generation mode, the objectives of control are to operate the system at the maximum efficiency and power. In this operation, the current pulse is positioned to occur while the rotor pole is departing from the stator pole (i.e. during negative inductance slope), then the current shape in Figure 3.14 (c) is a duplicate of mirror image of the motoring operation, shown in Figure 3.14(a). However, since there are no windings or permanent magnets on the rotor, an external setup of the magnetic field is necessary. Therefore, excitation from the source is required, and in this period energy is taken both from the supply and the shaft, and is stored in the field. After the excitation period the energy is returned to the source from the shaft with the magnetic field energy. Even in the generating mode, phase advancing of current is required at high speed to establish a desired current. But too much advance of the control signal will result in decreased generating power. The extreme case is shown Figure 3.14 (b), in which almost no net power-flow is measured in the dc link.

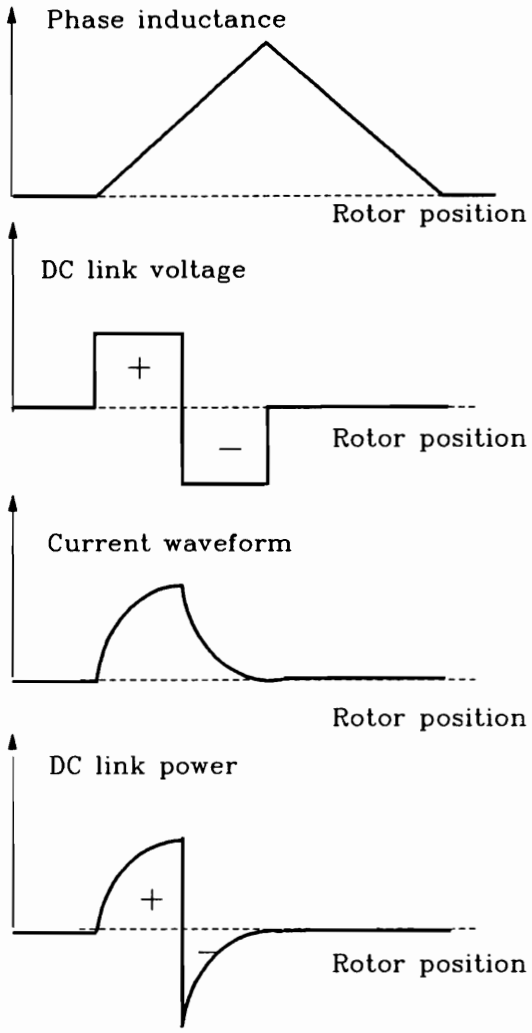

(a) Motoring characteristics

Figure 3.14: Relationship of inductance, voltage, current and power

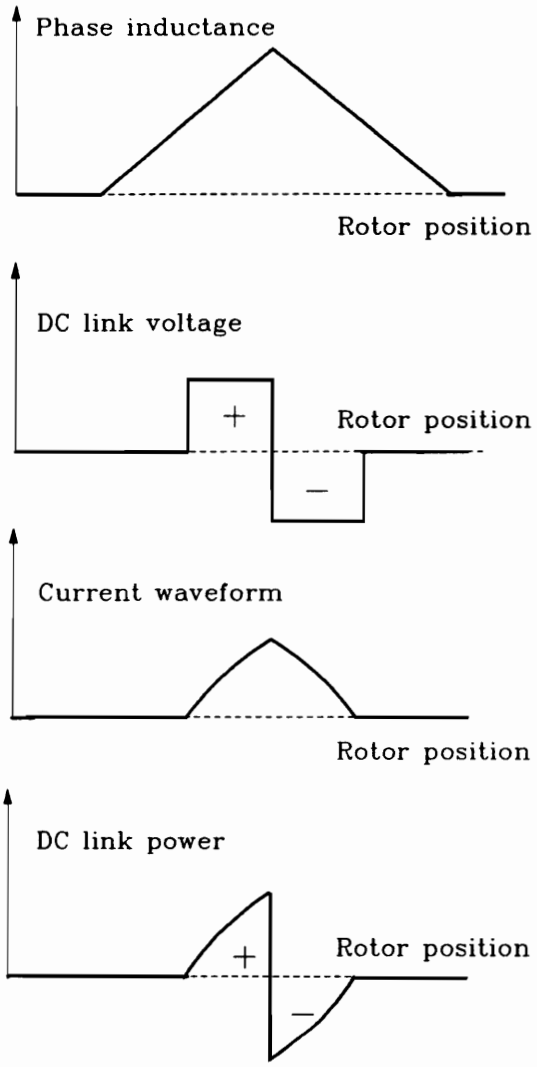

(b) Generation characteristics with extremely advanced current

Figure 3.14: Continued

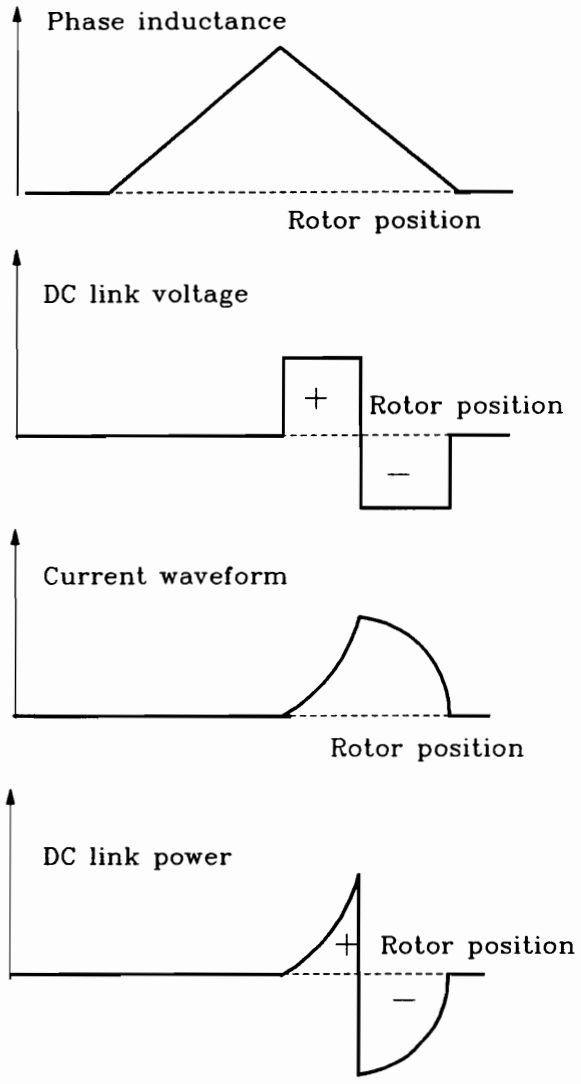

(c) Generation characteristics

Figure 3.14: Continued

On the contrary, retarding too far will also produce positive torque(motoring operation) because current is flowing during positive inductance slope. Since these limits are functions of the machine geometry, special care should be exercised at the machine design stage.

3.4.4 Design of the converter

The SRM drive, unlike other machines, can not operate without its power converter. It is known that the variable speed SRM drive offers a high system efficiency over a wide range of torque and speed. Various attempts have been made to estimate the converter volt-ampere ratings from linear and quasi-linear models of the SRM, but due to its nonlinear characteristics, none of them was complete. In this section, some design aspects about the SRM converter-design are provided.

Current rating

The current rating is defined as peak current rating and continuous current rating which is equal to, or greater than the rms current. Assuming flat-topped current pulse, the peak and rms current ratings are given in equations (3.8) and (3.9b), respectively. For convenience, they are rewritten,

$$I_{peak} = \frac{P_o}{\eta_s D V_{dc}} \tag{3.18}$$

where P_o is the peak output, D is the duty ratio, V_{dc} is the dc source voltage, and η_s is the efficiency of the system.

$$I_{rms} = \sqrt{\frac{1}{2\pi}\int_0^{\theta_c} {I_p}^2 d\theta} \tag{3.19a}$$

$$= \sqrt{\frac{\theta_c}{2\pi}} I_p \tag{3.19b}$$

if $\theta_c = \frac{2\pi}{q}$ then $I_{rms} = \frac{I_p}{\sqrt{q}}$ where q is the number of phases, θ_c is the conduction angle for each phase, and I_p is the peak current value.

Since all the semiconductor devices (T1-T6, D1-D6, Da-Dd and Ta-Td) constitute the current path in series, and the converter does not allow any current overlap, the devices

have the same the peak current rating. The number of switches in the front-end converter is solely dependent on the number of phases of the supply, which is usually three-phase. Thus, the device counts are fixed such as six diode-switch(switching-block) pairs. One pair of switching block conducts when power is processed through the converter. Therefore the rms rating of the front-end converter may be differently defined in single pulse mode as the following.

$$I_{FCrms} = \frac{P_o}{\sqrt{p}\eta V_{dc}} \tag{3.20}$$

where, p is the number of supply phases, $V_{dc} = 1.35V_{ll}$, and V_{ll} is the rms line to line voltage of the three-phase supply. Then the machine side converter rms current rating is determined as follows.

$$I_{MCrms} = I_{FCrms}\frac{\sqrt{p}}{\sqrt{q}} \tag{3.21}$$

where, q is number of machine phases.

Voltage rating of the devices

Despite the cascaded connections of diode-switch in a switching block the voltage blocking is not shared by the two devices because each device blocks different polarity voltages. Thus, the minimum voltage rating of each device is dependent of the source voltage and is given

$$V_{min} = \sqrt{2}V_{ll} \tag{3.22}$$

where V_{ll} is the rms line to line voltage of the ac source. However due to the transient voltage at commutation and at turn-off, some voltage margin is desirable.

Input side capacitor

When the switches of the same leg in the front-end converter are turned off, the ac line current need a path to flow and it is provided by the capacitors in the ac supply. Their minimum voltage rating and sizes are given by

$$V_{min} = \sqrt{2}V_{ll} \tag{3.23}$$

$$C = L_l\left(\frac{i_m}{V_{min}}\right)^2 \tag{3.24}$$

where, L_l is the stray inductance of the circuit and i_m is the maximum instantaneous current when the two switches are turned off.

3.4.5 Theoretical and experimental results

Theoretical results

The voltage across a phase winding is closely associated with the flux linkage(of a winding) which varies cyclically with rotor position, θ and phase current i. From the equivalent circuit for SRM phase winding shown in Figure 3.15(a), the general voltage equation for a phase winding is given by

$$\begin{aligned} \pm v_{dc} &= iR_e + \frac{d\Psi(\theta,i)}{dt} && (3.25a) \\ &\quad + \text{nonlinear circuit-component voltage-drop} \\ &= iR_e + L(\theta,i)\frac{di}{dt} + i\frac{dL(\theta,i)}{dt} - M(\theta,i)\frac{di}{dt} && (3.25b) \\ &\quad + \text{nonlinear circuit-component voltage-drop} \end{aligned}$$

where, R_e is the circuit equivalent resistance including winding resistance(R_w), M is the mutual inductance due to coupling between phases, L is self inductance.

Neglecting the nonlinear circuit-component voltage drop, the circuit resistance except winding resistance, and assuming self inductance L in independent of current, the equation is given by

$$\begin{aligned} \pm v_{dc} &= \frac{d\Psi(\theta,i)}{dt} + iR_w && (3.26a) \\ &= L\frac{di}{dt} + i\frac{dL}{dt} + iR_w && (3.26b) \\ &= L\frac{di}{dt} + i\frac{dL}{d\theta}\frac{d\theta}{dt} + iR_w && (3.26c) \\ &= L\frac{di}{dt} + i\frac{dL}{d\theta}\omega + iR_w && (3.26d) \end{aligned}$$

where, $\omega = d\theta/dt$, the rotational angular speed. Therefore the equivalent circuit diagram becomes as shown in Figure 3.15(b).

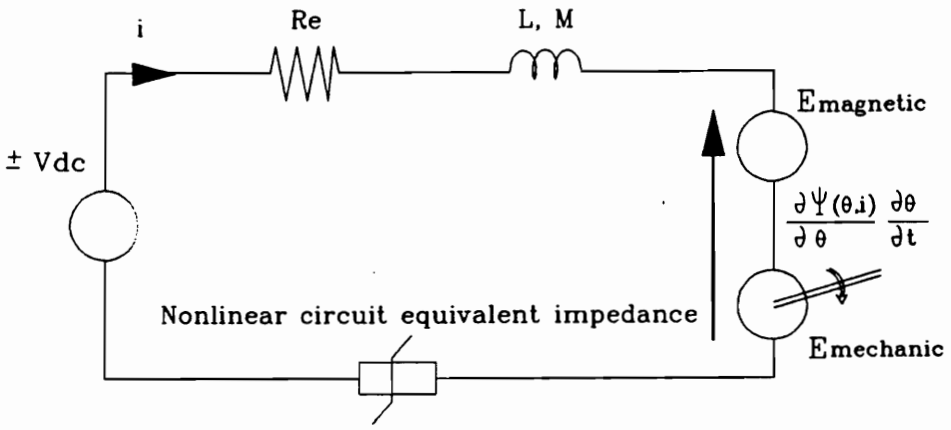

(a) Equivalent circuit of a phase winding

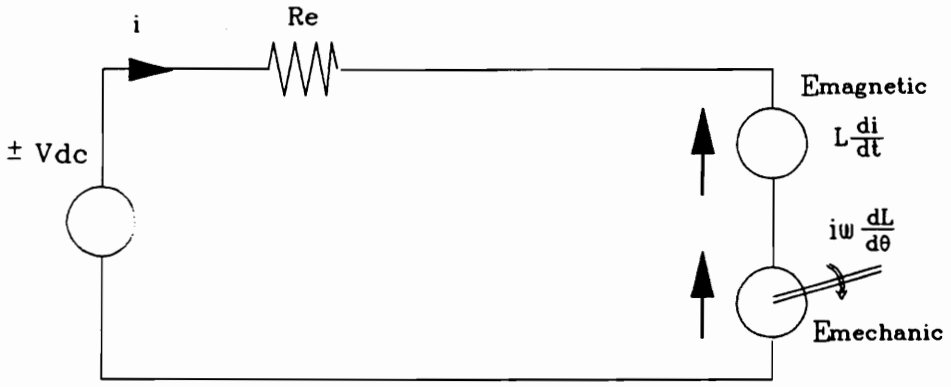

(b) Simplified equivalent circuit

Figure 3.15: Equivalent circuit of a phase winding

The instantaneous electric power to a phase winding is given by

$$P_W = \pm v_{dc} i \tag{3.27a}$$

$$= Li\frac{di}{dt} + i^2\omega\frac{dL}{d\theta} + i^2 R_w \tag{3.27b}$$

$$= \frac{d}{dt}(\frac{1}{2}Li^2) + \frac{1}{2}i^2\omega\frac{dL}{d\theta} + i^2 R_w \tag{3.27c}$$

$$= P_{Wmagetic} + P_{Wmechanic} + P_{Wcopper} \tag{3.27d}$$

The first term of the equation is the variation of the stored magnetic field-energy in a phase winding, the last term stands for the winding copper-loss. The term in the middle of the equation represents the mechanical power output and it may be expressed alternatively as

$$P_{Wmechnic} = T_e\omega \tag{3.28}$$

where T_e is the electromagnetic torque. In motoring operation, T_e is positive in polarity, but in generation mode it becomes negative. It implies that if mechanical power is externally supplied in the generation mode, the machine can generate electric power. The mechanical equations describing the interactions between the load torque T_l and the electromagnetic torque is given by

$$J\frac{d\omega}{dt} + B\omega = T_e - T_l \tag{3.29}$$

$$\frac{d\theta}{dt} = \omega \tag{3.30}$$

where J is the moment of inertia, and B is the coefficient of viscous friction. Flux linkage in each phase and rotor position are obtained by solving the differential equations (3.26a), (3.29) and (3.30) using numerical integration. Since flux linkage and rotor position are known, the phase current can be found from the $\Psi(\theta, i)$ data.

The predicted results of the scheme in the steady state are obtained using Backward-Euler method for the solution of differential equations. The results shown in Figure 3.16 includes phase-voltage, line-current and instantaneous power for ac source, and phase voltage, current and inductance variation for the SRM machine. The commanded speed and torque profiles are also available. The front-end converter is basically phase-controllable. Therefore, the current can flow at any phase of the source voltage.

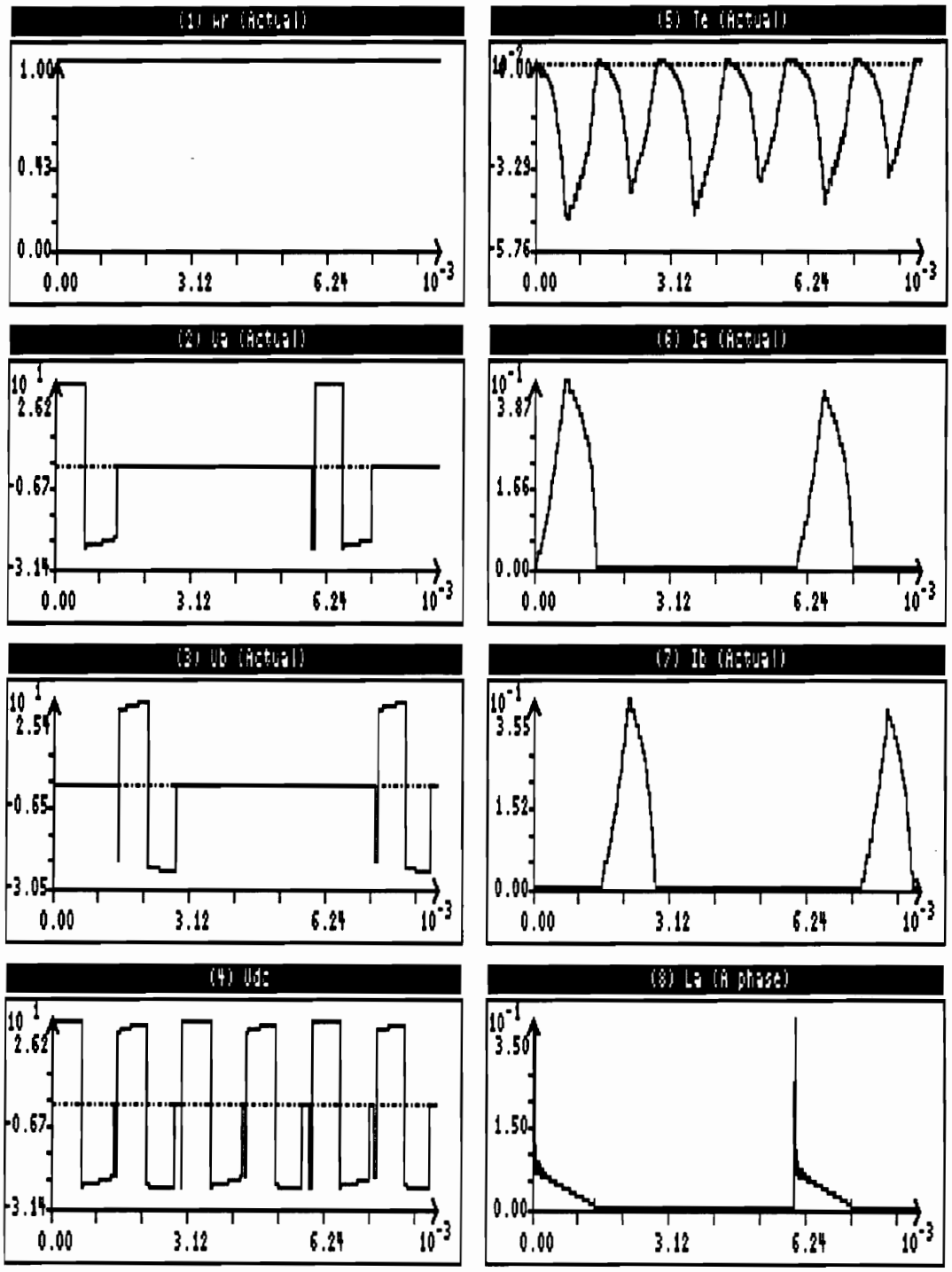

Figure 3.16: Theoretical results of a VSCF with an SRM

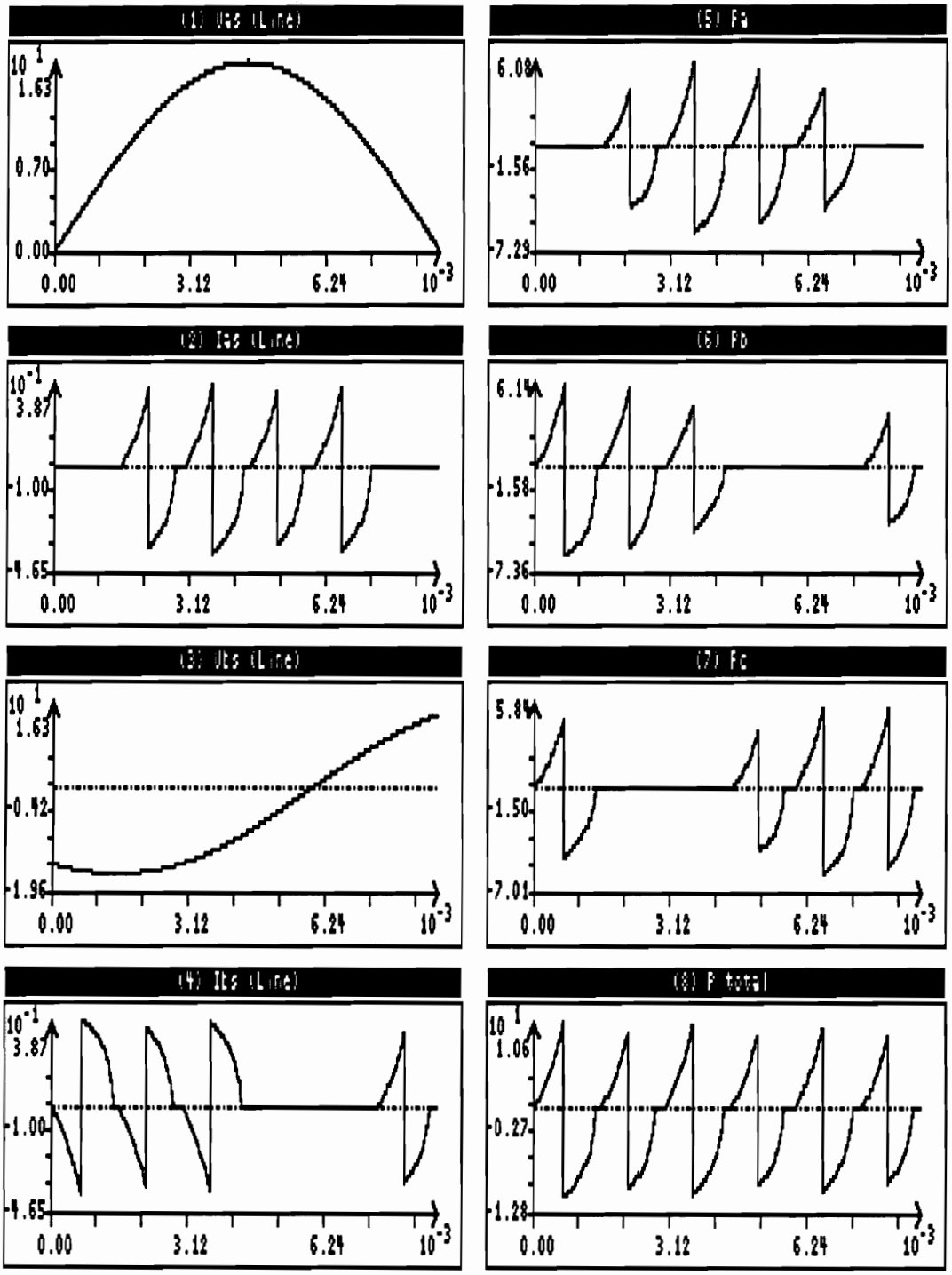

Figure 3.16: Continued

The phase relationship between the phase voltage and current shown in the results is set at $\alpha = 0°$, similar to a thyristor-based phase-controlled rectifier. Dc link voltage is maximized at the activation angle. The instantaneous dc link power(P_o) and shaft-power(P_i) are determined by

$$P_o = \frac{1}{N}\sum_{i=0}^{N-1} v_a(t_i)i_a(t_i) + v_b(t_i)i_b(t_i) + v_c(t_i)i_c(t_i) \tag{3.31}$$

$$P_i = \frac{1}{N}\sum_{i=0}^{N-1} T(t_i)\omega(t_i) \tag{3.32}$$

where, N is the number of simulation points, $v_a(t_i), v_b(t_i)$ and $v_c(t_i)$ are the phase voltages at time of t_i, $i_a(t_i), i_b(t_i) and i_c(t_i)$ are the line currents, $T(t_i)$ and $\omega(t_i)$ are the shaft-torque and the rotational angular-speed, respectively. 2.5 μs of time step is used in the digital computer simulation. Consequently, the system efficiency across the machine is defined as,

$$\eta = \frac{\text{Output power from dc link}}{\text{Input power to the shaft}} \tag{3.33a}$$

$$= \frac{P_o}{P_i} \tag{3.33b}$$

Experimental results

The feasibility of the scheme is verified by the comparison of the theoretical and experimental results. The oscillograms of the dc link voltage and current are found in Figure 3.17 (a). With the same time scale at the machine speed of 1800 RPM(1 pu), the instantaneous power waveform is shown in Figure 3.17 (b) which contains the dc link current, too. In power waveform instrumentation, a multiplication chip, XR-2208, is used. The chip has bandwidth of 8-MHz. The dc link current and the attenuated dc voltage are two inputs to the chip, and the power is directly measured at the output pin. From the measured value the actual power is calculated by

$$P_o = k_s k_v k_i \times \text{ Measured voltage at chip terminal} \tag{3.34}$$

where, k_s, k_v and k_i are chip scale factor, voltage gain and current gain, respectively.

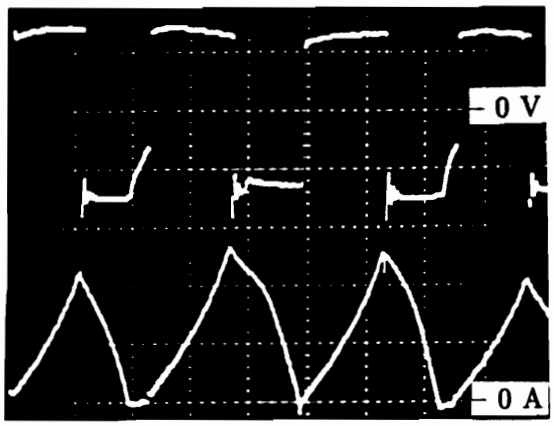

10 V/div

0.2 A/div

0.5 ms/div

(a) Dc link voltage and current

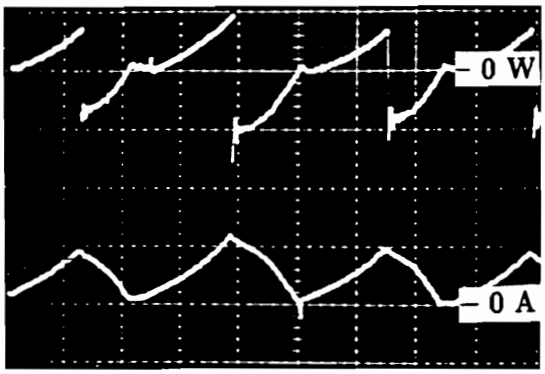

11 W/div

0.5 A/div

0.5 ms/div

(b) Dc link power and current

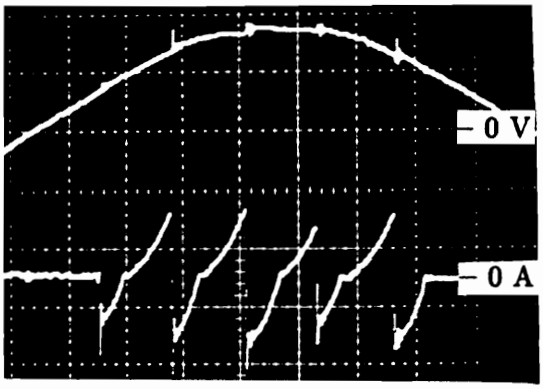

10 V/div

0.5 A/div

1 ms/div

(c) Ac phase voltage and line current

Figure 3.17: Experimental results of a VSCF with an SRM

Since the voltage is a bipolar quasi-square wave, the instantaneous power waveform is almost a linear expansion of the current in magnitude except polarity change due to the voltage polarity. The oscillations in the power waveform come from the voltage oscillations at the moments of commutation. It is due to the switching of a highly inductive circuit. Figure 3.17 (c) shows the waveforms of phase-voltage and current of the ac mains. The humps in the voltage can be removed by using a low pass filter on the supply side. The bipolarity current explains that only one current path is provided for the field energization and regeneration. In other words, only two phases out of the three phases of the supply are used as the current path at a given time.

Two operation modes are discussed in the following using the expanded current and power waveforms. These waveforms also validate the profiles shown in Figure 3.14.

Motoring mode: As shown in Figure 3.14 (a) a motoring torque is produced by energizing a phase winding during the period when the inductance is increasing. The machine takes power from the ac source up to the point where commutation occurs. The energy taken from the three-phase mains is converted to mechanical output, magnetic field energy and is partly lost in the converter and machine. After the point where commutation occurs, the stored field energy is partly returned to the source, and during this period the front-end converter changes the polarity of the dc link voltage. Some of the field energy is converted to further mechanical output and losses. The converter and machine also take parts of the energy in the form of losses. Experimental measurements of the dc-link current and power in the motoring mode is shown in Fig 3.18 (a), where the net average power is positive.

Generation mode: If a phase winding is energized, while the rotor is moving away from the fully aligned position (i.e. during the decreasing inductance), power is generated. Figure 3.18 (b) is taken after advancing the current far from the generation mode. The winding is energized by taking energy from the source during inductance rising period (producing positive torque) and it returns energy to the source during inductance decreasing period (taking energy from the shaft). The waveforms are taken with the machine running. In this operation, no average power was measured in the dc link.

That is, during the generation mode the machine returns power as much as it has taken from the source during the motoring mode. The current takes the shape shown in Figure 3.18 (c) , which is a mirror image of Figure 3.18 (a). During the rising current portion, the machine takes energy from the three-phase mains and shaft, and stores energy in the field. During the generation period, the system takes energy from the shaft and returns it to the source.

Figure 3.19 contains the impacts of the current advancing angle, θ_a on the output power. It depicts the output power on the ideal phase-inductance profiles as a function of rotor position. For dwell angle, $\theta_c = 7°$ and speed of 1800 RPM, power output at dc link are predicted at two voltage levels, $v_{dc} = 0.5$ and 1.0pu. Experimental results have been taken for $v_{dc} = 0.5$pu. The results show that the maximum power is obtained with a significant retarding of θ_a. To maximize the power output, the excitation current should attain its rated value. But, the advance of θ_a more toward the peak inductance with constant θ_c opposes the increase of current. For the given conditions, the system gives the maximum output power around 39° from the unaligned rotor position.

The output power and efficiency at various speed are included in Figure 3.20, for $\theta_a = 39°$ and $\theta_c = 7°$. The maximum power is predicted and measured near the machine speed of 0.8 pu as shown in Figure 3.20 (a). Decreasing speed reduces the power output of the machine, and in a high speed range the desired current can not be attained due to short rising time and high back-emf. The efficiency shown in Figure 3.20 (b) is almost constant for the entire operating speed range. It can be explained by the comparable losses; copper losses in the low speed range and windage/frictional losses in the high speed range.

3.5 Conclusion

In this chapter, the operation of SRMs was studied in detail. The discussion includes the basic principles of SRM drive, topology review and the application of SRM to VSCF scheme using a new converter topology. The inherent nonlinearity of the machine has been explored using the characteristics such as output power and efficiency vs. speed and output power vs. current advancing.

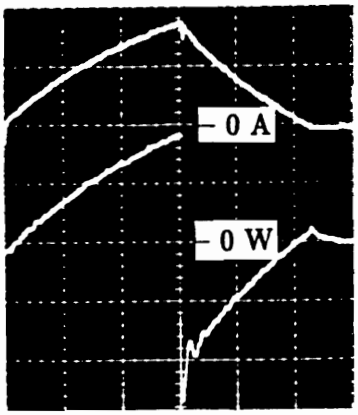

0.2 A/div

4.4 W/div

0.2 ms/div

(a) Winding current and power in motoring mode

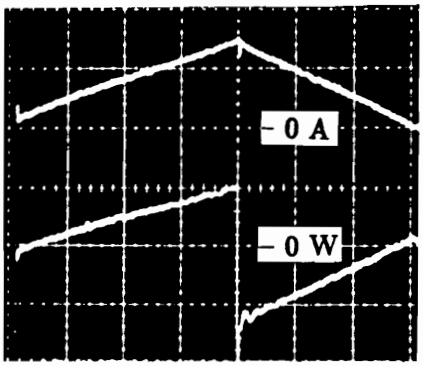

0.2 A/div

4.4 W/div

0.2 ms/div

(b) Misplaced–current operation

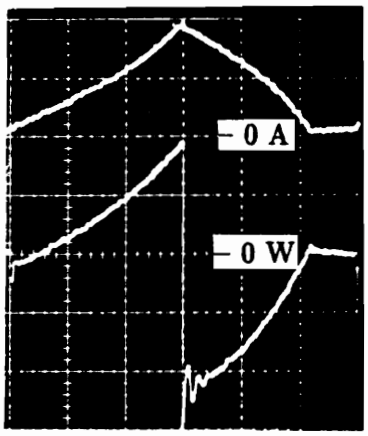

0.2 A/div

4.4 W/div

0.2 ms/div

(c) winding current and power in generation mode

Figure 3.18: Current and power flow of a phase winding in each operating mode

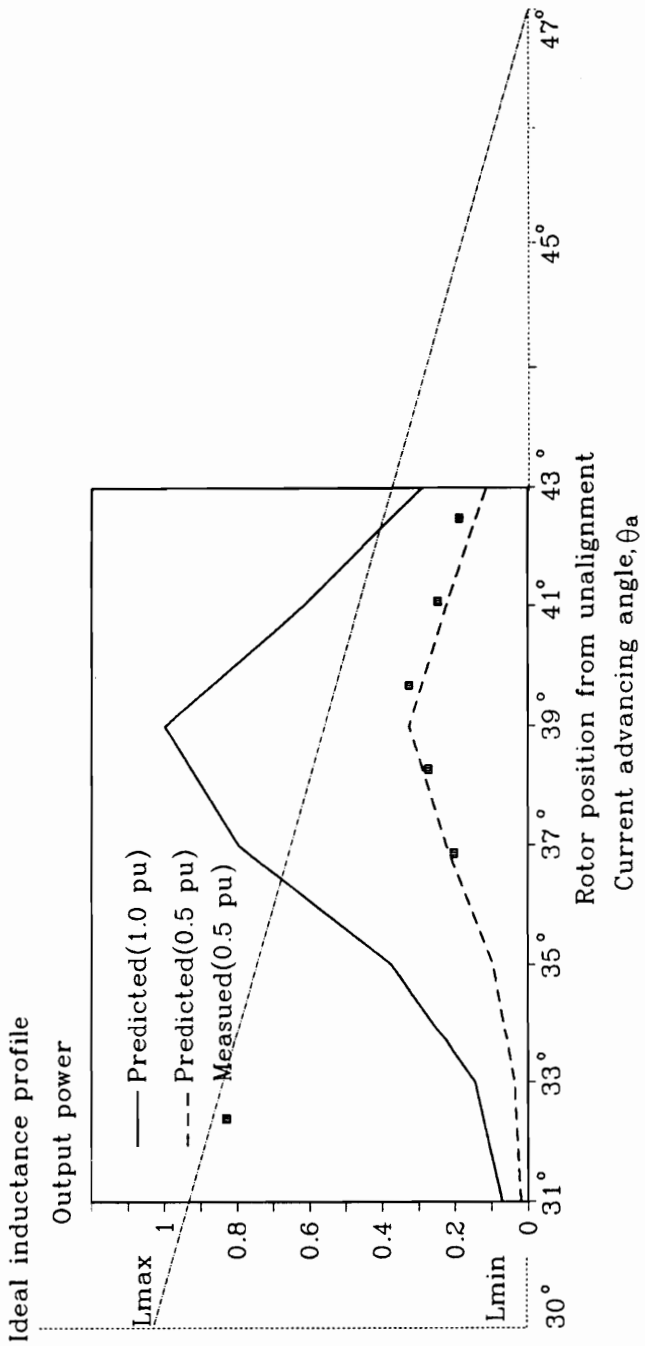

Figure 3.19: Output power vs. rotor position

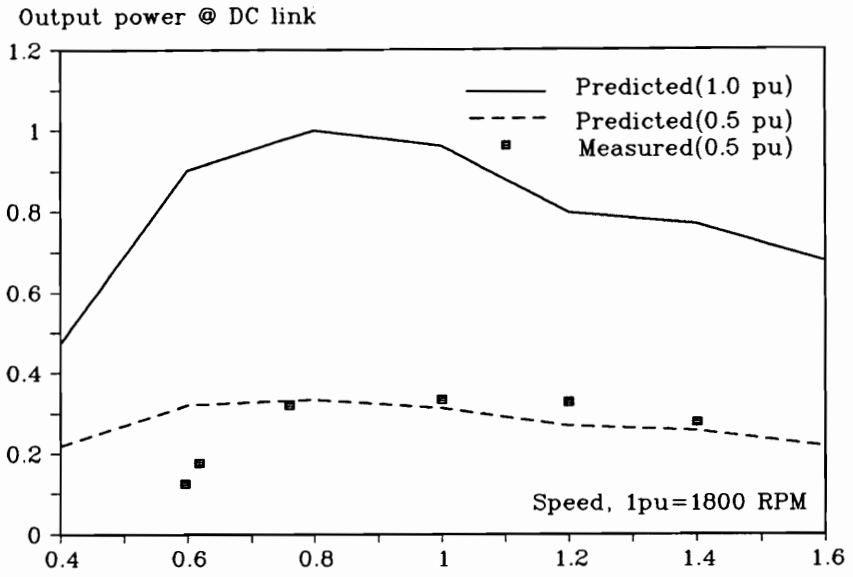

(a) Output power vs. speed for 0.5 and 1.0 pu of Vdc

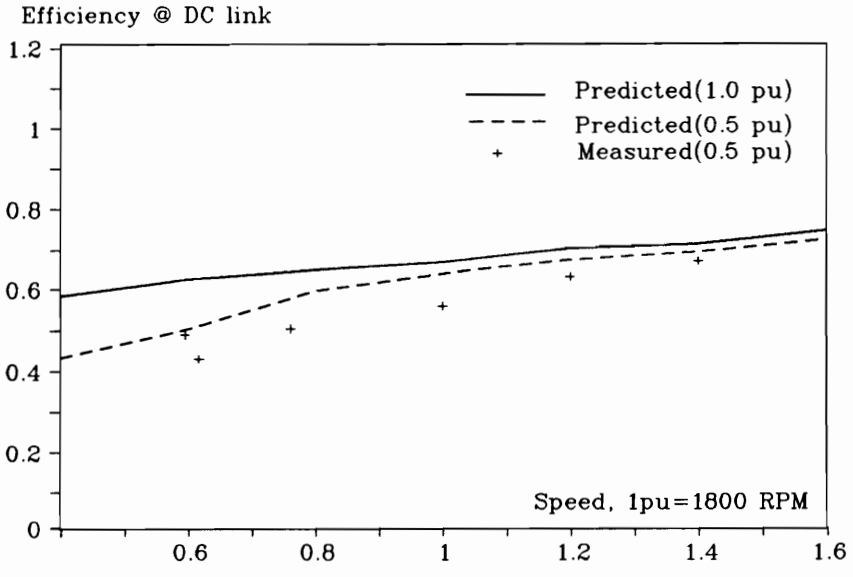

(b) Efficiency vs. speed for 0.5 and 1.0 pu Vdc

Figure 3.20: Impacts of speed change on output power and efficiency

The proposed topology has distinct features such as unidirectional current-flow and bipolarity of dc-link voltage. The topology is able to convert power directly from three-phase ac source to an SRM and vice versa without any dc link capacitor. However, simulation results of the converter show large ripple in the torque due to the lack of current overlapping capability, which results in acoustic noise. Through this study, the possible use of SRMs in the VSCF applications is clearly confirmed by the good correlation between the theoretical and experimental results with respect to the following characteristics.

(i) Phase voltage and line current in the ac source.

(ii) Voltage and power in the dc link.

(iii) Winding current and inductance profiles.

(iv) Relationships between power and efficiency vs speed.

(v) Relationship between power vs current advancing angles.

Based on these observations, the following original contributions are made in the study of VSCF power conversion scheme with the SRM:

(i) A novel VSCF power conversion scheme with the SRM has been proposed.

(ii) The converter topologies with no dc link capacitor have been proposed. This feature enhances the reliability of the power conversion scheme and reduces the weight of the converter system.

(iii) The proposed converter topologies directly links the constant frequency ac source to the SRM and they provide for four quadrant operation. This feature makes it attractive for starter-generator applications such as in aerospace, hybrid electric vehicles and remote power stations.

(iv) Various control modes of the proposed scheme have been studied, modeled and analyzed, and experimental correlation is obtained on many key issues.

(v) The feasibility of the proposed VSCF power conversion scheme is demonstrated both by simulation results and experimental verification.

Chapter 4

AN AC TO DC POWER CONVERSION SCHEME

VSCF schemes supply various three phase and single phase loads. Most of these loads are variable speed ac or dc motor drives. Under these circumstances, unity power factor and distortion free operation of theses drive schemes is desirable. Phase-controlled ac to dc power conversion has the disadvantages of low power factor and harmonic pollution on the utility side, particularly in the case where dc voltage regulation is required. This chapter presents a one-stage single-phase controlled rectifier which has a wide output variation on the dc output while maintaining unity power factor and sinusoidal current on the input side. This scheme also provides galvanic isolation which is required in most industrial applications with a transformer of small size, compared to the ones used with the phase-controlled converters. Three control strategies for the operation of the converter are proposed and verified experimentally. The harmonic spectra on the ac and dc sides are analytically derived. The low frequency harmonics of the ac line current have been eliminated by PWM and higher orders could be filtered out depending on the control strategies.

Nomenclature

L_s, C_s	Inductance and capacitance of low pass filter
f_c	PWM carrier frequency
f_r	Resonance frequency of a notch filter
C_i, C_t	Ac capacitances for inductive currents
k	Number of pulses per cycle
D	Duty ratio
I_o	Fundamental component of ac line current
I_n	n-th order hamonics of ac line current
V_s	Rms voltage of ac source
V_o	Fourier series of dc output voltage
V_{dc}	DC component of output voltage
θ_{ii}	Dividing point of i-th pulse for control strategy III
θ_{i1}	Chopping point on pulse leading edge for control strategy III
θ_{i2}	Chopping point on pulse tailing edge for control strategy III

4.1 Introduction

In ac to dc power conversion, it is timely to consider the minimization of its negative impacts on the ac utility such as low power factor and harmonic distortion. Even though the standards on power factor and harmonics have not been enforced, utilities are expected to demand better quality because of poor power factor operation resulting in over-sizing of the power conductors and continuing degradation of the power quality. Line-filter capacitor of a diode-bridge or a phase-controlled rectifier causes short duration of conduction which in turn results in large pulse-currents. Such pulse-currents are rich in harmonics and have the following disadvantageous features:

(i) They might introduce unnecessary tripping of the protective circuit breakers.

(ii) They need over-sized EMI filters.

(iii) They cause more losses in the power device due to higher peak current for the same power rating requiring better thermal management of the converter.

To separate the effect of the faults on the dc side and surge from the utilities, transformer ohmic-isolation is a usual practice in the industrial applications. In this chapter a single-phase PWM ac to dc converter has been studied to offset and minimize these problems. High-frequency switching PWM converter can reduce the size of the EMI filters, the heat sinks, and the isolation transformer, thus minimizing weight, size, and cost of the converter.

4.2 Description of Systems and Ratings

4.2.1 Operation principles

Referring to Figures 4.1 and 4.2, the scheme consists of four bilateral switches, a high frequency transformer, and a diode bridge rectifier, and low pass filter on ac side. Output filter is optional and is excluded in the study.

The control logic is designed to synchronize two pairs(S1 & S4, S2 & S3) of switches in Figure 4.1. To apply a high frequency voltage across the transformer from 60 Hz source, the source voltage has to be chopped at a certain rate. If the chopping points are determined by control strategy, one voltage pulse out of every two is applied in one direction across the transformer winding, and the next pulse in the other direction as shown in Figure 4.3. It shows a simulated voltage waveform across the transformer primary winding, in which every pulse has equal area(i.e. equal volt-second). Thus, the source seen from the transformer is high frequency ac voltage.

4.2.2 AC filter ratings; L_s, C_s, C_i and C_t

L_s and C_s are determined on the basis of the carrier frequency of the converter. In the PWM converter, with a carrier-frequency of f_c, the first two lowest harmonics are $f_c \pm$ 60 Hz. These harmonics can be screened with a notch filter with a zero or a pole at the resonant frequency, $f_r = f_c$.

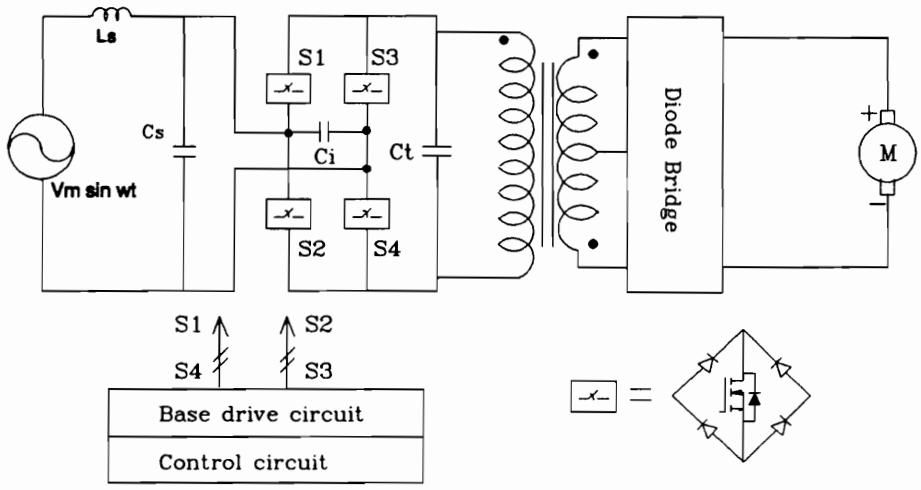

Figure 4.1: Overall power conversion scheme

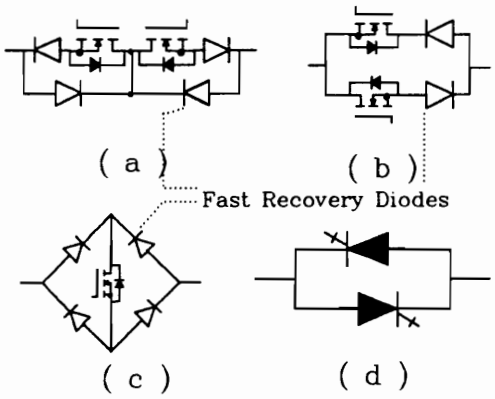

Figure 4.2: Bilateral switches

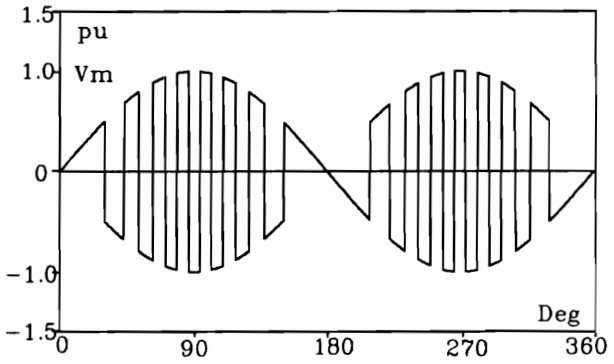

Figure 4.3: Equal volt-second chopping

In the case of a PWM converter with the ac source frequency of f_s and carrier frequency of f_c Hz, (where $f_c = kf_s$, and k is integer), the low-order harmonics can be filtered with an inductance of L_s and capacitance C_s, where

$$L_s = \frac{1}{4\pi^2 (kf_s)^2 C_s} \tag{4.1}$$

and k is the order of the harmonic.

Due to the high-frequency transformer-leakage inductance and the stray inductance of the circuit during turn-off of both the switches in the same leg, the current needs a paths to flow. They are provided by C_t and C_i. Their minimum voltage ratings and size ratings are given by

$$\text{Minimum voltage rating of } C_t(\text{ or } C_i) = V_m \tag{4.2}$$

$$C_t(\text{ or } C_i) = L_l(\frac{i_m}{V_m})^2 \tag{4.3}$$

where, where V_m is the peak voltage of the ac source, L_l is the sum of the transformer leakage-inductance and the stray-inductance of the circuit, i_m is the maximum current to be switched off by the bidirectional switch.

4.2.3 Bilateral switches

Four configurations of bilateral switches shown in Figure 4.2 can be considered in the scheme. The switch configuration shown in Figure 4.2 (a) is made of two active switches and four fast-recovery diodes. This arrangement has more loss due to higher voltage drop of two fast-recovery diodes. In manufacturing process the fast-recovery diodes have more recombination-centers, compared to the regular ones and those impede the current flowing. Figure 4.2 (b) has low voltage drop. Thus, it is more advantageous for high-frequency application. The switch structure of Figure 4.2 (c) is easy to control because only one unidirectional-switch is used with a diode-bridge and this has the same voltage drop as 4.2 (a). The last, Figure 4.2 (d), comprises two four-layer semiconductor devices which have no body diodes and have self turn-off functions in them such as IGBT's and GTO's. GTO's doped with heavy metal(without anode short) can withstand high reverse voltage, and it draws large current from gate circuitry when switched on and off. However, since the presently available IGBT's do not have reverse blocking capability, series diodes may

be required. In this study the third configuration with the fast recovery blocking-diodes is used due to the simplicity of the operation. When the high voltage fast-recovery diodes are considered, four-diode configurations are more expensive compared to the two-diode two-active switch configurations. If the loss and heat dissipation are the major concerns, then the structure, 4.2 (d) is recommended. Neglecting the stray inductance of the circuitry, the diode and the switching-device ratings are dependent on the power output which the converter deals with.

$$\text{Minimum voltage rating} = V_m. \tag{4.4}$$

Considering the stray inductance of the circuit and the leakage inductance of the transformer, a margin is required for the voltage rating to account for a voltage spike at turn off. Assuming the transformer ratio, n=1,

$$\text{Current rating} = \frac{1}{2}\frac{VA}{V_m/\sqrt{2}} \tag{4.5}$$

where VA is the volt-ampere of the transformer or the power rating of the scheme.

4.2.4 High-frequency transformer

The center-tapped transformer is preferable to reduce the voltage drop due to diodes. Once the VA rating of the transformer is decided, other subsystem ratings follow subsequently.

4.2.5 Diode bridge

High-frequency transformer necessitates a fast-recovery diode-bridge and its ratings are as follows:

$$\text{Minimum voltage rating} = \sqrt{2}V_s \tag{4.6}$$

$$\text{Current rating} = I_s/\sqrt{2} \tag{4.7}$$

where V_s and I_s are the transformer secondary rated voltage and rated current, respectively.

4.3 Control and Operation of the Scheme

Three control strategies are developed and compared from the viewpoints of harmonic spectra and ease of operations. Particular attention has been directed in eliminating the

low order harmonics on the ac side to reduce the input filter size. The requirement of high-frequency transformer is explicable by the requirement of high power density, low cost and compactness, etc. However, due to the non-sinusoidal voltage applied across the transformer in the scheme, some care is necessary in the use of the transformer to avoid core saturation. A design consideration of the transformer required by all the control strategies of the proposed scheme is that flux-linkages are balanced in each cycle. In this scheme, however, due to sine-wave characteristics the volt-second area is not equal, if it is chopped at equal time interval. However, by varying the chopping interval, the sinusoidal voltage can be chopped such that each pulse has the same volt-second. In that case, the minimum switching interval for the equal volt-second area occurs at near the peak, where the pulses are almost square waveforms. Therefore, the switching frequency for the same volt-second area is the highest near the peak as shown in Figure 4.3. From the discussion, it can be inferred that the cause of the transformer saturation is the pulses near the peak when the pulses at equal intervals of a sinusoidal voltage are used as inputs to the high frequency transformer.

Using the simulation results the merits and demerits of each strategy are discussed in the following. The analytical expression for the harmonics of the ac line-current is also derived for the last two strategies.

4.3.1 Strategy I: Constant-interval chopping strategy

This strategy is developed using double edge modulation. For clarity, only a resistive load with no filters on both ends of the scheme is considered with low carrier-frequencies throughout the discussion. Each pulse shown in Figure 4.4 (b), or (d) has the same area (or volt-second). Every other pulse is applied to the transformer winding in the opposite polarity as shown in Figures 4.4 (a) and (c). Thus, the magnetic resetting is achieved in the transformer.

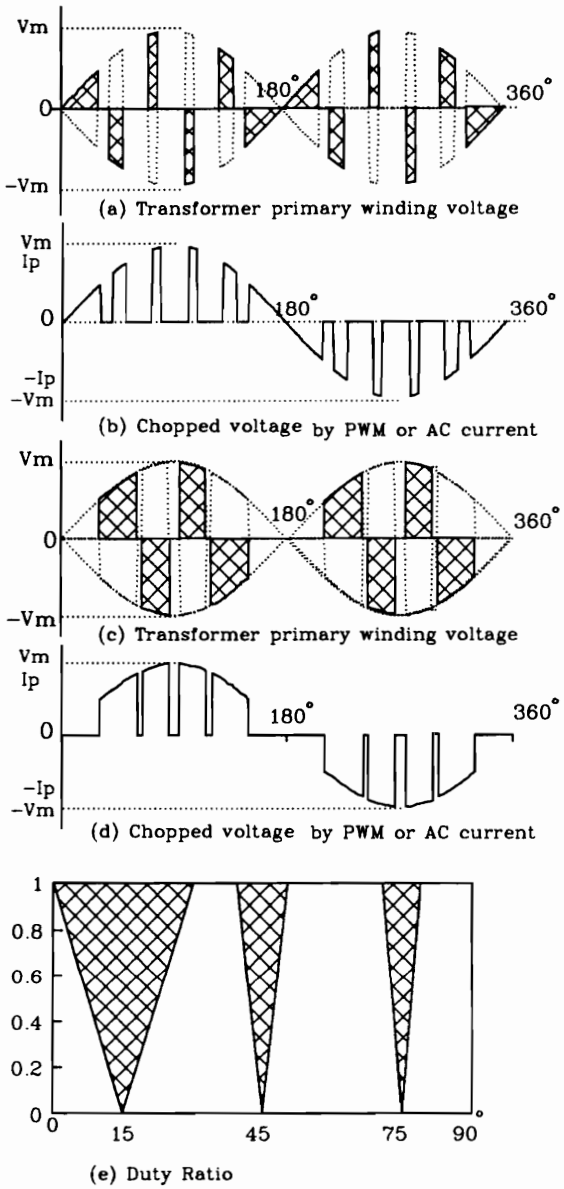

Figure 4.4: Control strategy I

Comparing Figures 4.4 (a) and (c) it is obvious in the strategy that, due to variation of the pulse area, the maximum dc output voltage is a function of the first-pulse area whose duty ratio is determined (hereafter referred to as base pulse) as

$$\text{Duty ratio} = \frac{\text{base pulse conducting angle}}{\text{base pulse angle } (or\ 2\pi/k)} \tag{4.8}$$

where k is the number of pulses per cycle. Figure 4.4 (e) provides the conduction interval in the case of six pulses per half cycle as a function of duty ratio. It has a simple triangular shape, which results in simple implementation of the scheme. This shows only one-quarter of a full waveform, but, due to its symmetry, it contains all the information required. Figure 4.5 (a) shows that the maximum dc output voltage is dependent on the base pulse. The base pulse which gives the maximum output-voltage is varying in step according to the number of pulses as shown in Figure 4.5 (b). The dc output is changed by varying the duty ratio. However the odd number harmonics as low as the 3rd show up on the ac side as shown in Figures 4.5 (c) and (d) for the cases of Figures 4.4 (b) and (d), respectively. The rich harmonics in low frequency make strategy I less useful in practice.

The next two strategies are made by eliminating the low order harmonics using high carrier-frequencies. Special care has to be taken, to avoid the transformer saturation. First, the relationship between the carrier frequency and the input-current harmonic spectra is identified by deriving an analytical equation. The current waveform, Figure 4.6 (e) on the ac side is obtained by multiplying the sinusoidal waveform, 4.6 (a) and the switching signal function, Figure 4.6 (d) for the case of six pulses per half cycle. In the following two strategies the duty ratio (or D) is defined as the ratio of dc control-voltage level to the carrier magnitude. The Fourier series of the waveform, Figure 4.6 (d) is a function of duty ratio, D and the number of pulses per cycle, k (or carrier frequency). It is expressed as

$$F_c(\theta) = D + \sum_{n=1}^{\infty} \frac{-2}{n\pi} \sin\{n\pi(1-D)\} \cos(kn\theta). \tag{4.9}$$

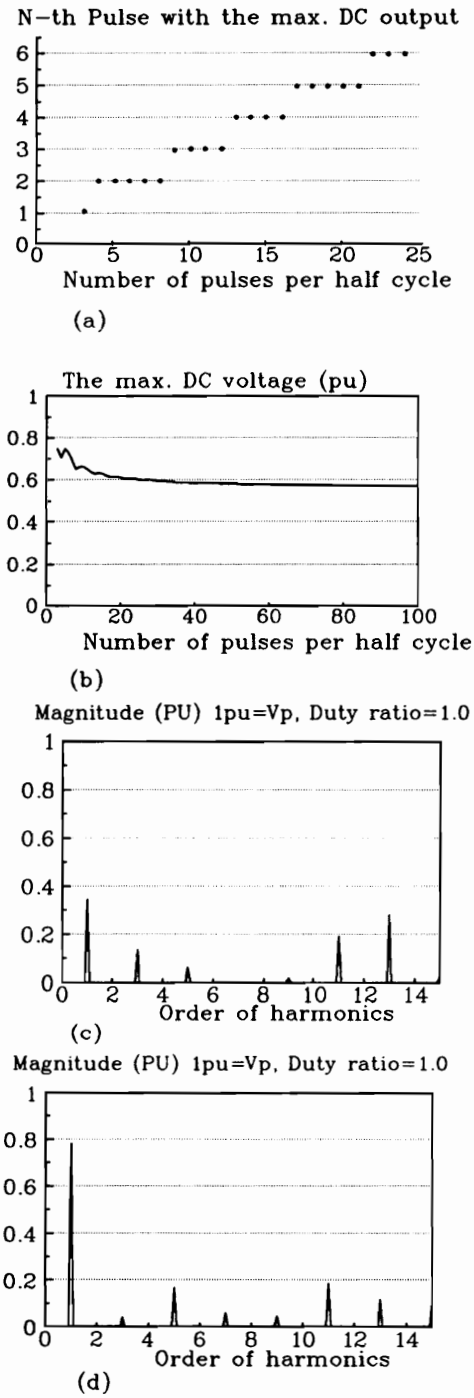

Figure 4.5: Dc voltage and harmonics for control strategy I

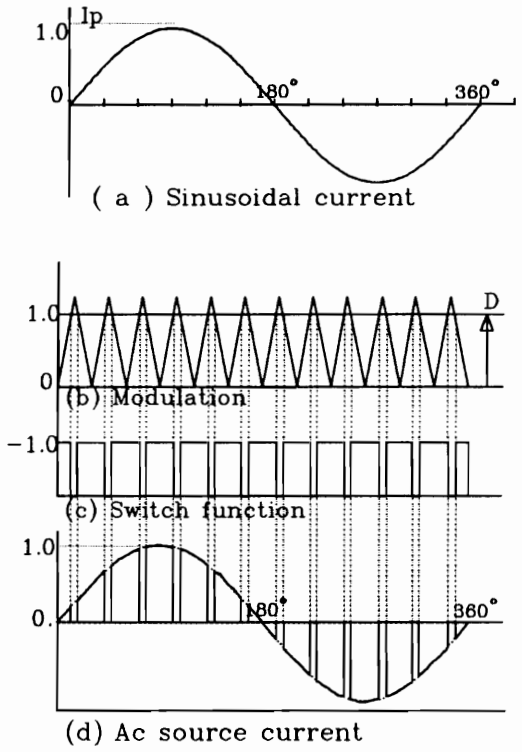

Figure 4.6: PWM modulation for control strategies II and III

The resultant of the multiplication of Figures 4.6 (a) and (d) is given as

$$I(\theta) = I_0 \sin\theta + \sum_{n=1}^{\infty} I_n \sin(kn-1)\theta - \sum_{n=1}^{\infty} I_n \sin(kn+1)\theta \tag{4.10}$$

where D and k are duty ratio and number of pulses per cycle, respectively, and I_0 is the magnitude of the fundamental components and is expressed as

$$I_0 = D\, I_p \tag{4.11}$$

I_n is the $kn \pm 1$ th order harmonic-current magnitude and is given as

$$I_n = \frac{I_p \sin(n\pi(1-D))}{n\pi}. \tag{4.12}$$

The fundamental component I_0 is proportional to the duty ratio, and the next two lowest harmonics are k+1 th and k-1 th harmonics. The two harmonics have same magnitudes except the phase difference of 180° as shown in Figure 4.7 (a). Depending on the number of pulses, k(for carrier frequency, kf_s) the harmonics can be eliminated up to k-2 th order. Using the analytical equations (4.11) and (4.12) , generalization of the relationships between the harmonic amplitudes versus duty ratio for the harmonics is made possible. It is shown in Figure 4.7(b) for n=1, 2, 3. The magnitudes of kn±1 th harmonics are given in equation (4.12). They have a period of π/n radian with the maximum magnitudes of $I_p/(n\pi)$ at $D = 1/2n$ $(0 \leq D \leq 1, n = 1,2,3\ldots)$. In the equation (4.10), there is no cosine term, which makes the scheme with unity displacement factor.

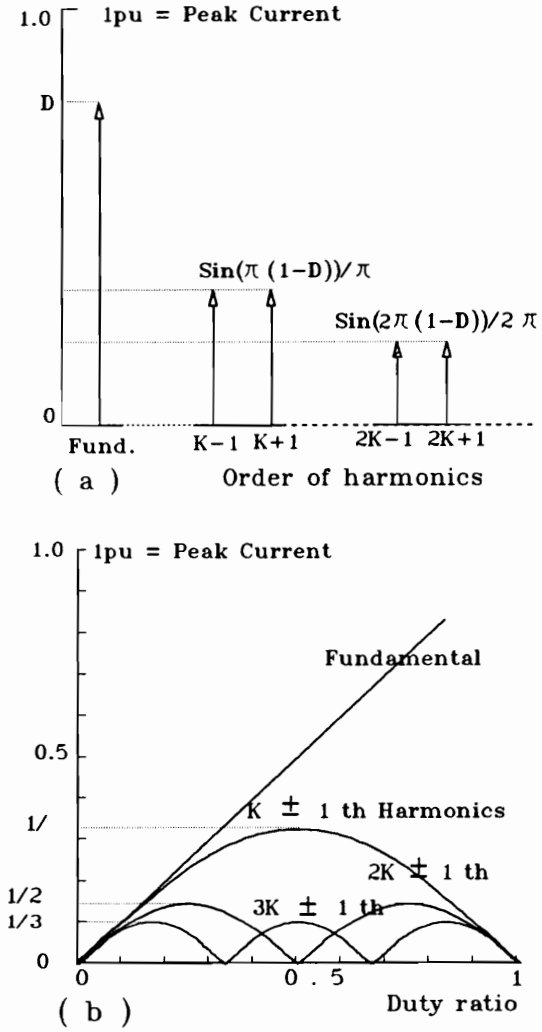

Figure 4.7: Input ac line current harmonic spectrum for control strategies II and III

Similarly the voltage waveform on the dc side is expressed as

$$
\begin{aligned}
V_o \;=\; & \left(\frac{2\sqrt{2}D}{\pi} - \sum_{n=1}^{\infty} \frac{4\sqrt{2}D}{\pi(4n^2-1)} \cos 2n\theta \right. \\
& - \sum_{n=1}^{\infty} \frac{4\sqrt{2}\sin n\pi(1-D)}{n\pi^2} \cos kn\theta \\
& + \sum_{n=1}^{\infty} \frac{4\sqrt{2}}{\pi(4n^2-1)} \cos 2n\theta \\
& \left. \times \sum_{n=1}^{\infty} \frac{2\sqrt{2}\sin n\pi(1-D)}{n\pi} \cos kn\theta \right) V_s
\end{aligned}
\tag{4.13a}
$$

where V_{rms} is the rms voltage of the transformer secondary for the duty ratio unity. Its harmonic spectrum is shown in Figure 4.8. For convenience of drawing and writing the equations, the rms voltage is assumed to be 1 pu hereafter. The dc component is given as

$$V_{dc} = \frac{2\sqrt{2}D}{\pi} V_s. \tag{4.14}$$

4.3.2 Strategy II: Carrier chopping strategy

It has been shown that the harmonics lower than k-1 th order can be eliminated by the carrier frequency of kf_s. Every other pulse is applied to the transformer winding in the opposite polarity. It is easy to implement but the utilization rate of the transformer is low. The conduction angle for the windings with k=12 is presented in Figure 4.9 (a) with the transformer primary voltage waveform in (c). There is no possibility of transformer saturation for this strategy. It has been tested using a simplified equivalent circuit, and its result is given in Figure A.6 of Appendix A. It shows that the flux is varying according to the applied voltage. And it does not saturate since the transformer is reset every applied voltage cycle.

4.3.3 Strategy III: Carrier and even-chopping strategy

Harmonic elimination is fulfilled in the same way as strategy II. Thus, it has the same harmonic spectrum in the ac line current as strategy II for the same carrier frequency. However, it is different from strategy II in that its switching frequency is twice the carrier frequency. Each pulse area is evenly divided into two segments.

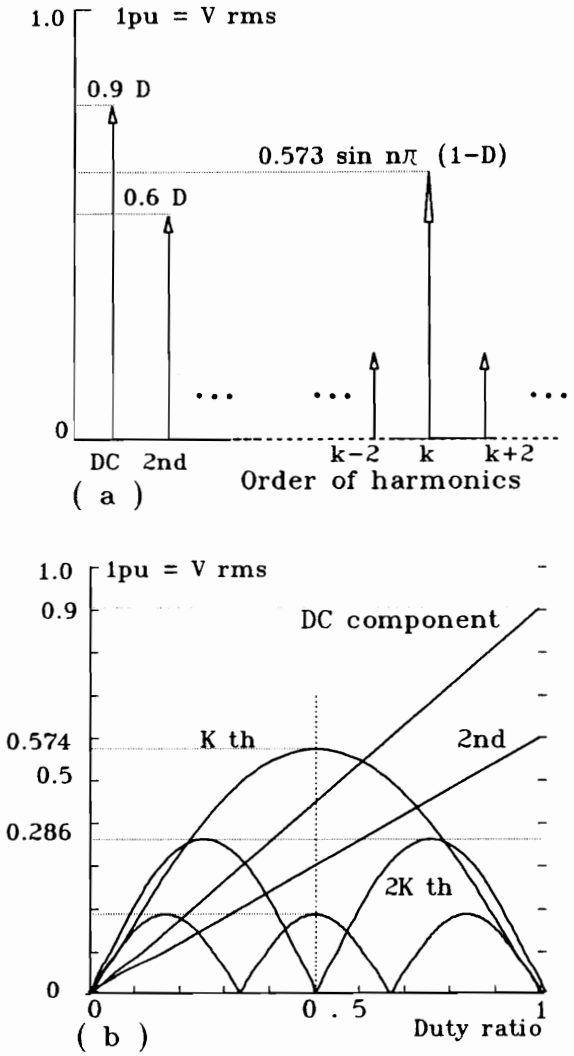

Figure 4.8: Output voltage harmonic spectrum for control strategies II and III

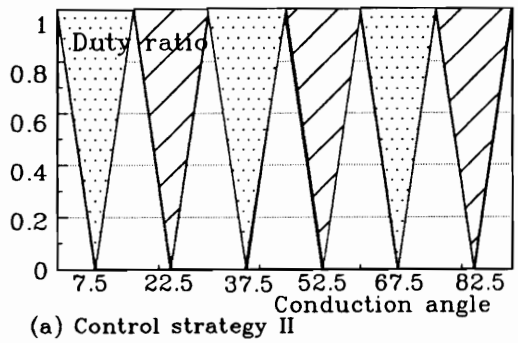

(a) Control strategy II

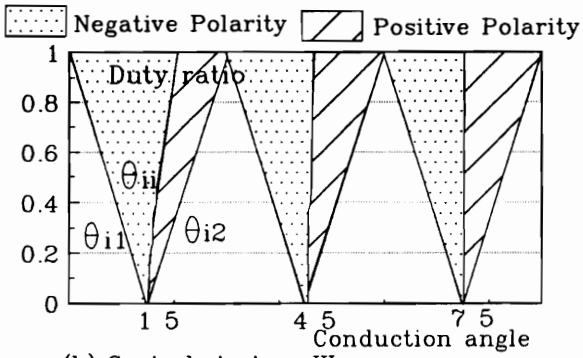

(b) Control strategy III

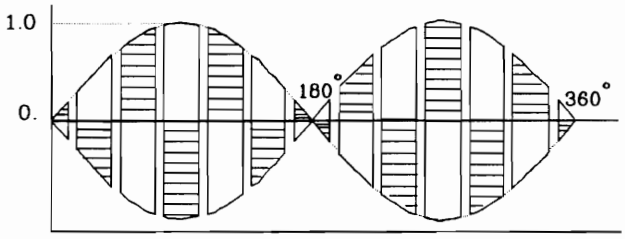

(c) Transformer primary winding voltage for control strategy II

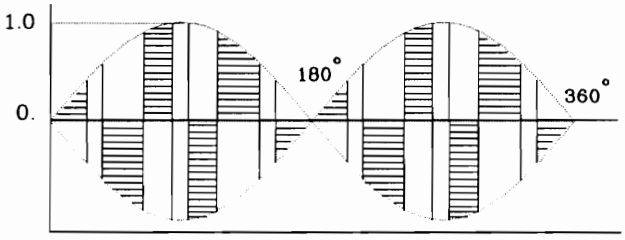

(e) Transformer primary winding voltage for control strategy III

Figure 4.9: Voltage waveforms and duty ratios

One of the two segments is applied to the winding in the positive polarity and the other is applied in the negative polarity. Thus, the transformer is reset within each carrier frequency. This strategy is difficult to implement because the dividing point is not defined as a single function for varying duty ratio. However, if an on-board computing using a microcomputer or microprocessor is considered, it can be easily implemented. In this study, it is implemented using carrier-waveforms stored in EEPROMs.

The dividing points are given as

$$\theta_{ii} = \cos^{-1}\left(\frac{\cos\ \theta_{i1} + \cos\ \theta_{i2}}{2}\right). \tag{4.15}$$

The dividing point and conducting angle of each winding versus duty ratio with k=6 is shown in Figure 4.9 (b). The voltage waveform across the transformer primary winding is shown in Figure 4.9 (d).

4.4 Theoretical and Experimental results

The theoretical and experimental results from a laboratory prototype are compared to verify the validity of the proposed scheme for the second and third strategies. For the second strategy, a 20kHz of carrier frequency is used with a small size of low-pass filter (142 μH, 2μF) on the ac input side. This study uses a carrier frequency of 2.4kHz for control strategy III without any filters in the power circuit.

4.4.1 Experimental results for strategy II

Figure 4.10 shows the ac line current, transformer voltage and ac source voltage waveforms. No phase delay between ac voltage and current is observed.

4.4.2 Experimental implementation for strategy III

Figure 4.11 shows the brief experimental set up. The zero crossing signal from the ac source voltage gives the reset signal to the four digital counters each cycle. The EPROMs have 8k bytes of memory. Triangular carrier waveforms are stored in the EPROM-I and the waveforms corresponding the pulse polarity to the transformer is stored in the other EPROM.

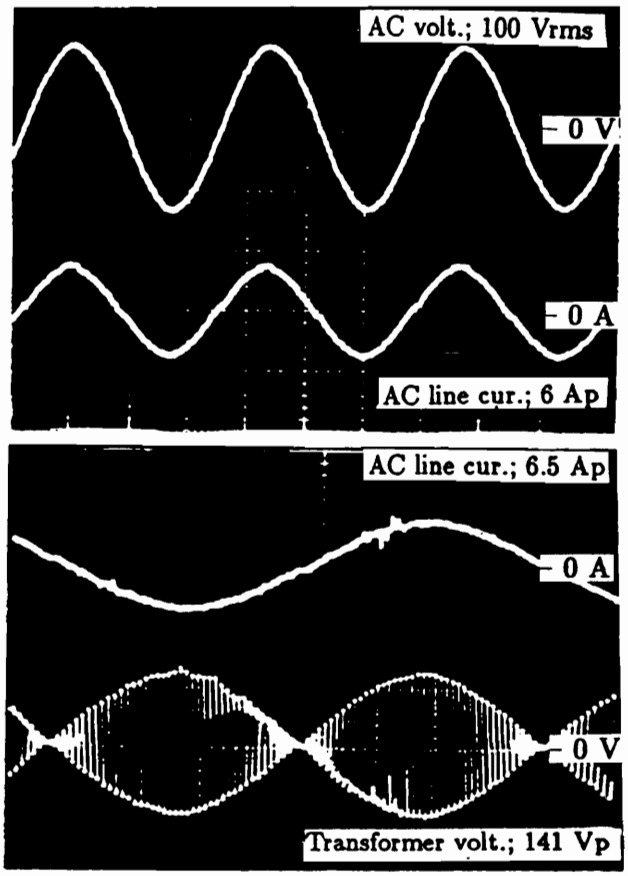

Figure 4.10: Waveforms for control strategy II

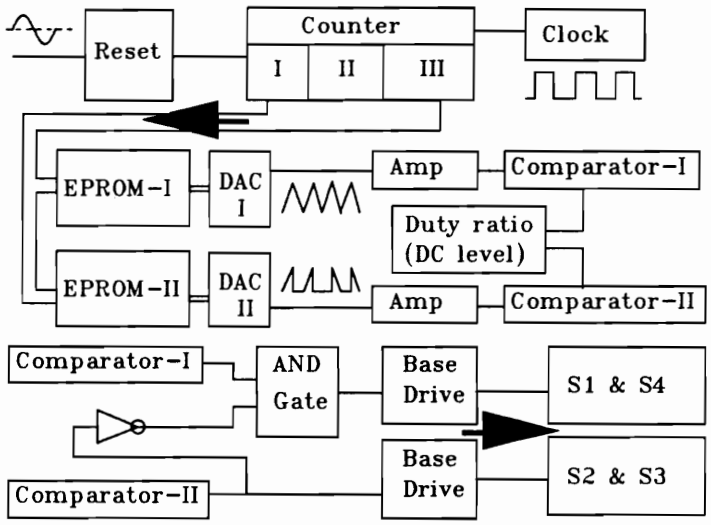

Figure 4.11: Experimental setup for control strategy III

These two waveforms from the EPROMS amplified and compared with dc voltage to control the duty ratio. The outputs of the comparators are fed to base drive through optocouplers. The output of the comparator-I gives the total energy transferring time through the converter for each carrier. The second comparator output is used to determine the half volt-second area of each pulse obtained by comparator-I. Therefore the output of the second comparator turns on one of the switch-pairs S_1 and S_4 (or S_2 and S_3) and the rest of the first comparator output turns on the other switch pair. Doing so, one half volt-second of each pulse is applied to the transformer and the next half is applied in the opposite polarity. On the secondary of the transformer fast-recovery diode full-bridge is connected to rectify the high frequency ac source. The related waveforms of this control circuit are shown in Figure 4.12. The circuit details and control board for this control strategy are included in Figures A.4 and A.5 of Appendix A.

4.4.3 Predicted and experimental results for strategy III

Dc output-voltage variations

The theoretical and experimental dc voltage variation against the duty ratio is shown in Figure 4.13. The discrepancy between the predicted and experimental results at higher duty ratio comes from the voltage drop across the devices (MOSFETs) due to higher current. 1 pu dc output voltage is the rectified voltage at a duty ratio of unity.

Resistive load

Figure 4.14(a) shows the waveforms for the resistive load at the duty ratio (D) of 0.5. The predicted and experimental harmonic spectra for the ac line current are shown in Figures 4.14 (b) and (c), respectively. The magnitude of the fundamental ac component is 0.5 pu which is already predicted in Figure 4.7, where 1 pu is the peak current as shown in Figure 4.6. The predicted results are also obtained using the equations derived in section 4.3.1. The first ac line current harmonics are found near the carrier frequency as shown in Figure 4.14 (b) and (c).

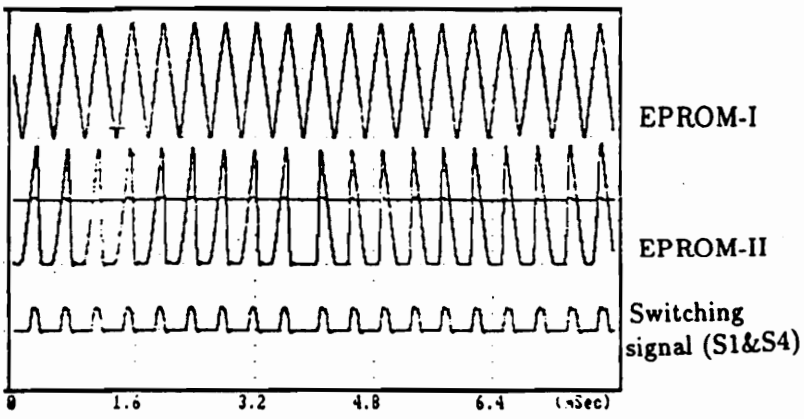

Figure 4.12: Experimental output from the control circuit for control strategy III

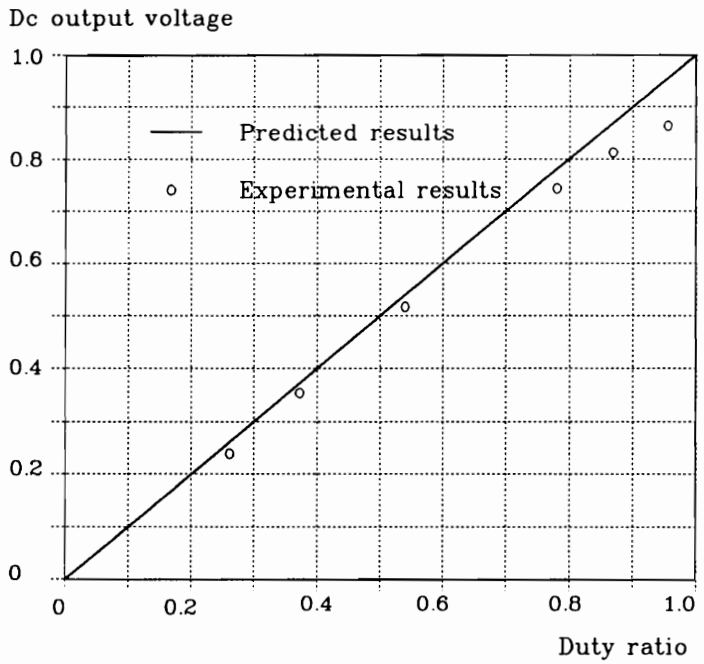

Figure 4.13: Duty ration vs. output voltage

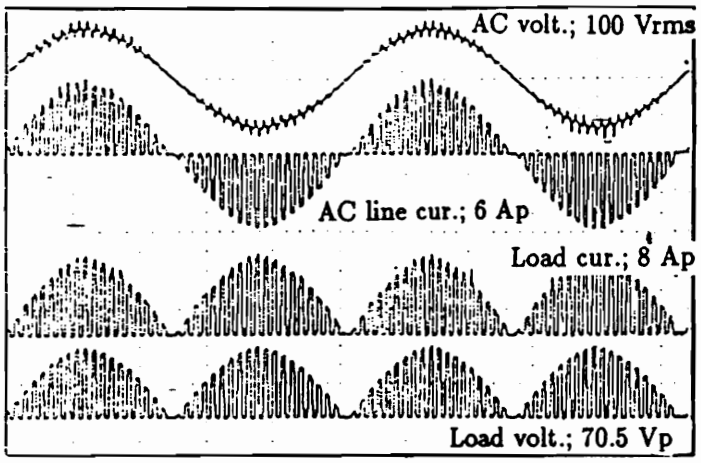

(a) Experimental Waveforms

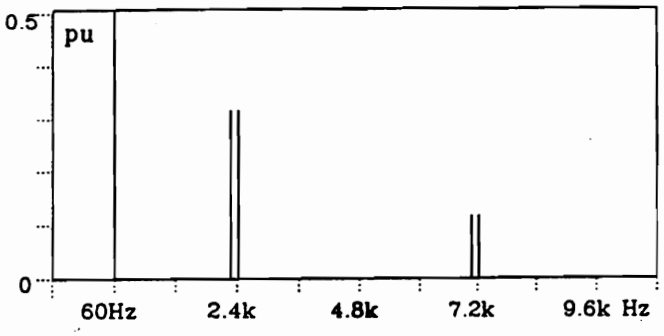

(b) Predicted AC line current harmonics

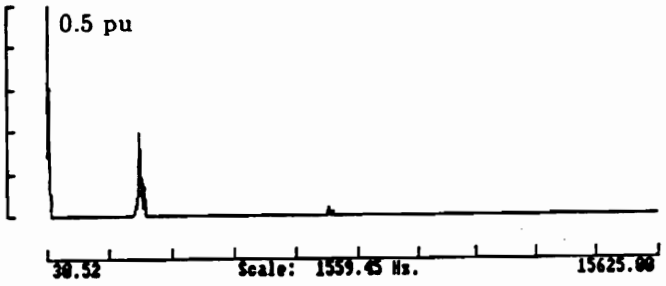

(c) Measured AC line current harmonics

Figure 4.14: Ac line current harmonics

The even order harmonics and the side band harmonics are predicted in Figure 4.8 for the rectified dc voltage. The experimental measurements and predicted results are compared in Figure 4.15 (b) and (c).

Dc motor load

The waveforms and the harmonic spectra are shown in Figure 4.16 for the case of a dc motor load. Due to the back emf of the dc motor the current is discontinuous.

RL load

The waveforms for an RL load are shown in Figure 4.17 (a). The phase delay of the source current is noticed due to the load power factor. This results in introducing the odd harmonics in the ac line current as shown in Figure 4.17 (b).

Devices stress and transformer voltage waveforms

The device stress and the transformer secondary voltage waveforms are shown in Figure 4.18 with the ac source voltage and ac line current for the RL load. For the resistive load the maximum voltage stress across the switching devices is the same as the source peak voltage. However for the RL-load the voltage stress across the devices increases as the load increases due to the effect of the load inductance.

4.4.4 Discussion of experimental work

Control strategy II

In this study, 20kHz of a bipolar triangular wave from a function generator is used with comparator chips to control the duty ratio. The advantage of this strategy is the simple control circuitry.

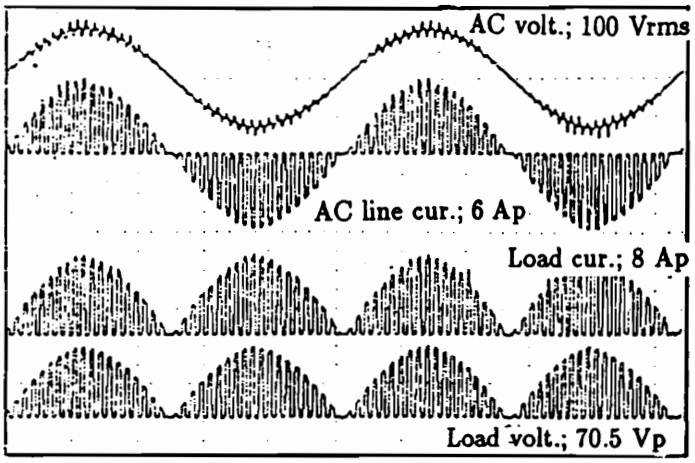

(a) Experimental Waveforms

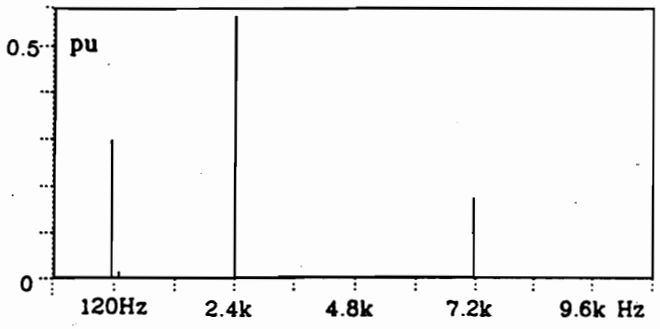

(b) Predicted DC output harmonicx

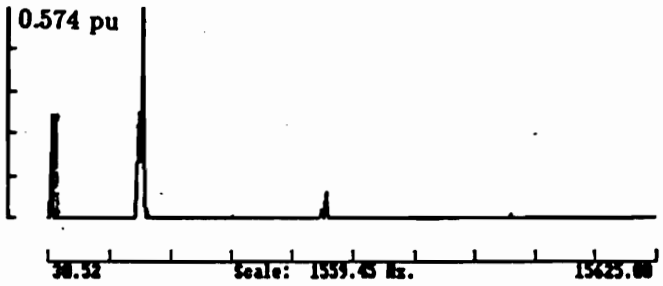

(c) Measured DC output harmonics

Figure 4.15: Dc output voltage harmonics for resistive load

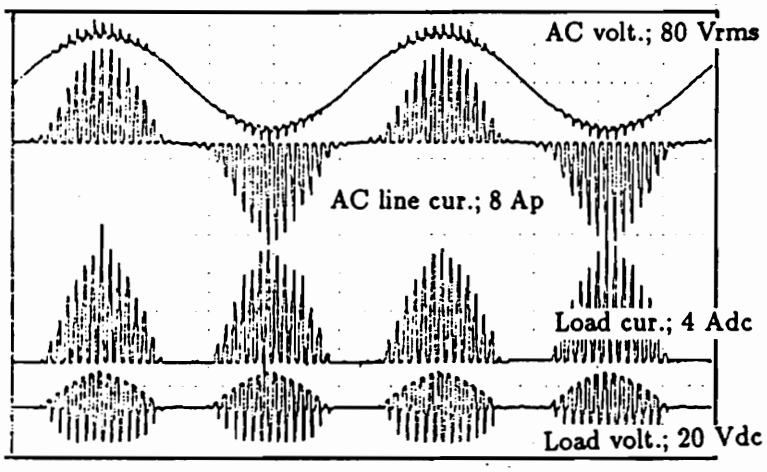

(a) Experimental Waveforms

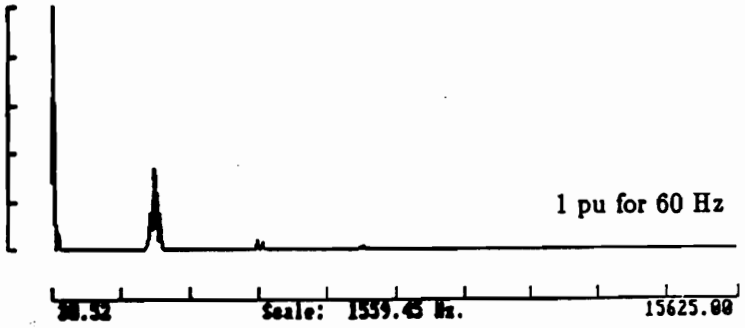

(b) Measured AC line current harmonics

Figure 4.16: Waveforms and harmonics for dc motor load

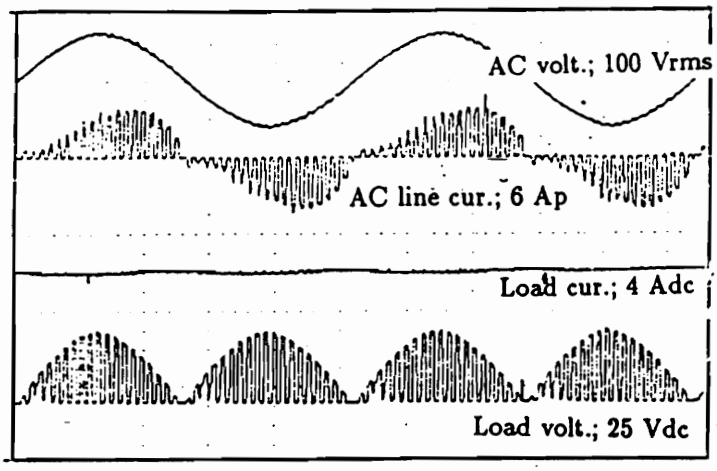

(a) Experimental Waveforms

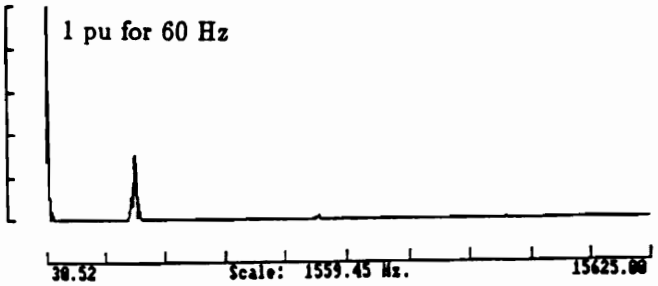

(b) Measured AC line current harmonics

Figure 4.17: Waveforms and harmonics for RL load

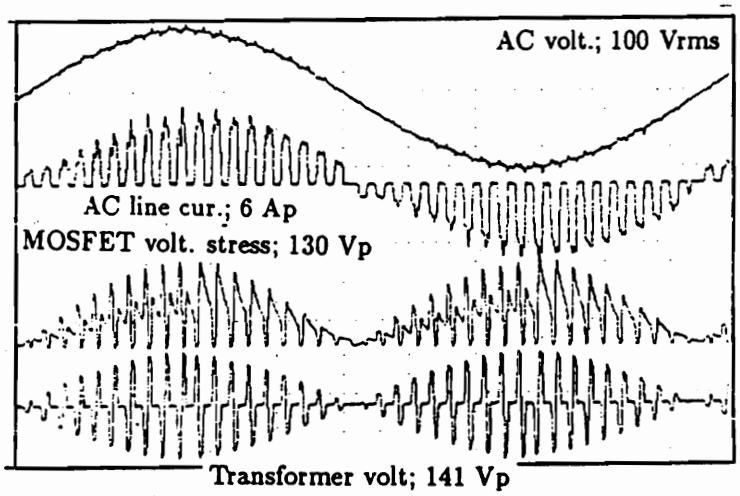

Figure 4.18: Experimental waveforms of device and transformer

Control strategy III

In the implementation of control strategy III, a carrier frequency of 2.4kHz is generated and used to verify the validity of the converter. No filters are connected to the both ends of the converter for the clarity of the waveforms. The transformer with single secondary winding is used with a full-bridge rectifier consisting of fast-recovery diodes.

4.5 Conclusions

The following conclusions are derived from this study:

(i) A power circuit topology capable of unity displacement-factor with sinusoidal input current is proposed.

(ii) Three control strategies are proposed for the operation of the converter and they are simulated and analyzed. Two of the strategies have been designed and realized in hardware and experimentally verified for various loads.

(iii) Harmonic analysis for two control strategies has been derived in analytical form and verified experimentally on a laboratory prototype. Low-frequency harmonic elimination in the input current was feasible up to the desired frequency-ranges.

(iv) One-stage power conversion with a wide-variation in dc output voltage and galvanic isolation with a high frequency transformer of compact size are achieved.

Chapter 5

CONCLUSIONS

Objectives:

The goal of this dissertation was to explore and define the electrical constant frequency (VSCF) power conversion schemes using PM brushless and switched reluctance generators. To meet this goal the following research objectives were addressed:

(i) Analysis and design of the VSCF power conversion schemes.

(ii) Improvement of the overall efficiency of the schemes.

(iii) Introduction of forced commutation to remove the constraints on the frequency range.

(iv) Reduction of harmonics.

(v) Improvement in power factor.

(vi) Wide range of speed of operation, maintaining all the above objectives.

Applications:

The schemes may find applications in the following:

(i) Wind power generation.

(ii) Naval or aircraft on board ship power generation and processing.

(iii) Jet engine starter-generator in aerospace applications.

(iv) Stand alone power generation for remote stations.

Contributions:

In the course of the study, the following contributions are made:

(i) An integrated system consisting of PM brushless and switched reluctance generators, and self commutating converters were modeled, simulated, analyzed, and experimentally verified.

(ii) Two novel schemes for the VSCF scheme with a PMSM and an SRM have been proposed.

(iii) The two proposed schemes have been designed, built, and tested to prove the feasibility of the scheme.

(iv) A new converter topology for four-quadrant operation SRM drives has been proposed and verified, which eliminates the dc link capacitor thus enhancing the reliability of scheme.

(v) Several control strategies for the scheme have been proposed, analyzed, and implemented on a laboratory prototype. They are directly applicable to ac to dc or dc to ac power conversion.

(vi) A new topology and three control techniques for single phase ac to dc power conversion were proposed, analyzed, and have been experimentally verified. This scheme provides isolation and compactness to the VSCF scheme. Thus, it makes the system even ideal for the applications with constraints of critical limits on volume and weight.

Recommendations for the future work

The following recommendations are made to extend the work described in this dissertation.

(i) Development of a dynamic model for the simulation and analysis of the VSCF power conversion schemes.

(ii) Comparison of these two schemes with wound rotor and induction generators.

(iii) Topology exploration for the SRM which is capable of wave shaping of the input/output current and torque ripple reduction.

(iv) Performance analysis of the scheme at extreme operating conditions.

(v) Evaluation of the schemes for various applications.

(vi) Fault tolerance test of the scheme during normal operation.

REFERENCES

[1] Z.M. Salameh and L.F. Kazda, "Analysis of the Steady State Performance of the Double Output Induction Generator", IEEE Trans. on Energy Conversion, Vol.EC-1, No.1, Mar. 1978, pp26-32

[2] K.Natarajan and et al., "Modeling and Design for Wind Power Conversion Scheme Using Self-Excited Induction Generator", IEEE Trans. on Energy Conversion, Vol.EC-2, No.3, Sept. 1987, pp506-512

[3] H.L. Nakra and B. Dube, "Slip Power Recovery Induction Generator for Large Vertical Axis Wind Turbines", IEEE Trans. on Energy Conversion, Vol.EC-3, No.4, Dec. 1988, pp733-737

[4] R. Krishnan and G. H. Rim, "Modeling, Simulation and Analysis of Variable Speed Constant Frequency Power Conversion Scheme with a Permanent Magnet Brushless DC Generator", IEEE Trans. on Industrial Electronics, Vol. 37, No.4, pp 291-296, August 1990.

[5] R. Krishnan and G. H. Rim, "Performance and Design of a variable speed constant frequency power conversion scheme with a permanent magnet synchronous generator", IEEE IAS Conference Record, pp 45-50, Oct. 1989

[6] R. Krishnan and G. H. Rim, "Design and Operation of Adjustable Power Factor Sinusoidal Converter for Variable Speed Constant Frequency Generation with PMSG", IEEE IAS Conference Record, pp 835-842, Oct. 1989

[7] T.S. Key and J.E. Leeman, "Power Conditioning Development for Grid-Connected Residential Photo voltaic Applications", Sandia Report, Aug. 1987

[8] K. Taniguchi and et al., "High-Performance Slip Recovery Induction Motor", IEE Proc., Vol. 134, Pt.B, No.4 Jul 1982, pp193-197

[9] J.A. Wilson, "The Forced-Commutated Inverter as a Regenerative Rectifier", IEEE Trans. on Industry Applications, Vol.IA-14, No.4, Jul/Aug, 1978, pp335-340

[10] L.H. Walker, "Forced Commutated Reactive-Power Compensator", IEEE Trans. on Industry Applications, Vol.-22, No.9, Nov/Dec 1986, pp1091-1104

[11] J. Arrillaga, "High Voltage Direct Current Transmission", Peter Peregrinus Ltd., London, UK. 1983

[12] D.Y. Chen, "Power Semiconductors and Magnetic Devices ", Class Note for EE5984, Dept. of Elect. Eng., VPI & SU, Spring 1991

[13] S. Rahman, "Alternative Energy Systems", Class Note for EE4364, Dept. of Electric. Eng., VPI & SU, 1989

[14] R. Hendricks, "Electronic Magnetic and Photonic Materials", Class Note for Mate4214, Dept. of Material Science, VPI & SU, Spring 1991

[15] H.P. Patel and R.G. Hoft, "Generalized Techniques of Harmonic Elimination and Voltage Control in Thyrister Inverters: Part 1-Harmonic Elimination", IEEE Trans. on Industry Applications, Vol.IA-9, No.3 May/Jun 1973, pp 310-317

[16] D.A. Grant, "Technique for Pulse Dropping in Pulse-Width Modulated Inverters", IEE Proc., Vol.128, Pt.B, No.1, Jan. 1981, pp 67-72

[17] J.A. Houldsworth and D.A. Grant, "The Use of Harmonic Distortion to Increase the Output Voltage of a Three-Phase PWM Inverter", IEEE Trans. on Industry Applications, Vol.IA-20, No.5, Sept/Oct 1984, pp 1224-1227

[18] S.R. Bowes and R.I. Bullough, "Harmonic Minimization in Microprocessor Controlled Current Fed PWM Inverter Drives", IEE Proc., Vol.134, Pt.B, No.1, Jan 1987, pp 25-41

[19] P.D. Ziogas, "PWM Control Techniques for Rectifier Filter Minimization", IEEE Trans. on Industry Applications, Vol. IA-21, No.5, Sept/Oct 1985, pp 1206-1214

[20] M. Boost and P.D. Ziogas, "Audible Noise Reduction for Medium Power Inverters", IEEE PESC '90 Conference Record, 1990, pp 714-722

[21] V.R. Stefanovic, "Power Factor Improvement with a Modified Phase-Controlled Converter", IEEE Trans. on Industry Applications, Vol.IA-15, No.2, Mar/Apr 1979, pp 193-201

[22] B.T. Ooi and et al., "A 3-Phase Controlled Current PWM Converter with Leading Power Factor", IEEE Trans. on Industry Application Vol.IA-23 Jan/Feb 1987, pp 78-84

[23] H.W. Dixon and B.T. Ooi, "Indirect Control of a Unity Power Factor Sinusoidal Current Boost Type Three-Phase Rectifier", IEEE Trans. on Industrial Electronics, Vol.35, No.4, Nov. 1988, pp 508-515

[24] H.S. Black, "Modulation Theory", D. Van Nostrand Co., Inc. 1953

[25] S.R. Bowes, et al., "Novel Approach to the Analysis and Synthesis of Modulation Processes in Power Converters", IEE Proc., Vol. 122, No.5 May 1975, pp507-513

[26] S.R. Bowes, et al., "New Sinusoidal Pulse-Width Modulation Inverter", ibid., 1975, pp1279-1285

[27] P.N. Enjeti, et al., "Programmed PWM Techniques to Eliminate a Critical Evaluation", IEEE IAS Conference Record, 1988, pp419-430

[28] S.R. Bowes, et al., "Transient Performance of Inverter Systems", IEE Proc., Vol. 129, Pt.B, No.6 Nov. 1982, pp507-513

[29] M.A. Boost and P.D. Ziogas, "State-of-Art Carrier PWM Techniques; A Critical Evaluation", IEEE Trans on Industry Applications, Vol.24, No.2, Mar/Apr, 1988, pp271-280

[30] T.H. Barton, "Pulse Width Modulation Waveforms, the Bessel Function Approximation", IEEE IAS Conference Record, 1978, pp1125-1130

[31] B. Mokrytzki, "Pulse Width Modulated Inverters for AC Motor Drives", IEEE Trans. on Industry and General Applications, Vol. IGA-3, No.6, Nov/Dec 1967, pp493-503

[32] S.B. Dewan and et al., "Output Voltage in Three-Phase Pulse Width Modulated Inverters", IEEE Trans. on Industry and General Applications, Vol. IGA-6, No.6, Nov/Dec 1970, pp570-579

[33] K. Taniguchi and et al., "A Three-Phase Sinusoidal PWM Inverter", IEEE IAS Conference Record, 1985, pp1269-1173

[34] D.A. Grant and et al., "Ratio Changing in Pulse-Width Modulated Inverters", IEE Proc., Vol.128, Pt.B, No.5, Sept. 1981

[35] D.A. Grant and et al., "A New High-Quality PWM AC Drive", IEEE Trans. on Industry Applications, Vol.IA-19, No.2, Mar/Apr 1983, pp211-216

[36] T.L. Grant and T.H. Barton, "Control Strategies for PWM Drives", IEEE Trans. on Industry Applications,Vol.IA-16, No.2, Mar/Apr 1980 , pp211-215

[37] J. Richardson and O.T. Kukrer, "Implementation of a PWM Regular Sampling Strategy for A.C. Drives", PESC '89 Record, 1989, pp649-656

[38] S.R. Bowes, "Steady-state Performance of PWM Inverter Drives", IEE Proc., Vol.130, Pt.B, No.4, Jul 1983, pp 229-244

[39] J. Zubek and et al., "Pulse Modulated Inverter Motor Drives with Improved Modulation", IEEE Trans. on Industry Applications, Vol.IA-11, No.6, Nov/Dec 1976, pp 695-703

[40] J.W. Dixon and et al., "Characteristics of A Controlled-Current PWM Rectifier-Inverter Link", IEEE IAS conference record, 1986, pp 685-691

[41] P. Enjeti, "New Current Control Scheme for PWM Inverters", IEE Proc., Vol.135, Pt.B, No.4, Jul. 1988

[42] S.R. Bowes, "Optimal PWM Microprocessor Controlled Current Source Inverter Drives", IEE Proc., Vol.135, Pt.B, No.2, Mar. 1988, pp 59-75

[43] A.W. Green, "3-Phase Voltage sourced reversible rectifier", IEE Proc., Vol.135, Pt.B, No.6, Nov., 1988, pp362-370

[44] A.W. Green, " Hysteresis Current-forced Three-phase Voltage-sourced Reversible Rectifier", IEE Proc., Vol.136, Pt.B, No.3, May 1989, pp 113-120

[45] S. Manias et al., "Three-Phase Inductor fed SMR Converter with High Frequency Isolation, High Power Density and Improved Power Factor", pp 183-191

[46] A.M. Campos et al., "UPS System Employing High Frequency PWM Techniques", IEEE APEC Conference Record, 1990, pp414-421

[47] T. Kagotani, "A Novel UPS Using High-Frequency Switch-Mode Rectifier and High-Frequency PWM Inverter", IEEE PESC '89 Conference Record, 1989, pp 53-57

[48] D.P.M. Cahill and B. Adkins, "The Permanent Magnet Synchronous Motor", IEE Vol.109, Pt.A, No.48, Dec. 1962

[49] P. Pillay and R. Krishnan, "Application Characteristics of Permanent Magnet Synchronous and Brushless DC motor for Servo Drives", IEEE IAS Conferences Record, 1987. pp 385-390

[50] P.W. Franklin, "Theory of The Three Phase Salient Pole Type Generator with Bridge rectified Output - Part 1 and 2", IEEE Trans. on Power Apparatus and System, Vol. PAS-91, No.5, Oct. 1972, pp1960-1975

[51] G.H. Rim, "Modeling, Analysis and Experimental Verification of Variable Speed Constant Frequency Power Conversion Scheme with a Permanent Magnet Synchronous Generator", M.S. Thesis, Dept of Electrical Engineering, VPI & SU, Blacksburg, VA 24061, Feb. 1988.

[52] R. Krishnan and et al., "Design Procedure for Switched Reluctance Motors", IEEE IAS Conference Record, Oct. 1986, pp 858-863

[53] T.J.E.Miller and et al., "Design of a Synchronous Reluctance Motor Drive", IEEE IAS Conference Record, Oct. 1989, pp 122-127

[54] R. Krishnan and et al., "A Design Procedure for Axial Field Switched Reluctance Motors", IEEE IAS Conference Record, Oct. 1990, pp 858-863

[55] L.E. Unnewehr and W.H. Koch, "An Axial air gap Reluctance Motor for variable speed Application", IEEE Trans. on PAS-93, 1973, pp 367-376

[56] C.C. Chan, "Axial-Field Electrical Machines-Design and Applications", IEEE Trans. on Energy Conversion, Vol.EC-2, No.2 Jun. 1987, pp 294-300

[57] J.W. Finch and et al., "Switched Reluctance Motors with Multiple Teeth per pole: Philosophy of Design", 2nd Int. Conf. on Elect. Mach. - Design and Application, Sept. 1985, pp134-138

[58] P.N. Materu and R. Krishnan, "Steady-State Analysis of the Variable-Speed Switched-Reluctance Motor Drive", IEEE Trans. on Industrial Electronics 1989, pp 523-529

[59] P.N. Materu and R. Krishnan, "Analytical Prediction of SRM Inductance Profile and Steady-State Average Torque", IEEE IAS Conference Record, Oct. 1990, pp 214-223

[60] P.J. Lawrenson and et al., "Variable-Speed Switched Reluctance Motors", IEE Proc. Vol.127, Pt.B No.4, Jul. 1980, pp 253-265

[61] J.M. Stephenson and J. Corda, "Computation of Torque and Current in Doubly Salient Reluctance Motors from Nonlinear Magnetisation Data", IEE Proc., Vol.126 No.5, May 1979 pp 393-396

[62] W.F. Ray and R.M¿ Davis, "Inverter Drive for Doubly Salient Reluctance Motor: Its Fundamental Behavior, Linear Analysis and Cost Implications", Electric Power Applications, Vol.2, No.6, Dec.1979, pp 185-193

[63] T.J.E.Miller, "Converter Volt-Ampere Requirements of Switched Reluctance Motor Drive", IEEE IAS Conference Record, Oct. 1984, pp 813-819

[64] R. Krishnan and P. Materu, "Analysis and Design of a New Converter Topology For Switched Reluctance Motor Drives", IEEE IAS Conference Record, Oct. 1989, pp 1181-1185

[65] C. Pollock and B.W. Williams, "A Unipolar Converter for A Switched Reluctance Motor", IEEE IAS Conference Record, Oct. 1988, pp 44-49

[66] R.M. Davis, "Inverter Drive for Switched Reluctance Motor Circuits and Component Ratings", IEE Proc., Vol.128,Pt.B,No.2 Mar., 1981, pp 126-136

[67] J.T. Bass and T.J.E. Miller, "Development of a Unipolar Converter for Variable Reluctance Motor Drives", IEEE IAS Conference Record, Oct. 1985, pp 1062-1074

[68] C. Pollock and B.W. Williams, "Power Converter Circuits for Switched Reluctance Motors with the Minimum Number of Switches", IEE Proc., Vol.137, Pt.B No.6, Nov. 1990

[69] R. Krishnan and P. Materu, "Analysis and Design of a Low Cost Converter for Switched Reluctance Motor Drives", IEEE IAS Conference Record, Oct. 1989, pp 561-567

[70] R. Krishnan and et al., "A Low Cost SRM Analog Controller", Electronic Motortechnics Feb./Mar. 1990, pp 19-23

[71] B.K. Bose and et al., "Microcomputer Control of Switched Reluctance Motor", IEEE IAS Conference Record, Oct. 1985, pp 542-547

[72] J. C. Moreira and T.A. Lipo, "Simulation of a Four Phase Switched Reluctance Motor Including the Effects of Mutual Coupling, Electric Machines and Power Systems, 16:281-299, 1989, pp281-299

[73] R.M. Davis and I. Al-Bahadly, "Experimental Evaluation of Mutual Inductances in a Switched Reluctance Motor", IEE Proceeding Pt.B, 1991 pp 243-248

[74] T.J.E. Miller and et al., "Four Quadrant Brushless Reluctance Motor Drive", IEEE IAS Conf. Record, 1988, pp 273-276

[75] S.R. MacMinn, "Control of a switched Reluctance Aircraft Engin Starter-Generator Over a Very Wide Speed Range", IECEC Proc. Aug. 1989

[76] T. Fukao, "Principles and Output Characteristics of Super High-Speed Reluctance Generator System", IEEE Trans. on Industry Applications Vol. IA-22, No.4 Jul./Aug. 1986, pp 702-707

[77] S.R. MacMinn and W.D. Jones "A Very High Speed Switched Reluctance Starter-Generator for Aircraft Engine Applications", NAECON Proc. May 1989

[78] N.H. Mvungi, "A New Sensorless Position Detector for Drives", IEE Proceeding Pt.B, 1989 , pp 249-252

[79] Motion Controls System Group, "SRMDYN", Dept. of Electrical Engineering, VPI & SU, Blacksburg, VA Aug. 1990

[80] R.A. Bedingfield, "Development of CAE System for SRM Drive System", M.S. Thesis, Dept of Electrical Engineering, VPI & SU, Blacksburg, VA 24061, Jul. 1991.

[81] P.N. Materu, "Design and Steady-state Analysis of the Switched Reluctance Motor Drives", Ph.D Dissertation, Dept of Electrical Engineering, VPI & SU, Blacksburg, VA 24061, Jul. 1989.

[82] L.X. Le and G. J. Berg, "Firing Circuit for a Three Phase SCR Voltage Controller", IEEE Trans on IE, Vol.IE-31, No.4 Nov. 1984, pp389-390

[83] M.A. Geisler, "Predicting Power Factor and Other Input Parameters for Switching Power Supplies", IEEE APEC Conference Record, Mar. 1990, pp 579-587

[84] A.R. Prasad and et al., "A Novel Passive Wave shaping Method for Single-Phase Diode Rectifiers", IEEE IECON Conference Record, Nov. 1990, pp1041-1050

[85] K. Thiyagarajah and et al., "A High Switching IGBT PWM Rectifier/Inverter System for AC Motor Drives Operating from Single Phase Supply", IEEE PESC Conference Record, June 1990, pp663-671

[86] Gyu-Ha Choe, et al., " An Improved PWM Technique for AC Choppers", IEEE Trans on Power Electronics Vol.4, No.4 oct. 1989

[87] K. Inagaki, et al., " A New Control Method for AC to DC Converters with High-Frequency Transformer Isolation", IEEE IAS Conference Record, Oct. 1989, pp 783-789

[88] C. Glaze, F. Forest and F. Charef, "Study of Power Bidirectional Switches Using Mos-Transistors", Third Internal Conference on Power Electronics and Variable-Speed Drives, IEE conference Pub. No. 271, July 1988, pp 51-53.

[89] K. Kit Sum, " Power Factor Correction for Single-phase Input Power Supplies", PCIM Dec. 1989, pp 18-22

[90] S. Manias and P. D. Ziogas, " A Novel Sine Wave in AC to DC Conversion with High-Frequency Transformer Isolation", IEEE Trans. on Industrial Electronics Vol. IE-32 No. 4, Nov 1985, pp 430-438

[91] M. J. Kocher and R. C. Steigerwald, "An AC to DC Converter with High Quality Input Waves", IEEE PESC Conf. Record, 1982, pp 63-75

[92] T. Kataok, et al., " A Pulse width Controlled AC to DC Converter to Improve Power Factor and Waveform of Ac line Current", IEEE Trans. on Industry Applications, Vol. IA-15 No.6 Nov/Dec 1979, pp 670-675

[93] G.H. Rim and R. Krishnan, " AC to DC Power Conversion with Unity Power Factor and Sinusoidal Input Current", IEEE APEC Conference Record Mar. 1991, pp400-406

[94] R. Krishnan, "Electronic Control of Machines", Prentice Hall, To be published 1991

Appendix A

SUPPLEMENTS

A.1 Supplements to Chapter 2

A.1.1 PMSG parameters

R_g = 1.4Ω Stator resistance

L_s = $8.7mH$ Line filter inductance

R_s = 2.967Ω Line filter resistance

L_d = $5.6mH$ Stator d-axis inductance

L_q = $5.8mH$ Stator q-axis inductance

P = 6 Number of poles

λ_m = $0.1546V/(rad/sec)$ Mutual flux linkage

B = $0.000388Nm/(rad/sec)$ Damping constant

J = $0.00176Kg - m^2$ Moment of inertia

A.1.2 Experimental set-up with a PMSM

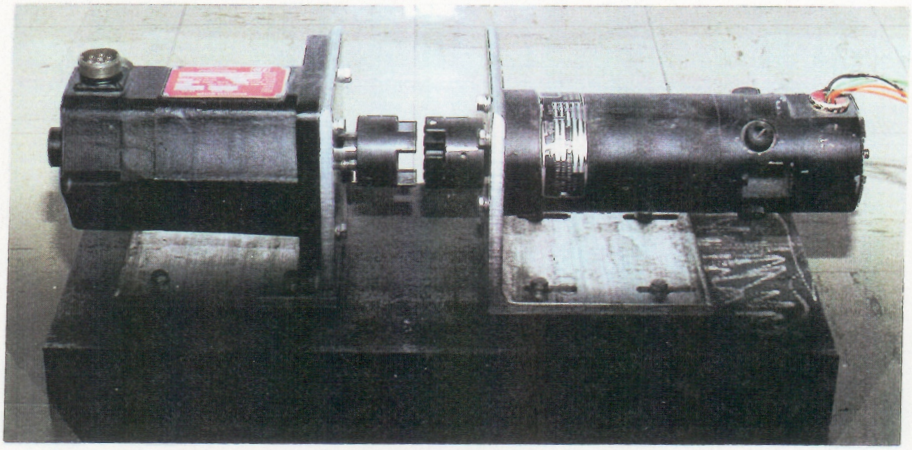

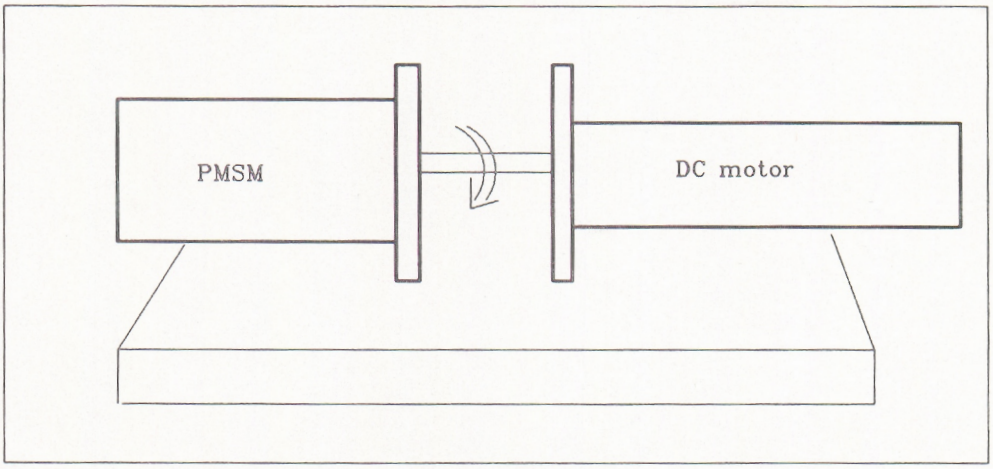

PMSM	DC motor
8.0 A continuous	8.4 V – 21.4 A continuous
35 A peak	28.9 V – 90 A peak
210 V line to line	3000 RPM
5000 RPM max	
2900 RPM rated	
2.48 Hp	

Figure A.1: PMSM connection to dc motor

A.2 Supplements to Chapter 3

A.2.1 Experimental set-up with an SRM

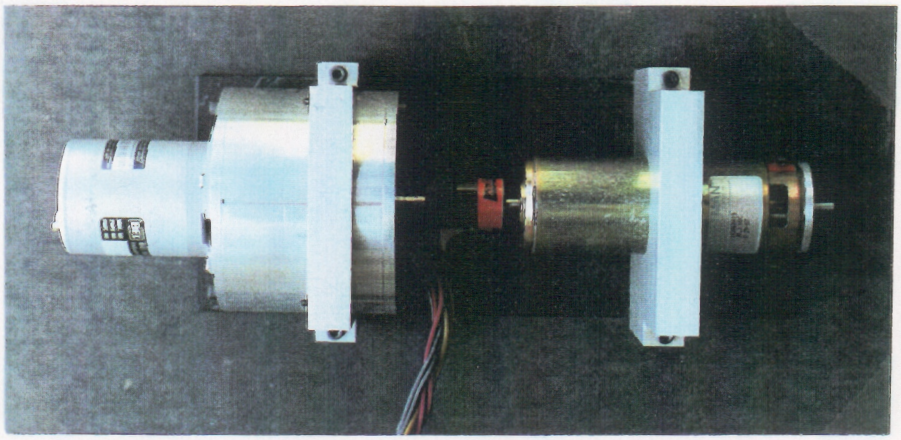

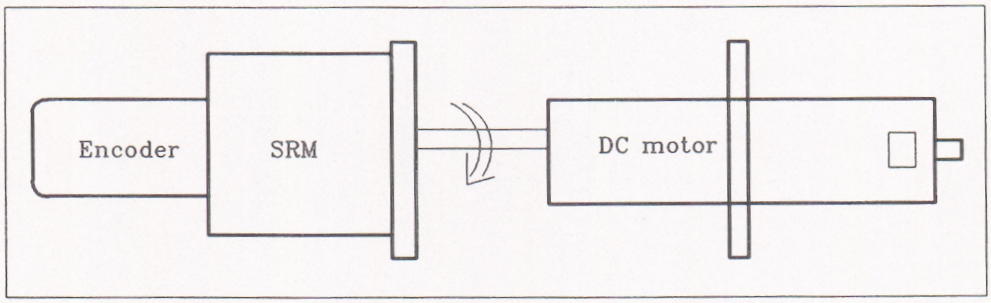

Encoder	SRM		DC motor
8 Bits Binary code	Stator O.D.=105.20 mm	Ns=8	12 A
	Stator I.D.=89 mm	Nr=6	30.3 V
	1800 RPM rated	$\beta s = 16°$	2800 RPM
	75 Watts @ 1800 RPM	$\beta r = 18°$	
	$J=3/10000$ Kg-m^2	Rs=1.6 Ohms	
	$B=10^{-8}$ Nm/(Rad/sec)		

Figure A.2: SRM connection to dc motor

A.2.2 Converter for VSCF with an SRM

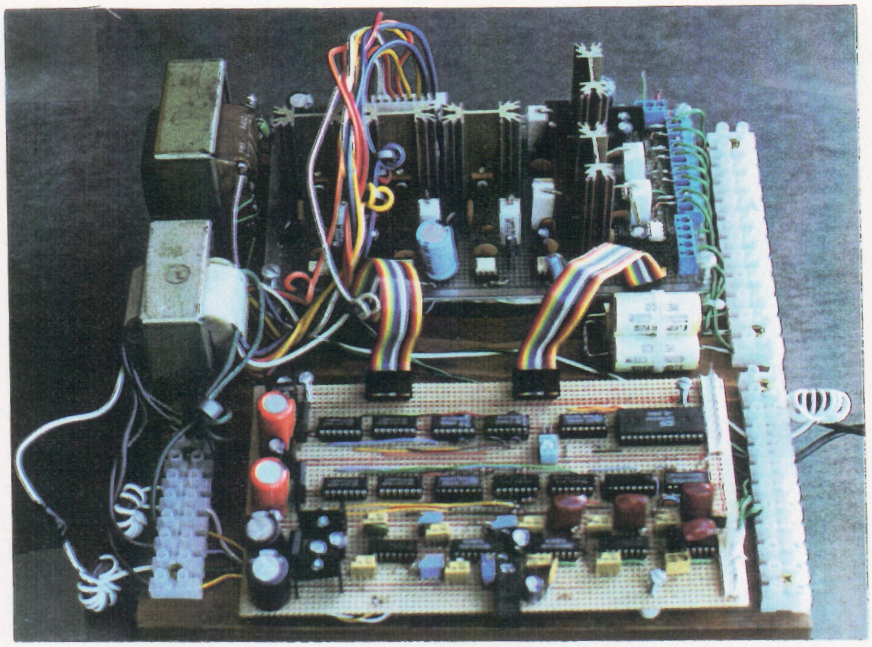

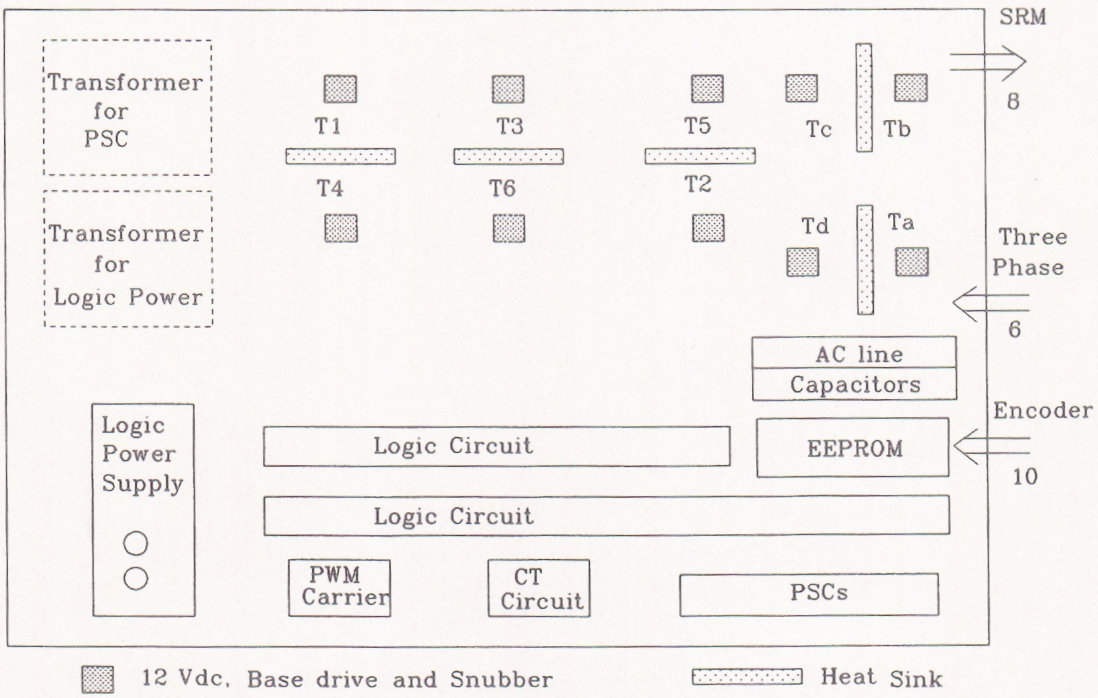

Figure A.3: Converter for SRM drive

A.3 Supplements to Chapter 4

A.3.1 Control board for AC to DC power conversion

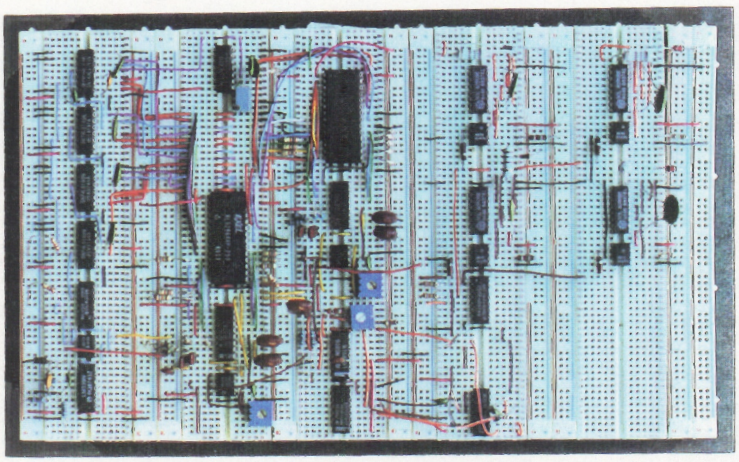

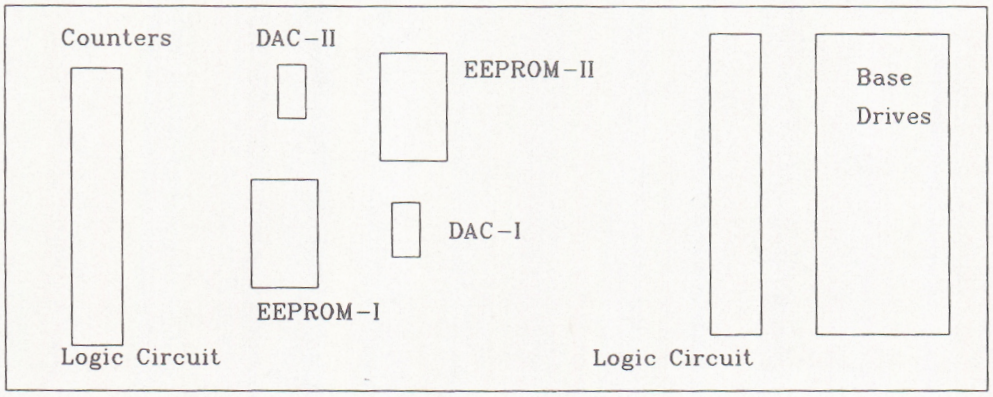

Figure A.4: Control board for AC to DC converter

A.3.2 Control circuit for ac to dc power conversion

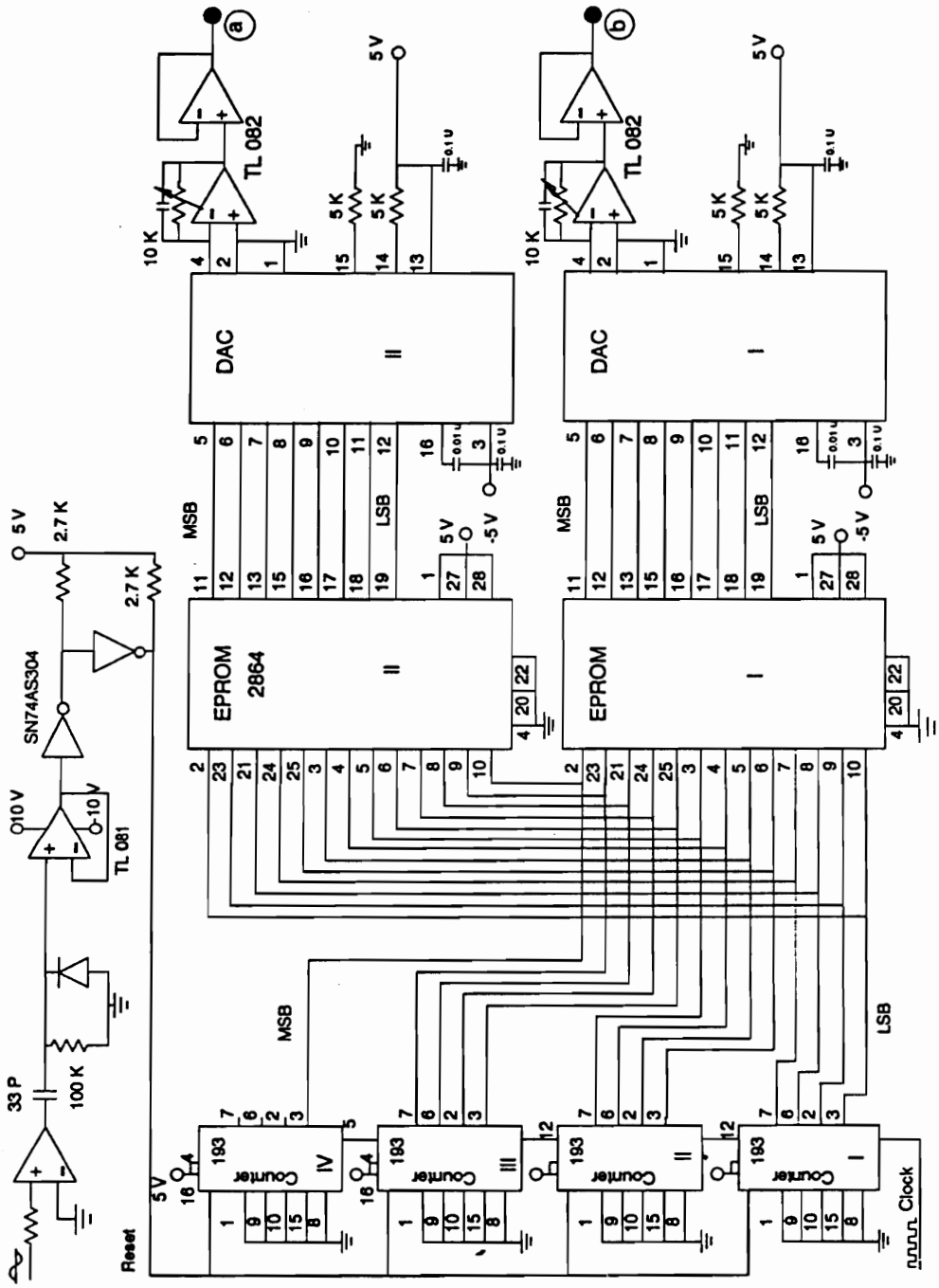

Figure A.5: Control circuit for ac to dc converter

A.3.3 Equivalent circuit and simulation results for control strategy II

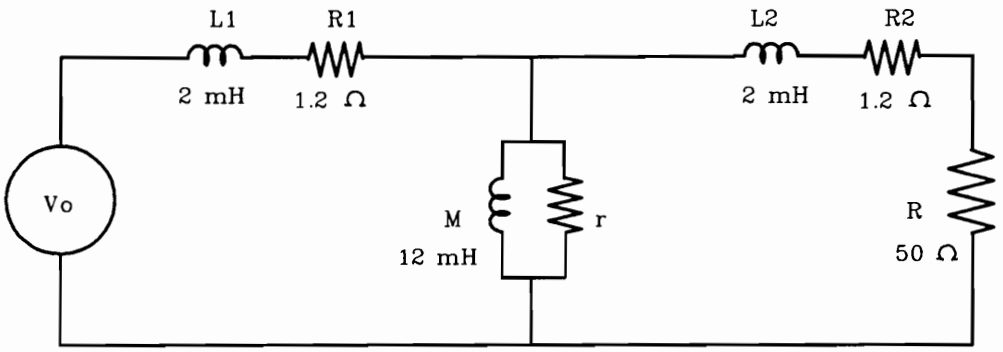

(a) Transformer equivalent circuit

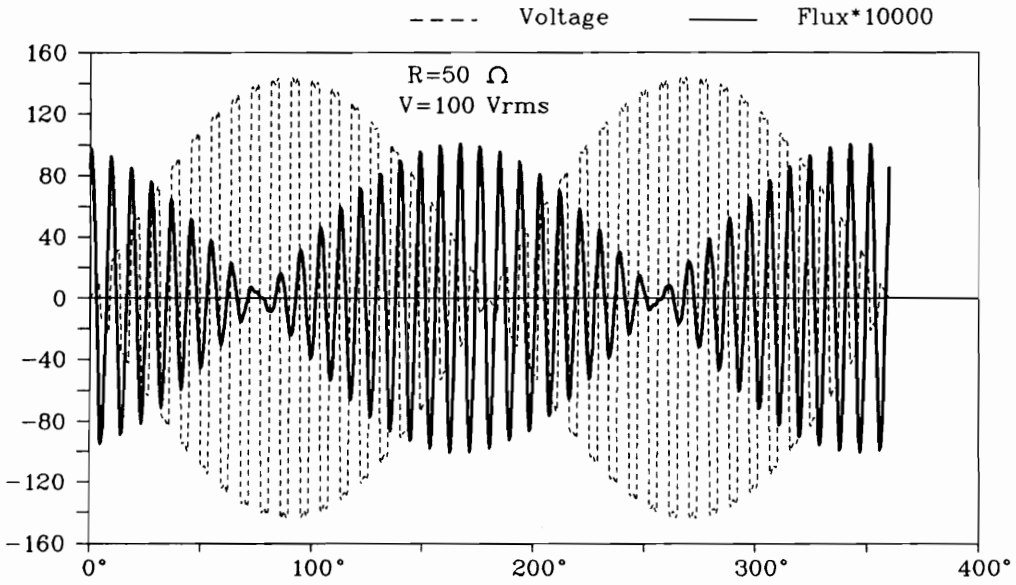

(b) Transformer voltage and flux

Figure A.6: Equivalent circuit and simulation results for control strategy II

Vita

Geun-hie Rim was born in Jeon-Ju, Korea on October 7, 1955. He received the B.S. degree from Seoul National University in 1978 and the M.S. degree from Virginia Polytechnic Institute in 1988 both in Electrical Engineering. Since 1978, he has been with Korea Elecrotechnology Research Institute, in Chang-Won, Korea as a senior research engineer in the power electronics division. During the course of this work he has been on study leave at Virginia Polytechnic Institute and State University to pursue his doctoral degree. His research interests are in the area of static power conversion and analysis and control of motor drives. He is a member of IAS, IES, PES of IEEE, and Phi Kappa Phi.

Geun-hie Rim